SEISMIC ANISOTROPY AND MANTLE FLOW BENEATH TURKEY

by

Gülten POLAT

Submitted to the Institute for Graduate Studies in
Science and Engineering Partial Fulfillment of
the Requirements for the Degree of
Master of Science
in
Geophysical Engineering

Boğaziçi University
2006

TABLE OF CONTENTS

ACKNOWLEDGEMENTS

My thesis advisor Prof. Dr Niyazi TÜRKELLİ has been considerably helpful and encouraging since the beginning of this study. I would like to thank him for his providing me an opportunity to work on my thesis in Department of Geological Sciences University of Missouri, Columbia, MO.

An important part of my thesis was completed during my stay at Missouri University, USA. I would like to thank Dr. Eric SANDVOL for his personality, guidance and hospitality. His physical insights, great deal of guidance and a lot of advices helped me for understanding the methodology. Prof. Dr Marian IVAN from Department of Geophysics, University of Bucharest, Romania and Assoc. Prof Hayrullah KARABULUT provided me with assistance at some stages of this work.

The waveform data used in this study were obtained from the Seismological Laboratory of BU-Kandilli Observatory and Earthquake Research Institute and GEOFON Data Center. I would like to thank all members of these institutions for providing researchers with available data.

I want to thank to all members of the Geophysical Department, especially Esen ARPAT , Prof. Dr. Cemil GÜRBÜZ, and Assoc. Prof Nurcan MERAL ÖZEL for their crucial comments and discussions and Dr. Ayşe Saliha TAŞPINAR who always encourages me to continue my education. I am grateful to Dr. Tolga KOMUT for his useful comments and advices. I couldn't express my feelings for Seda YELKENCİ because she always nicely listened my problems and helped me... I want to thank my good friends, Tugce AFACAN ERGÜN and Dogan AKSARI for their numerous advices.

I am grateful to Super Dorm Manager, Gülercan SELAMİOĞLU from Bogazici University for his invaluable advices and never-ending patience. In addition, I would like thank Guzide PORTAKALOĞLU and Yasemin İPEK CAN for their advices and help. I want to thank to my family, especially my mother, Seringül ÇİFTÇİ, for their supports, during my education.

LIST OF FIGURES

Figure B.5 A) Splitting versus BAZ (Back azimuth), **B)** Splitting versus the Moho incidence angle. Error bars represent 95% confidence intervals for each of the lag time estimates.

Figure B.6 The event 05164 22 44 may be shown as an example for a null at CLDR station (Φ= 75 ±3.55°, δt=2.05± 0.48 sec).

Figure B.7 A) Splitting versus BAZ (Back azimuth), **B)** Splitting versus distance (deg), **C)** Splitting versus the Moho incidence angle. Error bars represent 95% confidence intervals for each of the lag time estimates.

Figure B.8 A) Splitting versus BAZ (Back azimuth), **B)** Splitting versus distance (deg), **C)** Splitting versus the Moho incidence angle. Error bars represent 95% confidence intervals for each of the lag time estimates.

Figure B.9 A) Splitting versus BAZ (Back azimuth), **B)** Splitting versus distance (deg), **C)** Splitting versus the Moho incidence angle. Error bars represent 95% confidence intervals for each of the lag time estimates.

Figure B.10 A) Splitting versus BAZ (Back azimuth), **B)** Splitting versus distance (deg), **C)** Splitting versus the Moho incidence angle. Error bars represent 95% confidence intervals for each of the lag time estimates.

Figure B.11 This event 050611042 recorded by VANB station shows minimum transverse energy (Φ= 70°, δt=0.9 sec).

Figure B.12. Same of the Figure B.10 but for station BR13

Figure B.13 The event 041081558 may be shown as a good splitting at BR13 station (Φ= 76°, ±4.0°, δt=1.95± 0.35 sec).

Figure B.14 A) Splitting versus BAZ (Back azimuth), **B)** Splitting versus distance (deg), **C)** Splitting versus the Moho incidence angle. Error bars represent 95% confidence intervals for each of the lag time estimates.

Figure B.15 The event 05177 0823 may be shown as a splitting at CORM station (Φ= 40±10°, δt=0.75± 0.2 sec).

Figure B.16 A) Splitting versus BAZ (Back azimuth), **B)** Splitting versus distance (deg), **C)** Splitting versus the Moho incidence angle. Error bars represent 95% confidence intervals for each of the lag time estimates.

Figure B.17 The event 042781920 may be shown as a good splitting at DALT station (Φ= 5.0 ±8°, δt=1.5± 0.35 sec).

Figure B.18 A) Splitting versus BAZ (Back azimuth), **B)** Splitting versus the Moho incidence angle. Error bars represent 95% confidence intervals for each of the lag time estimates.

Figure B.19 The event 043492320 may be shown as an example at EDRB station for a good splitting estimate (Φ= -39° ± 42, δt=1.05± 1.25 sec).

Figure B.20 A) Splitting versus BAZ (Back azimuth), **B)** Splitting versus distance (deg), **C)** Splitting versus the Moho incidence angle. Error bars represent 95% confidence intervals for each of the lag time estimates.

Figure B.21 This 051380910 event may be shown as a good splitting at FETY station (Φ= -19° ± 25, δt=0.7± 0.45sec).

Figure B.22 A) Splitting versus BAZ (Back azimuth), **B)** Splitting versus the Moho incidence angle. Error bars represent 95% confidence intervals for each of the lag time estimates.

Figure B.23 A) Splitting versus BAZ (Back azimuth), **B)** Splitting versus distance (deg), **C)** Splitting versus the Moho incidence angle. Error bars represent 95% confidence intervals for each of the lag time estimates.

Figure B. 24 This 001661700 event may be shown as a good example for estimated splitting parameters at ISKB station ($\Phi = 37° \pm 12$, $\delta t = 1.35 \pm 0.3$ sec).

Figure B.25 A) Splitting versus BAZ (Back azimuth), **B)** Splitting versus distance (deg), **C)** Splitting versus the Moho incidence angle. Error bars represent 95% confidence intervals for each of the lag time estimates.

Figure B.26 A) Splitting versus BAZ (Back azimuth), **B)** Splitting versus distance (deg), **C)** Splitting versus the Moho incidence angle. Error bars represent 95% confidence intervals for each of the lag time estimates.

Figure B.27 A) Splitting versus BAZ (Back azimuth), **B)** Splitting versus distance (deg), **C)** Splitting versus the Moho incidence angle. Error bars represent 95% confidence intervals for each of the lag time estimates.

LIST OF TABLES

LIST OF SYMBOLS

λ	Elastic constant
μ	Elastic constant (Lame's constants)
ϕ	Fast polarization azimuth (splitting parameters, deg)
δt	Delay Time (splitting parameteres, sec)
β_0	Shear wave velocity (Swave)
ρ	Density
α	Compressional wave velocity (P wave)
Cijkl	The tensor of elasticity coefficients
LPO	Lattice Preferred Orientation
BAZ	Back azimuth
qSV	quasi-shear-waves
qSH	quasi-shear-waves
qP	quasi-compressional waves
i_c	Critical angle
R(t)	Radial component
s(t)	The radial waveform in isotropic medium
β	The angle between the fast and radial directions
T(t)	Transverse component
T_c (t).	Corrected transverse component
N	N-point digital time series
Δt	Time sampling interval
E_t (Φ, δt)	Transverse energy

w (w)	Wavelent function
λ_2^{min}	The sum-of-squares of a noise process
ν	Degrees of freedom
k	Parameters
α	Confidence level to be defined by values of λ_2 satisfying
F	F-distribution
A	The model parameter
A_i	An estimator of the parameter A
i,	Resample
L	The number of the bootstrapped
N *boot*	The bootstrapped noise sequence
N *original*	The original noise sequence
W	The white noise
KOERI	Kandilli Observatory and Earthquake Research Institute, Bogaziçi University

ABSTRACT

In this study, SKS and SKKS phases have been used for the analysis of shear wave splitting in order to investigate polarization anisotropy in the upper mantle beneath Turkey. To determine the shear wave splitting parameters (fast polarization direction and delay time), we have used teleseismic waveforms obtained from 21 broadband stations in Turkey. Shear wave splitting measurements are very important in determining the role of mantle flow in the geodynamics of the African-Arabian-Eurasian collison. The collision of the Arabian and African plates with Eurasia dominates the tectonic framework of the Eastern Mediterranean and Middle East (e.g., McKenzie, 1972; Jackson and McKenzie, 1988). The leading edge of the African plate is being subducted along the Hellenic trench at a higher rate than the relative northward motion of the African plate, required that the trench moves southward relative to Eurasia proper (e.g., Sonder and England, 1989; Royden, 1993). There are two adjacent subduction zones in the region: The Hellenic arc to the west and the Cyprian arc to the east. The Hellenic arc is characterized by a relatively steep, retreating subduction, whereas the Cyprus arc appears to involve a shallow subduction with two major seamounts (the Eratosthenes and Anixamander) impinging on the trench (Kempler and Ben-Avraham, 1987). Extension behind the Hellenic arc is arc-normal, whereas extension behind the Cyprus arc appears to be arc-parallel. Our results in Central Anatolia basically exhibits a NE-SW fast direction, while in Eastern Anatolia we have found a NE-SW fast direction and lag time consistent with the results obtained from temporary broadband stations of the eastern Turkey Seismic Experiment project within the Anatolian plate (Sandvol, 2003). These observations indicate that the anisotropic fabric could be relatively uniform throughout the upper mantle beneath the Anatolian plate. However, in the western Anatolia we have found a N-S fast direction that shows consistency with the directions of lithospheric extension inferred from GPS data. We have also found some evidence of trench parallel mantle flow as inferred from our results and those of Hatzfeld et al. (2001). Given the thin and hot lithospheric mantle beneath Turkey, it is unlikely that any of the observed anisotropy can be attributed to "frozen" or "fossilized" LPO induced splitting. Therefore, we believe that these observed changes in splitting reflect the variations in the asthenospheric flow along the African-Anatolian plate boundary.

ÖZET

Bu çalışmada, kesme dalgası ayrımlanma analizi ile Türkiye'nin üst mantosundaki polarizasyon anisotropisini araştırmak amacıyla SKS ve SKKS fazları kullanıldı ve bu analiz sonucunda gecikme zamanı ve hız polarizasyon yönü olmak üzere iki parametre elde edildi. Yöntemin uygulanması için gerekli olan telesismik veriler, Türkiye'deki 21 geniş bantlı sismik istasyonlardan elde edilmiştir. Afrika, Arap ve Avrasya levhalarının çarpışmasında etkin olan manto akışının belirlenmesinde, kesme dalgası ayrımlanması analizi büyük önem taşımaktadır. Arap, Afrika ve Avrasya levhalarının çarpışması Ortadoğu ve Doğu Akdeniz'in tektonik gelişiminde önemli bir rol oynamıştır (e.g., McKenzie, 1972; Jackson and McKenzie, 1988). Afrika levhasının uç kısmının Hellenik trenci boyunca dalması Afrika levhasının kuzey yönlü hareketine göreceli olarak daha yüksek seviyededir. Bu hareketin geçerli olabilmesi için Hellenik trencinin Avrasya levhasına göre güney yönlü hareket etmesi gerekmektedir (e.g., Sonder and England, 1989; Royden, 1993). Ege bölgesinde, batıdan gelen Hellenik ark ve doğudan gelen Kıbrıs arkı olmak üzere birbirine komşu iki dalma-batma zonu vardır. Hellenik arkı göreceli olarak dike yakın ve geri çekilme özelliğiyle tanımlanırken, Kıbrıs arkı yüksek açılı, uzun slab ve geri-çekilme özelliklerine sahiptir. Öte yandan, Kıbrıs arkında slab kısa ve ark üzerinde iki ana deniz dağı (Eratosthenes and Anixamander) mevcuttur. Bu deniz dağları özerleyen levhayla çarpışmış bulunmaktadır (Kempler and Ben-Avraham, 1987). Hellenic arkın arkasındaki genişleme arka normal iken Kıbrıs arkının arkasındaki genişleme arka paralel olarak görülmektedir. Analizler sonucunda, Orta Anadolu ve Doğu Anadolu bölgesinde KD-GB doğrultusunda hızlı yön ve bir saniyeden fazla gecikme zamanları bulunmuşur. Bu sonuçlar Sandvol'un (2003) Türkiye'deki Eastern Turkey Seismic Experiment projesinin geçici sismik istasyonlarını kullanarak elde ettiği sonuçlarla uyumludur. Bilindiği üzere, Batı Anadolu'da GPS çalışmaları, litosferik genişlemenin K-G yönlü olduğunu göstermiştir. Ayrıca, çalışmanın sonuçları Hatzfeld et al (2001).'in sonuçları ile karşılaştırıldığında bölgedeki çukurlukların manto akışı ile paralel yönde olduğu görülmektedir. Sonuçta, Anadolu levhası altında, üst manto boyunca düzenli anizotropik dizilimin ortama hakim olduğu gözlenmiştir. Elde edilen ayrımlanma analizi parametrelerine dayanarak Türkiye'nin altındaki, ince ve sıcak litosferik mantonun kaynağının fosil anizotropisi değil düzenli bir yapıya sahip olan astenosfer ile mekanik açıdan zayıf olan lithosfer arasındaki uyumdan dolayı oluştugu söylenebilir.

1. INTRODUCTION

Generally, seismic anisotropy occurs when elastic waves vibrate or travel in one direction faster than another. The propagation of seismic waves has revealed anisotropy in the Earth's interior. Predominantly, two types of anisotropy are observed. First type is azimuthal anisotropy in which both P- and S-wave velocities are dependent on the orientation of wave propagation. Second type is polarization anisotropy that is only valid for S-waves. If anisotropy is dependent on the direction of particle oscillation, it is called as polarization anisotropy. When a seismic wave in an anisotropic medium is recorded by a single station, we observe two different S-wave arrivals with different polarizations, rather than one S-wave. This is called *shear-wave-splitting*. In recent years, shear wave splitting has become a crucial method to map the seismic anisotropy in the upper mantle. A record of shear wave splitting gives us two pieces of information about the travel time difference and the direction of the polarization of the faster S-wave. They reflect the strength of anisotropy and the geometry of anisotropy structure, respectively. In determining splitting parameters, the quality of data is very significant because an increase in the quality of data can help us to determine shear-wave-splitting parameters more correctly. Many researchers prefer using core-refracted SKS and SKKS phases because they lead to the direct correlation of anisotropy with surface tectonic and geologic features and they are more beneficial than other phases such as PKP. In previous studies, Vinnik et al (1984) who are the first researchers of shear-wave splitting in core-refracted phases such as SKS. SKS phase has begun to be exploited extensively in teleseismic shear wave splitting (Kind et al., 1985; Silver and Chan, 1988; Vinnik et al., 1989; Ansel and Nataf, 1989; Savage et al., 1990) due to the fact that it can supply many advantages for investigating the Earth's interior.

One advantage of choosing SKS phase is that the observed anisotropy can be localized at the receiver side of the path due to the P to S conversion at the core-mantle boundary (CMB). Another one is the detectable energy on the transverse component in isotropic medium coul not be observed because SKS is radially polarized in an isotropic, spherically symmetric Earth. If the medium is anisotropic, it can be observed that SKS signifies deviations from these idealized features mentioned above. As a result of this, the effects of anisotropy and lateral heterogeneity can be simply distinguished. Hence, SKS gets an excellent diagnostic for finding out the presence of anisotropy. Thirdly, SKS approximately represents a vertical ray path through the mantle, so that the propagation direction is essentially constant; this allows a somewhat simpler analysis. The last advantage is that SKS is most clearly observed phase beyond 85 degrees. As a result of this advantage, the stable continental interiors can be investigated. Generally, teleseismic events are more suitable than local or regional events in order to sufficiently determine splitting parameters. Detailed information concerning the theory of shear-wave splitting and properties of anisotropy is given in Chapter II. We have taken into account all advantages of SKS phase as selecting the events. Therefore, we avoid using local and regional earthquakes because these types of events are especially not appropriate for investigating mantle seismic anisotropy that is most probably related to the lattice preferred orientation of anisotropic minerals (especially olivine) (Nicolas and Christensen, 1987; Mainprice and Silver, 1993; Ben Ismail and Mainprice, 1998). Moreover, splitting in teleseismic shear-waves such as SKS with steep arrival angles beneath the receiver provides perfect lateral resolution in the upper mantle. Therefore, anisotropy can be compared with surface tectonic and geologic properties possessing typical continental dimensions. There is one crucial advance in retrieving splitting information based on the utilization of SKS.

The study of seismic anisotropy began with a long theoretical treatise by Christoffel (1877) and was further advanced by Lord Kelvin (1904) in his Baltimore lectures and by Love (1944). Musgrave (1959) provided a review of the theory and practically applied to experimental studies of crystals. Seismologists realized that rocks have fabric and orientations that are clearly anisotropic. Radial anisotropy explained differences in velocities determined for Love and Rayleigh waves (Anderson, 1961). The early observations of azimuthal anisotropy were based on variations of velocity from Pn refraction data and were limited to characterizing upper mantle anisotropy (e.g., Hess, 1964). Analysis of surface waves that travel across the Pacific (Forsyth, 1975) is consistent with azimuthal anisotropy in the upper mantle (Smith and Dahlen, 1973). Silver (1996) provided a review of results from SKS phases received at continental stations. In addition to azimuthal anisotropy, extensive-dilatancy anisotropy (EDA) that is based on aligned cracks and microcracks was proposed by Crampin (1978). The microcracks are considered full of fluid in any point of the crust. The anisotropic poroelasticity (APE) due to the effects of stress on fluid-saturated cracked rock was also found by Zatsepin and Crampin (1995a).

Many seismic anisotropy treaties can be observed all over the world: Eaton (2004) studied in Great Slave Lake shear zone in the northern Canada to investigate lithospheric anisotropic structure by using teleseismic and magnetotelluric observations. Walker et al. (2001) examined shear wave splitting in order to constrain mantle flow in the vicinity of hotspots around Hawaii. Kubo et al (1995) applied shear wave anisotropy to SYOWA station in East Antarctica in order to reveal the seismic anisotropy of the crust and mantle. In addition, Zhao and Zheng (2005) performed an analysis of the SKS splitting to the North China Craton in order to analyze the seismic anisotropy of the crust and mantle.

As a new method, the cross-convolution for one and two-layer anisotropic earth methods was applied by Menke and Levin, (2003) in order to determine anisotropic earth models using observations of split shear-waves (such as SKS). Özalaybey and Savage (1994) studied shear wave splitting beneath Western United States. Özalaybey and Savage got the intriguing results that have also been confirmed using a double-layer waveform method and a more complete data set. Rümpker and Ryberg (2005) applied simultaneous inversion of shear-wave-splitting observations from seismic arrays along a 100-km profile located at the Dead Sea transform fault. The most significant anisotropic studies of the Earth are based on the upper crust. Records of local earthquakes from widely different areas of the world can be characterized with various sedimentary and crystalline geological regimes, displaying the shear-wave splitting phenomenon (Crampin, 1978; Kaneshima, 1990; Gamar and Bernard, 1997), which results in further understanding of the upper crust. A depth-varying crustal anisotropy based on vertical seismic profiling (VSP) experiment was recognized by Winterstein and Meadows (1991). Another intriguing study is related to a number of azimuthally symmetric compressive stresses. Tod (2001) applied shear-wave splitting to an isotropic crack distribution in order to determine the effects of applied stress and the fluid pressure in the medium.

Regarding the previous studies about shear wave splitting in Turkey, Sandvol (2003) applied shear wave splitting in Eastern Turkey in order to construct a reasonable geodynamic model for young continent-continent collision. Moreover, Hatzfeld (2001) employed shear wave anisotropy to understand the upper mantle beneath the Aegean related to internal deformation. Crampin (1993) analyzed shear-wave splitting from regional events in Turkey to find substantial shear-wave splitting (over 10%) in the Phanerozoic lower crust in western Turkey in which was accreted from the subduction of the Tethyan Sea. Peng and Ben-Zion (2005) analyzed spatiotemporal variations of crustal anisotropy along the Karadere-Düzce branch of the North Anatolian Fault (NAF) from similar aftershocks of the 1999 M7.4 İzmit and M7.1 Düzce earthquakes. As a result of this, splitting parameters averaged within each cluster indicates crucial variations for slightly different ray paths. Also, strong spatial variations of crustal anisotropy were observed in this area.

Generally, two methods are used for determining the shear-wave-splitting parameters in the most part of these researchs above. The first one is the method of Silver and Chan (1991) that estimates two parameters as the fast direction of shear–wave velocity and the cumulative lag time between the fast and slow components of the wave. Success of the method is based on the high quality of data due to an increase in signal to noise ratio. If data is not appropriate to analyze SKS phase, some filter techniques should be applied on data such as bandpass filter technique to observe SKS phase on the waveforms properly. However, we cannot reach expected results by filtering. Therefore, rigorous statistical analysis is required in order to solve such a problem. Because error analysis is hard to handle, a new method for nonlinear problems such as shear-wave-splitting determinations is developed. The method is referred as a bootstrap error estimation technique. The error estimation method consists of multiple inversions of simulated data that imitate the original data with different noise sequences (Efron and Tibshirani, 1991). Sandvol and Hearn (1994) modified bootstrap method by using bandlimited seismic data. Detailed information about these methods is given in Chapter II.

The goal of this study is to understand the role of mantle flow in the continent–continent collision by determining the parameters (fast polarization direction and delay time) of SKS splitting beneath all broadband stations in Turkey. Therefore, we examined only teleseismic (digitally recorded three component SKS-waveforms) events that are mentioned in Chapter III. In addition, event catalogue is given in the Appendix A. As interpreting obtained results, we must take into account the geological and geophysical background of the study area. Also, splitting measurements obtained from each station are given in Chapter III (See Appendix B for the complete list). The last chapter consists of previous studies about Turkey compared with obtained results. It is believed that in the light of these scientific implications, we could further explain the relationships between polarization, anisotropy and past and present tectonic processes in Turkey (e.g., Savage, 1999).

2. REVIEW OF THEORY

2.1. Anisotropy

Variation of the elastic parameters of a rock is a function of its mineral orientation. Anisotropy is the function of this variation. Seismic velocity anisotropy is commonly observed in the Earth's mantle, and sometimes in the crust. Nowadays, many seismologists pay attention on anisotropy because the anisotropy may be directly related to the deformation in the mantle and stress in the Earth's crust. Therefore, it can provide constraints on tectonic and geodynamic processes. Hooke's law defines an elastic body relation between stress and strain (Udias, A. 1999):

$$\tau_{ij} = C_{ijkl}\, e_{kl} \tag{2.1}$$

Anisotropy is not same as inhomogeneity, which refers to a localized change in physical parameters within a large medium. In this regard, the measurement of polarization anisotropy is generally reliable. The influence of heterogeneity is almost none with respect to the point of this view because waves in same propagation path can be easily analyzed. Moreover, there are two types of anisotropic structures: (a) lattice preferred orientation (LPO) and (b) layered structure (Figure 2.1). The elastic properties of isotropic materials are characterized by two elastic constants, the Lamé coefficients λ and μ, whereas anisotropic materials have many elastic constants. It is difficult to characterize elastic properties of anisotropic materials. Thus, in the extreme case of the most general anisotropy, 21 elastic constants get necessary. *Cijkl* is the tensor of elasticity coefficients and has 21 independent components for complete anisotropy without any kind of symmetry. In isotropic media, these independent components are reduced to two components (λ and μ) and the tensor is given at equation 2.2.

$$Cijkl = \lambda\delta_{ij}\delta_{kl} + \mu\left(\delta_{ik}\delta_{jl} + \delta_{il}\delta_{jk}\right) \tag{2.2}$$

In equation (2.2) δ_{ij} is the kronecker delta tensor. The 21 different components of C_{ijkl} in terms of λ and μ are given at equation. 2.3. If there is some kind of symmetry, this number is reduced. It is well known that there are 9 components for orthorhombic symmetry (olivine mineral) and 5 for hexagonal symmetry. Hexagonal symmetry has a principal axis. It is called transverse symmetry since any direction normal to this axis has the same properties (Figure 2.1).

$$C_{1111} = C_{2222} = C_{3333} = \lambda + 2\mu \tag{2.3}$$
$$C_{1122} = C_{1133} = C_{2233} = C_{2211} = C_{3311} = C_{3322} = \lambda$$
$$C_{1212} = C_{1313} = C_{2323} = \mu$$

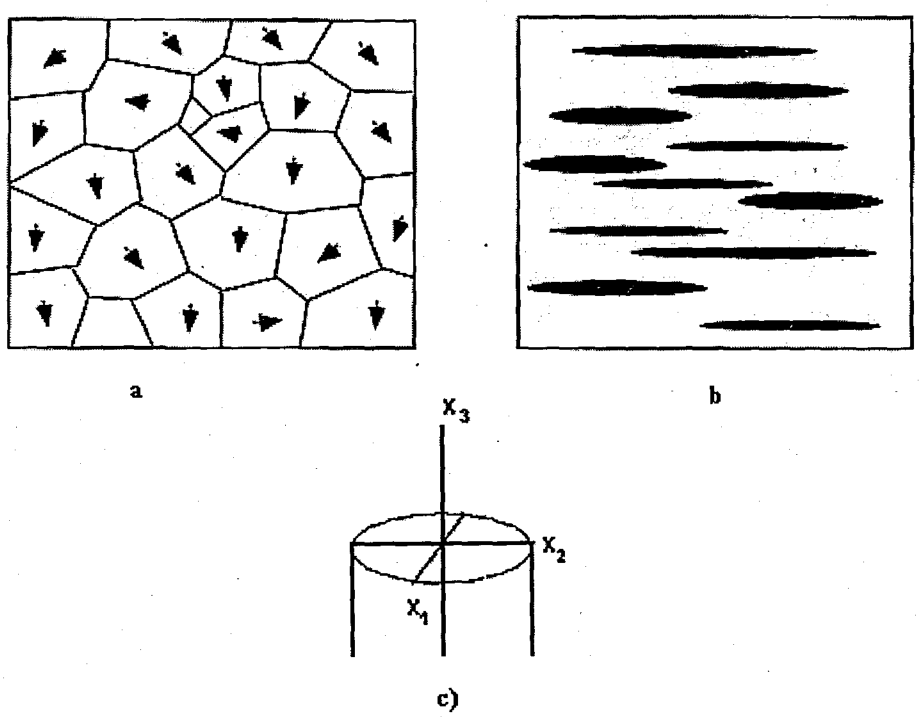

Figure 2.1 a) Lattice preferred orientation, b) Layered structure, c) The system of axis in medium with hexagonal symmetry and the principal axis in the X3 direciton. (Karato, 2003)

In isotropic media, seismic-wave velocities are independent of their direction of propagation. On the other hand, their polarizations depend just on the type of wave in isotropic media. There are two types of seismic waves: P-waves (compressional waves) and S-waves (shear-waves). The particle motion of the first wave (P-wave) is parallel to the propagation direction whereas the particle motion of S-wave is perpendicular to the propagation direction in isotropic, homogeneous and linearly elastic media and they are mutually orthogonal and have linear polarizations. The polarizations of P- and S-waves on a plane wavefront are shown via a cartesian coordinate system in the Figure 2.2. The vector L describes a motion with velocity α corresponding to longitudinal (P) waves. The vectors M and N describe motion of shear (SH and SV) waves, which is perpendicular to the direction of propagation with velocity β.

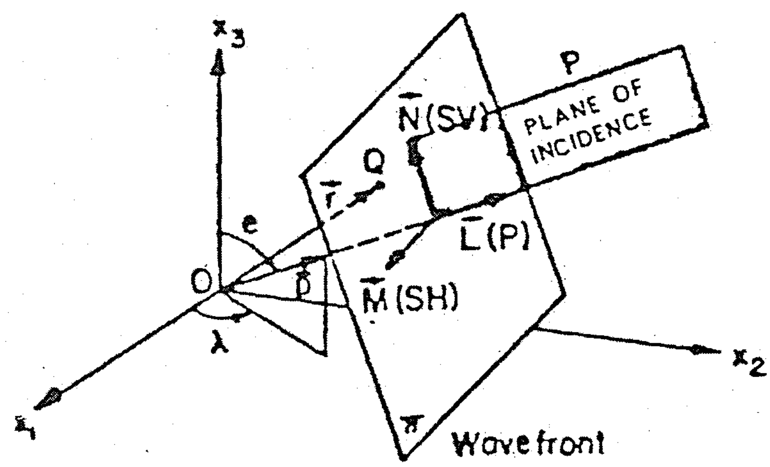

Figure 2.2. The polarization of P- and S-waves in isotropic media (Ben Menahem, 1981).

The theoretical velocities of α and β (equation.2.4) for a given isotropic material with two independent elastic constants λ and μ and the density of the material (ρ), are given by:

$$\alpha = \left[\left(\frac{\lambda + 2\mu}{\rho}\right)\right]^{1/2} \text{ and } \beta = \left(\frac{\mu}{\rho}\right)^{1/2} \tag{2.4}$$

According to the mentioned characterictic properties of the anisotropic media above, a teleseismic-shear-wave propagates through an anisotropic mantle as a pair of orthogonally polarized phases that travel at different speeds. According to propagation direction of waves towards the wavefront, the orientations of the polarization directions depend on the orientation of anisotropy. The delay time (*dt*) that accumulates between two phases is proportional to the raypath length and the magnitude of anisotropy sensed along the raypath. For a single horizontal anisotropic layer with a horizontal LPO of fast olivine a-axes, the observed fast polarization direction of a vertically traveling shear phase is horizontal and parallel to the LPO. In the case of a dipping axis of anisotropy, the fast polarization direction is not in the horizontal plane. Researchers only analyze horizontal seismograms for shear-wave splitting, and therefore only resolve the horizontal projection of the fast polarization direction, which refer to as the fast polarization azimuth (*phi*). In the case of multiple anisotropic layers, the observed splitting does not correlate directly with the individual splitting that occurs in each layer. For this reason, seismologists often refer to the observed splitting measurements (*phi* and *dt*) as "apparent" splitting measurements. For a layer with a dipping fast axis or two sublayers of different anisotropy, the apparent splitting measurements will change in a predictable fashion as a function of initial polarization azimuth, back azimuth, and incidence angle. Therefore, apparent splitting measurements can yield important insights into the kinematics and magnitude of active and past deformation in the Earth's interior.

2.2. Properties of olivine

It is generally accepted that seismic anisotropy results essentially from the lattice preferred orientations (LPO) of olivine crystals produced by solid-state flow in the upper mantle. The deformation–induced lattice preferred orientation of olivine crystals are shown at Figure 2.3. Therefore, olivine plays an important role for analyzing seismic anisotropy in the upper mantle. Olivine is a seismically anisotropic mineral that consists of a significant fraction of the upper mantle. It has maximum P- and S-wave seismic velocity anisotropy of 25% and 12%, respectively. When an aggregate of olivine grains is deformed through dislocation creep, a fabric or lattice-preferred orientation (LPO) develops where one or more of the three-olivine crystallographic axes have a preferred orientation. This leads to bulk anisotropy for the aggregate. The orientation of the bulk anisotropy depends on the set of dislocation slip planes that are active and located in the deformation accommodation areas and depends on the type of deformation. The fast direction of the bulk anisotropy is a proxy for mantle flow. Bulk anisotropy can also develop by the means of a preferred

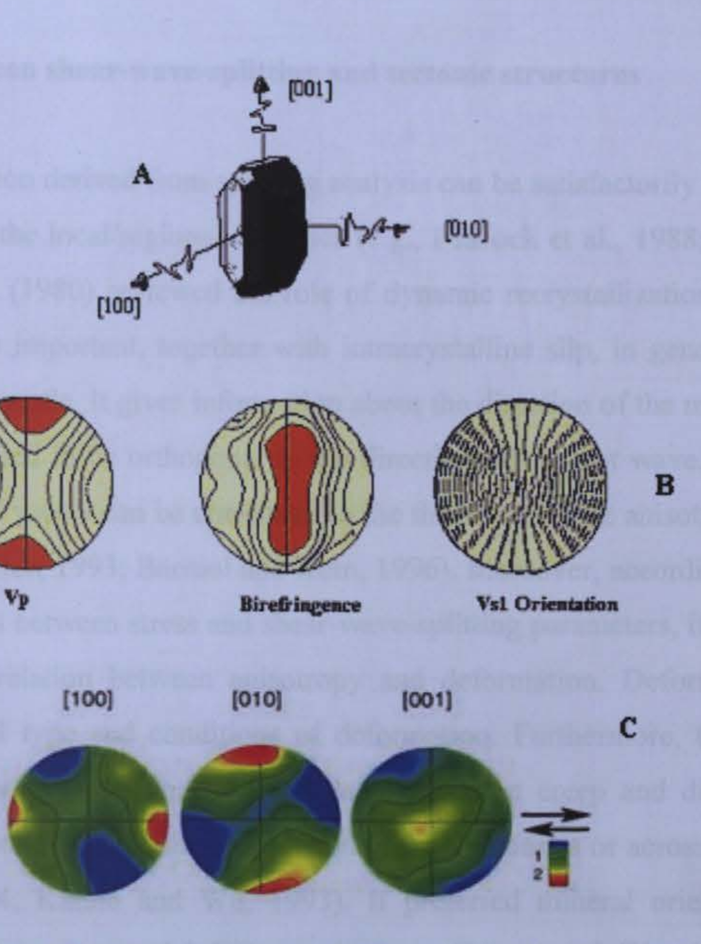

Figure 2.3 A) Olivine single crystal (Mainprice and Humbert, 1994), **B)** Olivine single crystal seismic properties (Vp and S-wave anisotropy) (Mainprice and Humbert, 1994), **C)** Lattice preferred orientation at the olivine mineral (Jung and Karato, 2001).

orientation of structures such as cracks and magma-filled lenses, or parallel layers of alternating seismic velocities. Considering its chemical composition, olivine is a natural mineral comprising a solid solution of approximately 92% magnesium or the silicate (forsterite) and 8% iron orthos silicate (fayalite). Forsterite (Mg_2SiO_4) is an olivine containing no additive but magnesium, while fayalite (Fe_2SiO_4) is an olivine containing no additive but iron. Between these two minerals, there is a continuum of olivines containing varying percentages of forsterite and fayalite in solid solution. Magnesium-rich olivine is the ingredient of the rock peridotite, the main component of Earth's upper mantle. Compression of olivine's atomic structure to its spinel phases under extreme pressure causes a seismic discontinuity at approximately 400 km and at approximately 670 km. These olivine–spinel phase transitions affect the mechanical properties of the whole mantle, which in turn determine the convective flow processes that drive plate tectonics.

2.3. Relation between shear-wave-splitting and tectonic structures

The stress direction derived from splitting analysis can be satisfactorily correlated to the breakout values or the local/regional tectonics (e.g., Peacock et al., 1988; Crampin et al., 1990). Karato et al (1980) reviewed the role of dynamic recrystallization and concluded that it may be very important, together with intracrystalline slip, in generating preferred orientations in the mantle. It gives information about the direction of the main stress acting in the area, considered to be orthogonal to the direction of the fast wave. The time delay between the splitted waves can be correlated to the thickness of the anisotropic layer (e.g., Barruol and Mainprice, 1993; Barruol and Kern, 1996). Moreover, according to mentioned views about relation between stress and shear-wave-splitting parameters, it can be said that there is a crucial relation between anisotropy and deformation. Deformation of rocks depends on mineral type and conditions of deformation. Furthermore, two deformation types are prominent in upper mantle conditions; diffusion creep and dislocation creep. Diffusion creep is solid-state diffusion between grain boundaries or across a crystal lattice (e.g., Nicolas, 1984; Karato and Wu, 1993). If preferred mineral orientations are not developed, the deformed material is isotropic (e.g., Karato and Wu, 1993). Secondly, dislocation creep causes lattice-preferred orientation (LPO). It is not created by grain-boundary migration.

2.4. Shear-wave splitting

Shear-wave splitting originates from linear polarized S-waves traversing an anisotropic medium that is known as shear-wave bi-refringence or shear-wave double–refraction (Figure 2.4). Nowadays, it is used as a method to investigate seismic anisotropy. In an anisotropic, homogeneous medium, three independent body waves are generated that have orthogonal planes of particle motions. These are usually called quasi-compressional waves (qP) and quasi-shear-waves (qSV and qSH), with names suggestive of the isotropic counterparts. It is well known that one of the primary effects is the separation of the isotropic S-wave into two quasi-shear-waves, which is called shear-wave splitting. These properties depend on the general stress-strain relationship expresses by Hook's law (equation2.1)

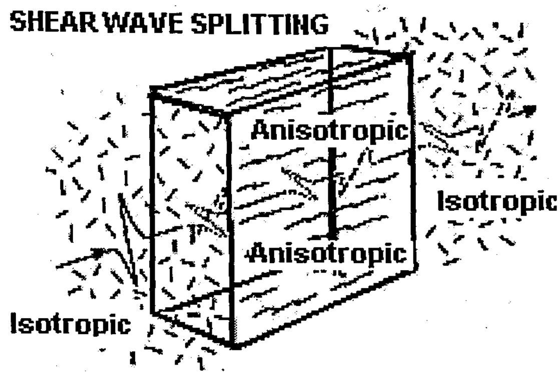

Figure 2.4. Showing the behavior of shear-waves in anisotropic media (Crampin, 1981).

for which the most general anisotropic medium has 21 independent elastic moduli. A single olivine crystal has orthorhombic symmetry. Symmetry increases in the structure reduces the number of moduli. In general, the propagation direction of these waves is not perpendicular to their wavefronts, so the particle motions differ from isotropic behavior. The velocities of these waves vary with the trajectory of the wave structure through the medium with respect to any axes of the symmetry in the structure. These kinds of discrepancies in observed S-waves help us to deduce the presence of anisotropy. Generally, it is believed that olivine-rich ultramafic rocks are the main rock types of the upper mantle.

2.5 Shear-wave splitting Analysis with SKS Phase

At the teleseismic distances, a very clear example of split shear-waves arriving at nearly vertical incidence at the station is provided by SKS-waves. SKS-waves travel as a P-wave within the liquid core of the Earth. It results from a P to S conversion at the core-mantle boundary (CMB) (Figure 2.5). Furthermore, we especially preferred SKS and SKKS phases as analyzing events because splitting in teleseismic shear-waves such as SKS with steep arrival angles beneath the receiver can provide excellent lateral resolution in the upper mantle. If the layer D" of the lowermost mantle is isotropic, upcoming SKS-waves should thus be polarized in the vertical plane in D". If the whole of the Earth is isotropic, SKS should appear as a pure S_v phase all the way towards the surface. As the SKS ray is

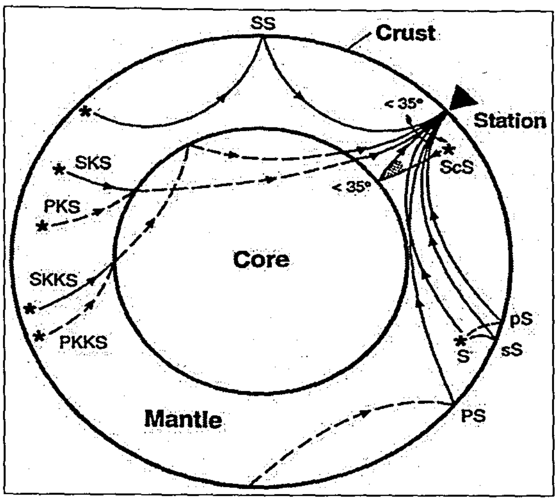

Figure 2.5. Ray trajectories of P- and S-waves are from the crust to the core (Savage, 1999).

nearly vertical beneath the station, it should be observed as a radially polarized phase in the horizontal plane (i.e., tangential to the great circle joining the station to the epicenter). On the other hand, if there is an anisotropic region somewhere along the upcoming SKS ray path, S-wave-splitting will occurs yielding two SKS-waves polarized at a right angle from each other. Finally, if the symmetry axes of the anisotropic region cause the splitting of SKS that have a fixed orientation in the space over a significant portion of the upcoming ray path, the two split SKS-waves can arrive at the station with a noticeable time difference. This can be interpreted in terms of preferred mineral orientations in the upper mantle. Moreover, the ray paths and geometries constrain the shear-waves because they arrive at near vertical incidence angle. This can found out from three component seismograms. Nuttli (1961) indicated that if the angle of incidence is greater than the critical angle (ic), some changes in particle motion of an incident shear-wave on the free surface can be observed (Figure 2.6). Laterally heterogeneous structures and scatterers may also be responsible for irregularities and anomalies of the particle motion of shear-waves. The effects of anisotropy can be easily distinguished from the effects of lateral heterogeneity by using polarization studies (Crampin, 1987). Indeed, a single or more anisotropic layer along the ray path can create shear-wave splitting. The critical angle is represented by,

$$i_c = \sin^{-1}\left(\frac{Vs}{Vp}\right) \tag{2.5}$$

Thickness of single layer (L), isotropic shear velocity (βo) and the delay time (δt) observed along a vertical ray path. These parameters are related to each other (Silver and Chain, 1988). (δt) = L ε / $\beta_{o,}$ ε (<<1) is the fractional difference in velocity between the fast and slow polarization directions. Where Vp and Vs are the near surface velocities of P- and S-waves respectively. The critical angle is approximately 35^0 accoording to Poisson' ratio of 0.25. Therefore, the simplifying solutions are made for many seismological problems.

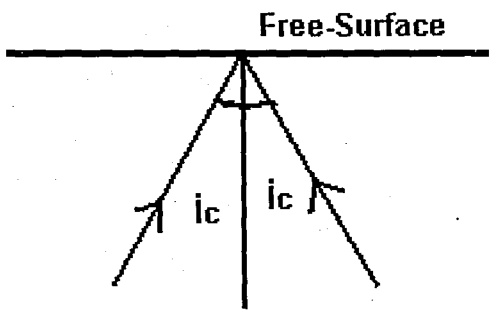

Figure 2.6. The cone explained by the critical angle.

3. ANALYSIS OF SKS ARRIVALS

3.1. Method

Nowadays, many methods have been used to determine the shear wave polarization direction and time delay result from shear-wave splitting. Ando et al (1983) developed one of these methods, which is based on the original horizontal seismograms. Horizontal seismograms are rotated to various azimuths. The polarization direction of the fast shear wave is the azimuth, which is determined from the amount of time seperation between the fast and slow shear-wave arrivals measured directly from the orthogonal seismograms. Secondly, Bowman and Ando (1987) determined the time delay by maximizing the cross-correlation function between the fast and slow components. Moreover, Menke and Levin (2003) applied the cross-convolution method with application to one to two-layer anisotropic earth methods in order to determine anisotropic earth models by using observations of split shear-waves (such as SKS). Shih et al (1989) maximized the ratio of the particle displacements' projection into a pair of orthogonal axes (aspect ratio) according to a function of azimuth. Maximum aspect ratio means that the azimuth of the pure linear particle motion is the fast polarization direction. Ryberg and Rümpker (2005) applied two different iterative approaches that utilies the inversion of the observed splitting parameters. First one is the local optimization technique (the downhill simplex method) and second one is a global genetic algorithm search in order to measure shear-wave splitting paramaters from observed SKS waveforms along a dense receiver profile and compare them with splitting parameters gained from numerical waveform modeling via anisotropic Earth models. Nearly all methods above have relative advantages and weakness in analysing shear-wave splitting. The advantage of the process is based on the amount of time seperation (time delay) between the split arrivals because the time delays based on usually of the order of a fraction of a second. Almost all of the methods are solely applicable to high frequency records that are collected from local events (Vinnik et al., 1989).

We approximately try to use two methods in this study. The method of Silver and Chain (1988) is generally applied to measure the splitting parameters from SKS arrivals. There are some factors, which encourage us to choose it for the study. It is briefly tried to explain that the shear-wave splitting parameters can be easily obtained from the horizantal component seismograms of the SKS-phase because the method takes complete advantages of the characteristic behaviours of SKS. In a laterally homogeneous Earth, the transverse component T(t) will be identically zero for a noise-free SKS seismograms because SKS is strictly polarized as Sv in the radial direction upon leaving the CMB on the receiver side. This feature of the SKS can be utilized as a constraint to find the splitting parameters (Silver and Chain, 1988). If anisotropy is detectable for near-vertical propagation, the radial and transverse components (equations 3.1 and 3.2. respectively) are related by,

$$R(t)=s(t)\mathrm{Cos}^2\beta+s(t-\delta t)\ \mathrm{Sin}^2\beta \tag{3.1}$$

$$T(t)=-1/2[s(t)-s(t-\delta t)]\ \mathrm{Sin}(2\beta) \tag{3.2}$$

where β is the angle between the fast and radial directions. If anisotropy is not observed, s(t) is the radial waveform.

In Figure 3.1 X(t) and Y(t) are the North-South (N-S) and the East-West (E-W) horizantal component seismograms, respectively. The ray back-azimuth measured clockwise from North is called as BAZ. Vectorially rotating the original horizantal component seismograms into the theoretical ray back azimuth direction give Radial (R) and Transverse (T) componets

$$R(t)=[X(T)COS(BAZ)+Y(T)SIN(BAZ)] \tag{3.3}$$

$$T(t)=[\ X(T)SIN(BAZ)-Y(T)COS(BAZ)] \tag{3.4}$$

T (t) is approximately zero. Its value depends on two conditions: anisotropy having very small (δt-0) or the back azimuth along the fast and slow polarization direction (β=0°, 90°, 180°, 360°) (Silver and Chan, 1988; Vinnik et al., 1989). Shear-wave-splitting parameters (Φ and δt) are found by using the transverse component of SKS due to the successfull elimination of the effects of anisotropy. This process is based on minimizing energy E_t (Φ, δt) at equation.3.5 on the corrected transverse component T_c (t). For a N-point digital time series, this is expressed as,

$$Et(\phi,\delta t) = 1 \Big/ N \sum_{i=1}^{N} Tc(t)^2 \Delta t = Minimum \tag{3.5}$$

where Δt is the time sampling interval. E_t (Φ, δt) (equation 3.6) is evaluated for many candidate values of Φ and δt by using Silver and Chain's method (1988) to locate the minimum energy with respect to the fast polarization direction Φ and the time delay δt. In addition, Parseval's theorem is used for the mentioning the approach above. The integrand is a product of Iw (w)I^2, and it was modulated by an oscillating function with maxima at w=(2n+1)π/δt and zeros at *w*=2nπ/δt. For δt=1 s, the maxima occur at 0.5 Hz, 1.5 Hz, 2.5 Hz, etc., zeros at 0 Hz, 1 Hz, 2 Hz, etc.

$$E_T = \sin^2(2\phi)\int_{\infty}^{\infty} |W(w)|^2 \sin^2(w\delta t)dw \tag{3.6}$$

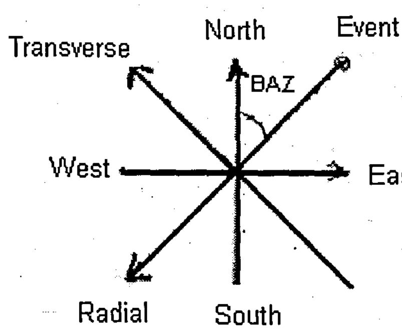

Figure 3.1. According to the recording coordinate system, schematic diagram illustrating transverse and radial directions on the horizantal plane (Arrows depict positive motion directions).

Moreover, the results of mantle azimuthal anisotropy are calculated by using teleseismic shear-waves. Therefore, shear-wave-splitting parameter determination gets a crucial technique in seismology. Generally, many stations are necessary to increase quality of obtained results. As processing the events, some problems could be observed. One of the most significant problems may be based on low quality of data so that rigorous statistical analysis gets necessary for correct estimation of shear-wave-splitting parameters. One of the most prominent nonlinear problems is the shear-wave splitting determination. Because of this, error analysis is very difficult for estimating precise splitting parameters. Sandvol and Hearn (1994) developed a bootstrap error estimation technique so that it has some problems. Therefore, we can benefit from the advantages of the two methods. The bootstrap method could be used to test the occurrence of shear-wave splitting and determine errors in the splitting parameters when splitting is observed. The bootstrap method consists of multiple inversions of simulated data that imitate the original data with differing noise sequences (Efron and Tibshirani, 1991). For bandlimited seismic data the method was modified to work and to be easily extended to other waveform inversion problems (Sandvol and Hearn, 1994).

3.1.1. Inversion method

The method of Silver and Chain (1991) is commonly used to invert SKS horizantal seismogram pairs. The two orthogonal shear-wave horizantal components are shifted as relative to one another and then they are rotated in terms of a polarization angle after original seismograms are become corrected by using the inversion process. It is well known that all of the shear-wave energy should be observed on the radial component of the corrected coordinate systems as the seismograms are shifted and rotated by the correct amount (Silver and Chain, 1991; Vinnik et al., 1992).

The corrected shear-wave-splitting parameters are found by using a direct grid search of the parameter space in order to find which set of parameters minimizes the energy in the corrected tangential component. The fast direction of shear-wave velocity and the cumulative lag time between the fast and slow components of the wave can be estimated by using the method of Silver and Chain (1991). The fast direction range is changed from -90° to 90° and the travel time variation between the fast and slow shear-wave is called as lag time, which signs positive. The disadvantage of the method is not directly to test the presence of shear-wave splitting because data with no shear-wave splitting exhibit ambiguity in the fast direction and always have a nonzero positive lag time. Sandvol and Hearn (1994) introduced a new method for testing the presence of shear-wave splitting. As the "polarization direction" is obtained, the initial inversion is applied. The polarization direction changes in the range within ± 45° of the fast polarization direction. In the method, one of the main objectives is to find the polarization direction for each bootstrap inversion. Then, the fast and slow direction can be distinguished from each other due to 90° apart between the fast and slow waves. Moreover, the shear-wave is propagating perpendicular to the polarization direction and the arrival times of the shear-waves in the polarization direction are different from each other. The difference is called as "relative lag time" and generally found for each bootstrap inversion. A positive or a negative relative lag time means that the polarization direction is identical with the direction of the fastest S-wave propagation neither the direction of the slowest S-wave propagation. The presence of shear-wave splitting can be recognized by a statistical test with using a new parameterization. Zero relative lag time on the confidence bounds indicates the absence of anisotropy whereas the confidence bounds including no zero relative lag time demostrate the presence of anisotropy. Silver and Chan (1991) used the inverse F test to analyze errors in the inversion for shear-wave splitting parameters by determining a confidence region for fast direction and lag time.

3.1.2. Error estimation

Error estimation plays crucial role in the measurement of shear-wave-splitting because evaluating the uncertainty of each measurement may support the quality of parameters. According to making an assumption, the root mean square (rms) amplitude for an n-point discrete time series, λ_2^{min} is the sum-of-squares of a noise process, which is approximately X^2 distributed. For v degrees of freedom and k parameters, taking the confidence region at the α confidence level to be defined by values of λ_2 satisfying (Jenkins and Watts, 1968; Bates and Watts, 1988), where f is the inverse of the F-distribution at equation 3.7 (Efron and Tibshirani, 1991) bootstrap methods, however, are free of any assumptions based on the distribution of the errors of the data or the model parameters and also are not critically dependent on estimating the number of degrees of freedom

$$\frac{\lambda_2}{\lambda_2^{min}} \leq 1 + \left(\frac{k}{(\nu - k)} \right) f \;\; k, \nu - k(1-\alpha) \tag{3.7}$$

3.1.3. Bootstrap Method

The variances of a problem can be determined by using the bootstrap method for an inversion (Tichelaar and Ruff, 1989). Bootstrap method works by using repeated inversions of bootstrapped data that contain the same information as the original data but have a different noise sequence (Sandvol and Hearn, 1994).

After first selecting an estimate of the noise sequence from the original data is a very helpful step for getting bootstrapped data, a bootstrap sequence simulates the noise. The last step is to add the bootstrap noise back to the original estimated signal in order to compose a bootstrap data set. It is well known that many scientists can use many different independent bootstrapped inversions in terms of their goals. As a result, for estimating a standard deviation, the set of bootstrapped solutions is applied at equation 3.8. The standard deviation of the model parameter is called as A that can be defined at equation 3.9.

$$\sigma boot = \frac{1}{(L-1)}\left[\sum_{i=1}^{L}\left(Ai-\hat{A}\right)^{T}\left(Ai-\hat{A}\right)^{1/2}\right] \tag{3.8}$$

$$\hat{A} = \frac{1}{L}\left(\sum_{i=1}^{L} Ai\right) \tag{3.9}$$

The term of A_i is an estimator of the parameter A (either of the shear–wave-splitting parameters), calculated for bootstrap resample i, and L is the number of the bootstrapped inversions (Tichelaar and Ruff, 1989). In order to work with the bootstrap technique, the errors in the data must be independent of each other (Efron and Tibshirani, 1991). Thus, this "classical" bootstrap error analysis cannot be performed on the bandlimited waveform data because the data points are not independently distributed (Efron and Tibshirani, 1991). That is, each data point must have the same statistical properties as the other data points, but each measurement must be independent of the others (Papoulis, 1991). Sandvol and Hearn (1994) modified the bootstrap error estimation method to account for correlated data such as that found in seismic waveforms. The modified bootstrap technique works with first estimating the shear-wave-splitting parameters for a pair of horizantal shear-wave seismograms. This is done by shifting and rotating the seismograms into the correct radial and tangential components (Silver and Chain, 1991).

The corrected tangential component is described by definition of their residual vector (i.e., noise sequence) (Sandvol and Hearn, 1994). Then, this original noise time sequence is used to construct a boootstrap noise sequence with the same statistical properties as the original noise but with a different numerical sequence. Each bootstrap noise sequence is constructed by convolving the original noise time sequence, a gaussian white noise time sequence and normalizing the resulting time sequence to have the same rms amplitude (equations: 3.10 and 3.11)

$$\sigma boot = \frac{1}{S}\left[\sum_{j=1}^{L} N(j)_{original} * W(i-j)\right] \tag{3.10}$$

where

$$S = \left[\sum N(j)_{boot} * N(j)_{original}\right]^{\frac{1}{2}} \tag{3.11}$$

N boot is the bootstrapped noise sequence, N original is the original noise sequence, and W is the white noise. Further randomization of the noise series can be gained by circularly shifting with using a random number of data points. Bootstrapped data sets are constructed by backrotating and then backshifting the corrected radial and tangential seismograms only using the bootstrapped noise sequence in place of the original corrected tangential component.

The flowchart (Figure 3.2) shows us to understand properties of the method clearly. As time series is backrotated and backshifted, alteration gains importance because the technique would only need it. Efron and Tibshirani (1991) mentioned that there is constrains on the number of bootstrap solutions to obtain required convergence.

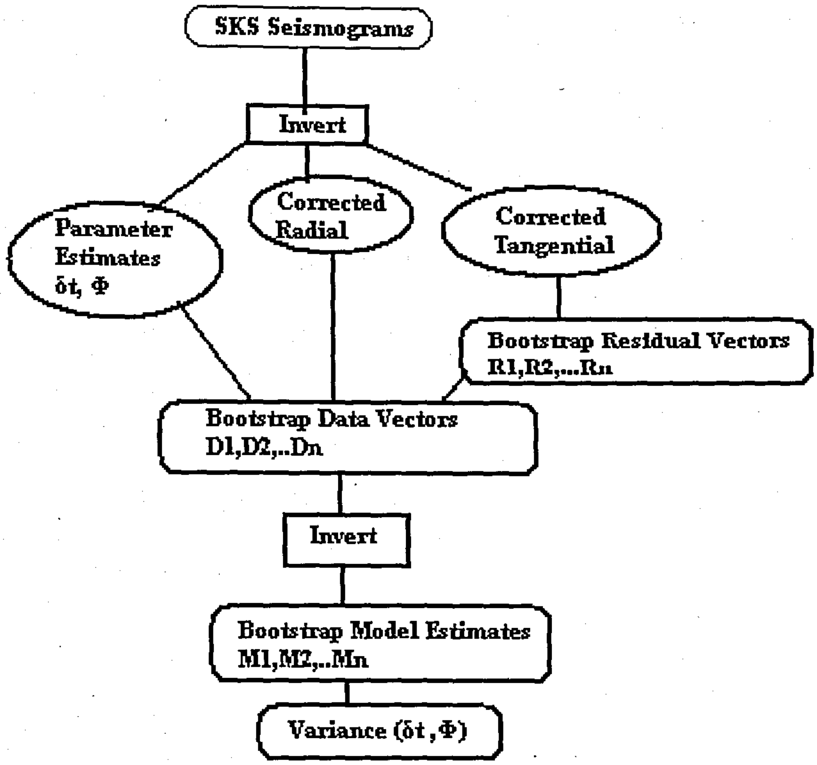

Figure 3.2 A flowchart of the modified bootstrap error estimation techniques to estimate errors in the inversion for shear-wave-splitting parameters.

3.2. DATA

3.2.1. Data selection

It is known that the past and the present tectonic processes can be clearly explained by polarization anisotropy. Hence, we tend to study upper mantle anisotropy beneath all stations in Turkey. Because of this study, we can easily map out the seismic anisotropy structure in the upper mantle by using the outcomes obtained from the process of the selected data. Moreover, in this study, we have examined teleseismic shear-waveforms, which were recorded by three components, digital KOERI broadband stations (Bogazici University, Kandilli Observatory and Earthquake Research Institude) and two permanent MALT and ISPB stations from the GEOFON network (Figure 3.3). These stations are listed in Table 3.1.

Figure 3. 3 The map shows broadband stations (KOERI) in Turkey.

The stations in the table 3.1 are permanent and they are broadband CMG-3TD (0.003 s to 10 Hz), CMG-6DT (0.03 s to 10 Hz), CMG-3ESPD (120s to50 Hz standard), CMG-40TD (0.03 s to 10 Hz), STS-1 (20 to 0.01 Hz), GEOTECH KS54000 (0.003 to 16 Hz) and STS-2 (20 to 0.01 Hz) seismometers. They were recorded continuously by a 24-bit digital acquisition system. Although, KOERI stations have 50 s sample intervals, MALT and ISPB stations have 100 s sample intervals. Approximately 400 earthquakes (Figure 3.4) with high signal to noise ratios are selected in terms of clear observation of SKS or SKKS on the teleseismic shear-wave forms in event catalog (Appendix A).

Figure 3.4 The used teleseismic events in this study

We collected seismograms from earthquakes that occured in a distance larger than 85 degree and that have a magnitude greater than 5.7. There is no constraint on depth range for events. Time scale is changed from 1996 to 2006.

Many S-waves from especially local earthquakes have angles of incidence much larger than the critical angle, in which case the shear-waves distorted due to the effect of the free surface (Nuttli, 1961; Kennett, 1991). In other words, large angles of incidence cause larger S-to-P conversions that can also distort horizontal particle motions. For this reason, only these records with S-wave incidence angles of 35^0 or less are used. Hales and Roberts (1970) developed the theoretical travel times for identification of SKS- and P-phase on the seismograms according to a travel-time polynomial. Then, Ray Buland developed FORTRAN programs to calculate travel times by using teleseismic body-waves through earth model IASP91 (Kennett and Engdahl, 1991). Although we collected the data in terms of mentioned criteria above, we could not obtain efficient events at some stations (Appendix B). The causes might consist of lack of sufficent amount of events and low quality of signal to noise ratio.

Table 3.1. Parameters of the used stations in this study

Stations	Latitude (deg)	Longitude (deg)	Elevation (m)	Seismometer
ANTB	36.8998	30.6538	120	CMG-6TD
BALB	39.64	27.88	150	CMG-40TD

BLCB	38.3853	27.042	379	CMG-6TD
BODT	37.0616	27.3103	209	CMG-3ESPD
BR131*	39.725	33.639	100	Geotech KS54000
CANB	40.0167	27.0625	2094	CMG-6TD
CEYT	37.011	35.7478	1292	CMG-3ESPD
CLDR	39.144	43.9172	548	CMG-3ESPD
CORM	40.1785	34.6302	1100	CMG-3ESPD
CUKT	37.2473	43.6077	209	CMG-3ESPD
DALT	36.7692	28.6372	200	CMG-3ESPD
DATB	36.729	27.5778	1946	CMG-3ESPD
EDRB	41.847	26.7437	132	CMG-40TD
FETY	36.6353	29.0835	1000	CMG-3ESPD
HDMB	36.964	32.486	366	CMG-6TD
ISKB	41.0657	29.0592	53	CMG-3TD
ISPB	37.8227	30.5222	381	STS-1
KARA	37.261	35.0547	649	CMG-3ESPD
KRTS	36.573	35.375	1087	CMG-3ESPD
KOZT	37.481	35.8268	381	CMG-3ESPD
KVTB	41.0807	36.0463	500	CMG-40TD
MALT	38.313	38.427	1835	STS-2
MERS	36.868	35.8268	1910	CMG-3ESPD
MLSB	37.2953	27.7765	1038	CMG-40TD
PTKB	38.8923	39.3923	1630	CMG-3ESPD
SEMD	37.3473	44.5208	938	CMG-3ESPD
SIRT	37.501	42.4392	1227	CMG-6TD
SVSB	39.9175	36.9925	924	CMG-3TD
URFA	37.441	38.8213	702	CMG-3ESPD
VANB	38.595	43.3888	829	CMG-3TD

(* Keskin: Belbaşı station in Ankara).

3.2.2. Processing Data

After selecting available data, basic preparation procedure were applied to the data recorded by the stations (Figure 3.3). Some of these steps in the procedure consist of filtering and windowing. Moreover, frequency filtering was often applied to the data in order to increase the signal to noise ratio. Filtering removes noise from signal which could be important for resolving anisotropy, especially anisotropy that gives rise to small *dt* (e.g., crustal anisotropy). Teleseismic signals that are used in splitting analysis have the dominant frequency of usually ~0.1-0.15 Hz. Noise often begins to approach signal strength at frequencies greater than 0.2 Hz. Consequently, a cutoff at 0.2 Hz significantly increases the signal-to-noise ratio of the data. Indeed it is not difficult to find a time window that brackets a noisy split broadband waveform that yields very small error bars and/or inaccurate measurement. Therefore, filtering may be necessary to make accurate determinations of the initial polarization azimuth for SKS and SKKS phases. In addition, these phases are important for investigating variations in splitting.

Before the beginning of the data process, we made some assumptions. As the first, the anisotropic medium is laterally homogeneous. Secondly, there is coherent anisotropy symmetry. Thirdly, receiver side seismic polarization anisotropy was determined by using SKS and SKKS core phases. After these kinds of the assumptions, all the events were selected manually according to their horizontal components with a window approximately from 10 or 15 second before SKS or SKKS wave to 15 or 20 seconds after these phases. Then, we applied a filter with a 0.01-0.2 Hz bandpass to the waveforms. After the filtering, the horizontal waveforms were cutted in terms of the predicted SKS or SKKS arrival time, which is calculated by IASP91 travel time table.

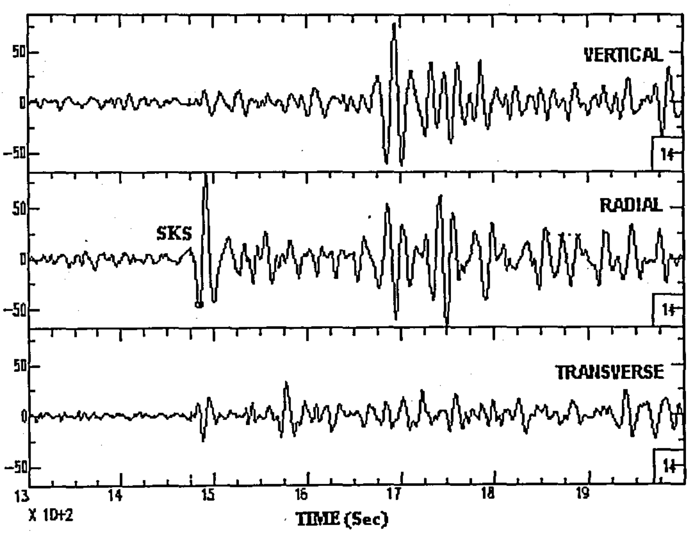

Figure 3.5. Three component seismograms of core-refracted phases (SKS) recorded at BALB station. Approximate arrival times of SKS are indicated on radial component. Crucial SKS energy can be dedicated on the transverse component.

In the next step, the cutted events were processed with the method of Silver and Chain (1991). If the result is not satisfied, the bootstrap technique (Sandvol and Hearn, 1994) may be used. After this data analysis, we obtained two parameters that are the polarization direction of the first arrival phase (fast direction) and the time delay (lag time) between the fast and the slow polarizations. These are defined as a split shear wave. Three components of SKS (vertical, radial, and transverse) for station BALB and the event 051642244 is depicted in Figure 3.5.

Also, Figure 3.6 shows an example of the applied processes on the raw data in this study (Figure3.6). Figure 3.6.A shows the original (uncorrected) radial and transverse components and right side of this Figure (a) shows particle motion of them. If SKS energy is observed on transverse component, this is accepted as an evidence for presence of seismic anisotropy. Figure 3.6.B shows super position of the fast and slow components that are determined in terms of estimated splitting parameters and right side of this Figure (b) indicates particle motion of them. The particle motion of slow and fast components is expected to be elliptical. In addition, Figure 3.6 C demostrates super position of the shifted fast and slow components and also right side of this Figure (c) shows particle motion of these shifted components. On the other hand, Figure 3.6.E indicates the minimizing transeverse energy on the transverse component in terms of estimated splitting parameters (top trace of Figure 3.6).

The bottom traces of Figure 3.5 shows superposition of corrected radial and transverse components and right side of this trace indicates their particle motion that gets linear. The splitting parameters $\Phi = 25^{o}$ and $\delta t = 1.2$ s are determined by the method of Silver and Chain (1991) for this event. Then energy of transverse component of SKS phase has been removed in terms of the estimated splitting parameters (Figure 3.6). The particle motion of the waveforms are used in this study to check the estimated parameters because elliptical particle motions are indicative of shear wave splitting (right side of Figure 3.6).

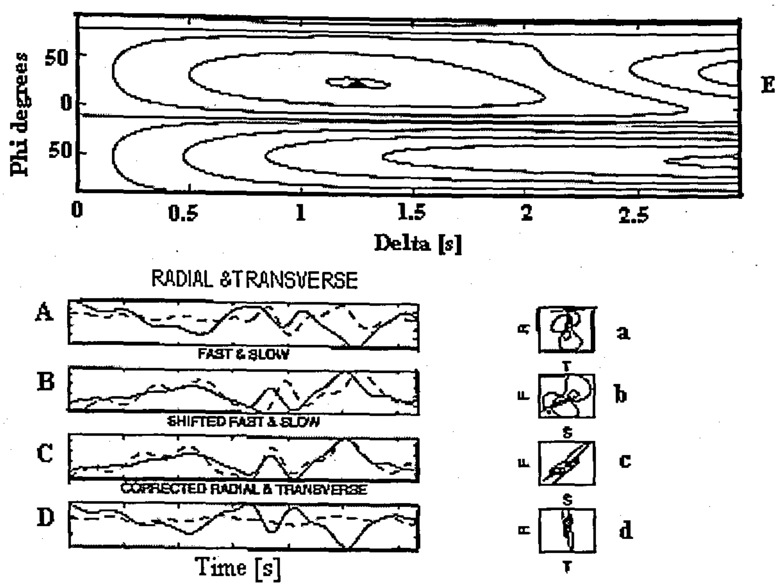

Figure 3.6 The event 051642244 may be shown as a good splitting at BALB station (Φ= 25±17.27 °, δt=1.25±).

The method described the inverse f test method for the error analysis. For each set of possible parameters, the test is applied to measure whether or not the split parameters are within the bounds of a 95 % confidence region. Sandvol and Hearn (1994) developed the bootstrap error estimation technique for shear wave splitting inversion. There were some ambiguities regarding the error estimates using the method of Silver and Chan (1991). Therefore, the bootstrap error estimation technique can be used as a robust technique to estimate errors correctly. We analyzed 400 sets of the high quality (minimum calculated Signal to Noise ratio allowed greater than 3) SKS and SKKS phases for evidence of shear wave splitting. We could not obtained suitable events from some stations such as SIRT, SEMD and DAT etc. because the quality of data is very poor due to the fact that the signal to noise ratio is very low. In the light of mentioned processing steps above, the flow chart was made to clearly show applied steps in process (Figure 3.7).

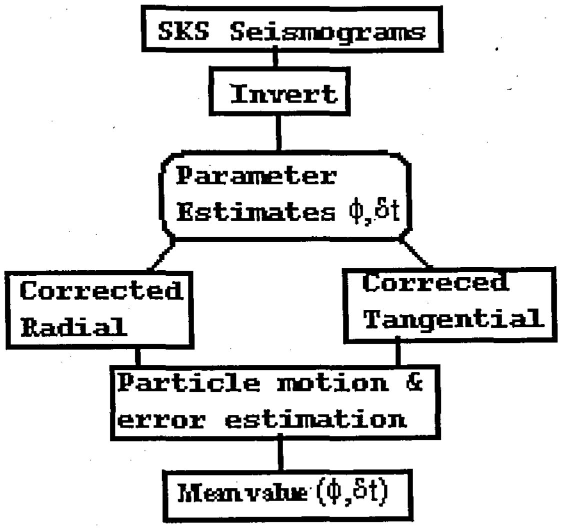

Figure 3.7 The flow chart shows our processing steps in this study.

3.3. RESULTS

3.3.1 Results of the estimated splitting parameters for each station

Tables from 3.2 to 3.4 include the estimates of splitting parameters for each station. Quality factor was ascribed to each estimated splitting parameters due to the signal to noise levels of the high quality SKS radial components. If observable energy on the transverse SKS components is not detected clearly, delay time may be zero as well as the event back azimuth (BAZ ±n 90°, n=1, 2, 3). The resulting splitting parameters for each station are respectively given below. Almost all of our results are given in Appendix B We observed evidence of distance or possibly azimuth dependence on splitting at nearly used stations (Figure 3.3). Generally, there was a little variation in the fast direction with ray parameter or BAZ. However, consistent variations between lag time and azimuth are observed. The variations in shear wave splitting lag times with incidence angle might indicate a purely horizantal symmetry for the stations of ANTB, CLDR, DALT, FETY, HDMB, URFA. In these stations steep incident waves could have smaller lag times than incident waves, which are oblique. However, the observed differences (> 0.5 seconds) show that the lateral variations in the thickness and the strength of anisotropic layer is responsible for the results. The variations in lag times decrease with increasing incidence angle. This is consistent with an inclined symmetry axis for these stations (BALB, BLCB, BR13, CORM, ISKB, ISP, MALT and SVSB). This may results from localized mantle shear. In addition, there are some variations at another stations except mentioned before. These variations could not be observed obviously at EDRB like other stations such as BODT. In addition, SKS or SKKS phases can not be clearly observed on the waveforms that recorded by KARA, SIRT, DATB, KOZT, CEYT, SEMD, CUKT, KRTS, BR232 and MERS stations. There are two possible reasons that lead to insufficient results: low quality of data due to signal to noise ratio and lack of several events.

ANTB

Splitting parameters obtained from ANTB station show fast polarization directions oriented around approximately N-S for the events with a back azimuth range between 73°-259° (Table 3.2). The simple mean value of fast polarization direction is -7.0°±13.7°. As calculating average value of the station's fast direction, we used only one event that is suitable for our criteria mentioned above. Otherwise, unreasonable results get irreversible due to the scatter in distribution of fast polarization directions. The mean value of the delay time is 1.4± 0.5 seconds. Obtained estimated splitting parameters are plotted as a function of back azimuth (BAZ), distance and incidence angle at Figure 3.8. Error bars represent 95% confidence intervals for each of the lag time estimates. Although the azimuthal coverage for ANTB station was not good, it is obviously seen that consistent variations are observed as a function of incidence angle with the lag time increasing at this station (Figure 3.8).

Table 3.2. ANTB splitting Measurements

EVENT ID	Δ (deg)	BAZ (deg)	Φ (deg)	δt (sec)	QUALITY
0516319 26	104.88	209.23	-7	1.4	Good
0516422 44	109.23	259.19	-2	1.8	Good
0516610 13	18.51	73.01	19	0.0	Good
0524612 38	93.27	204.37	73	1.2	Good
0525104 10	94.04	86.015	46	1.7	Good

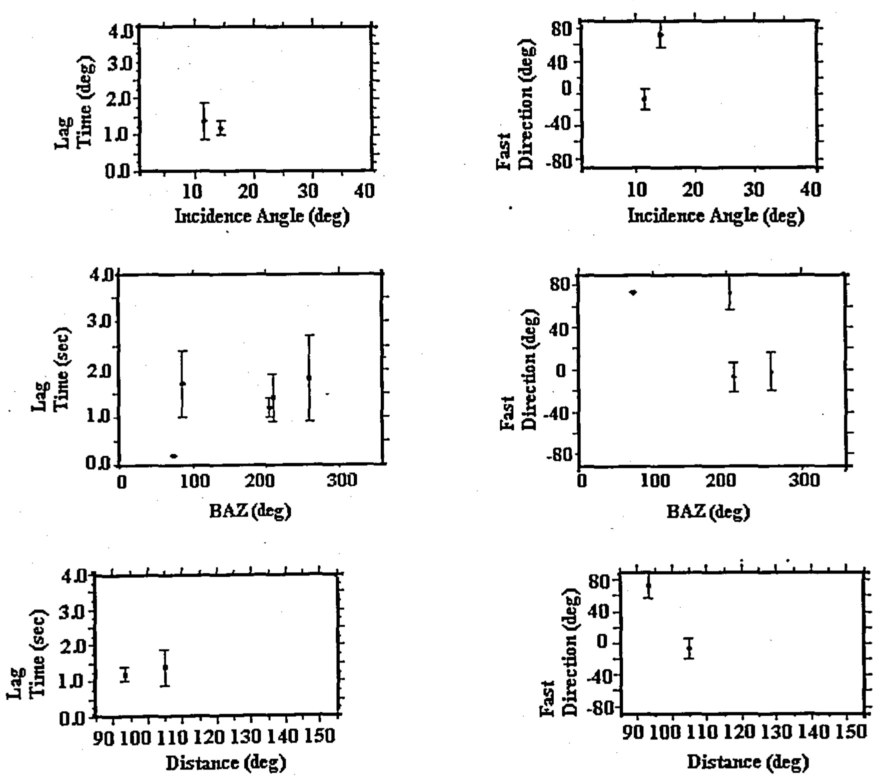

Figure 3.8 A) Splitting versus BAZ (Back azimuth), **B)** Splitting versus distance (deg), **C)** Splitting versus the Moho incidence angle. Error bars represent 95% confidence intervals for each of the lag time estimates.

BALB

The results of splitting parameters at BALB indicate a perfect consistent fast polarization directions oriented around NE-SW for the events with a back azimuth range between 54°- 282° (Table 3.3). The mean value of consistent fast polarization directions is 19.1°± 23.2°. The mean value of the delay time is 1.4 ± 0.6 seconds. Weighted means of the shear wave splitting parameters are calculated with eleven events that are suitable for our criteria. Estimated splitting parameters are plotted according to back azimuth (BAZ), distance and incidence angle in Figure 3.9. Figure 3.10 and Figure 3.11 show that transverse energy is minimized on the Transverse component in order to find splitting parameters for SKS or SKKS phase. In addition, the event 051642244 is a good example for understanding how corrected and uncorrected radial components are related to corrected and uncorrected transverse components in Figure 3.9. The event 051642244 may also be shown as a good splitting at BALB station (Φ= 25±17.27°, δt=1.25± 0.59 sec). In addition, this event 050611042 may be shown as a good null at BALB station (Φ= 82° ±27.12,δt=3.0± 3.4 sec at Figure 3.11). Error bars in Figure 3.9 represent 95% confidence intervals for each of the lag time estimates. The azimuthal coverage for BALB station was better than ANTB station, whereas inconsistent variations are observed as a function of incidence angle with the lag time increament at BALB station (Figure 3.9).

Table 3.3. BALB Splitting Measurements.

EVENT ID	Δ (deg)	BAZ (deg)	Φ (deg)	δt (sec)	QUALITY
01261 02 19	102.33	8 9.55	9.0	2.1	Good
01261 02 19	102.33	89.55	42.0	0.0	Good
01265 03 23	98.15	281.87	81.0	0.0	Good
02214 2311	86.19	54.78	10.0	1.1	Good
02214 2311	86.19	54.78	89.0	2.4	Good
03117 22 57	102.46	269.66	29.0	1.3	Good
03125 15 50	97.16	83.78	6.0	2.2	Good
03134 07 40	87.04	102.90	66.0	0.0	Good
03134 0740	87.04	102.90	-55.0	0.0	Good
03146 23 13	90.21	81.12	-58.0	1.6	Good
03208 11 41	104.84	256.09	26.0	1.5	Good
03315 18 48	93.81	56.98	10.0	1.2	Good
04028 22 15	99.32	86.33	28.0	0.8	Good
04 036210 5	105.88	81.39	18.0	1.2	Good
04108 15 58	102.72	89.02	-81.0	0.0	Good
04114 01 50	99.70	94.10	87.0	0.0	Good

04182 23 37	94.78	85.02	-70.0	1.8	Good
05061 10 42	103.41	87.37	-12.0	0.0	Good
05 06110 42	103.41	87.37	82.0	0.0	Good
05078 17 34	150.70	60.96	-2.0	1.4	Good
05080 12 43	106.34	251.33	20.0	2.2	Good
05096 10 46	117.57	245.68	69.0	0.0	Good
05138 09 10	106.30	208.22	20.0	0.0	Good
05163 19 26	106.22	208.41	24.0	0.0	Good
05164 22 44	107.62	258.52	32.0	1.4	Good
05164 22 44	107.62	258.52	25.0	1.2	Good

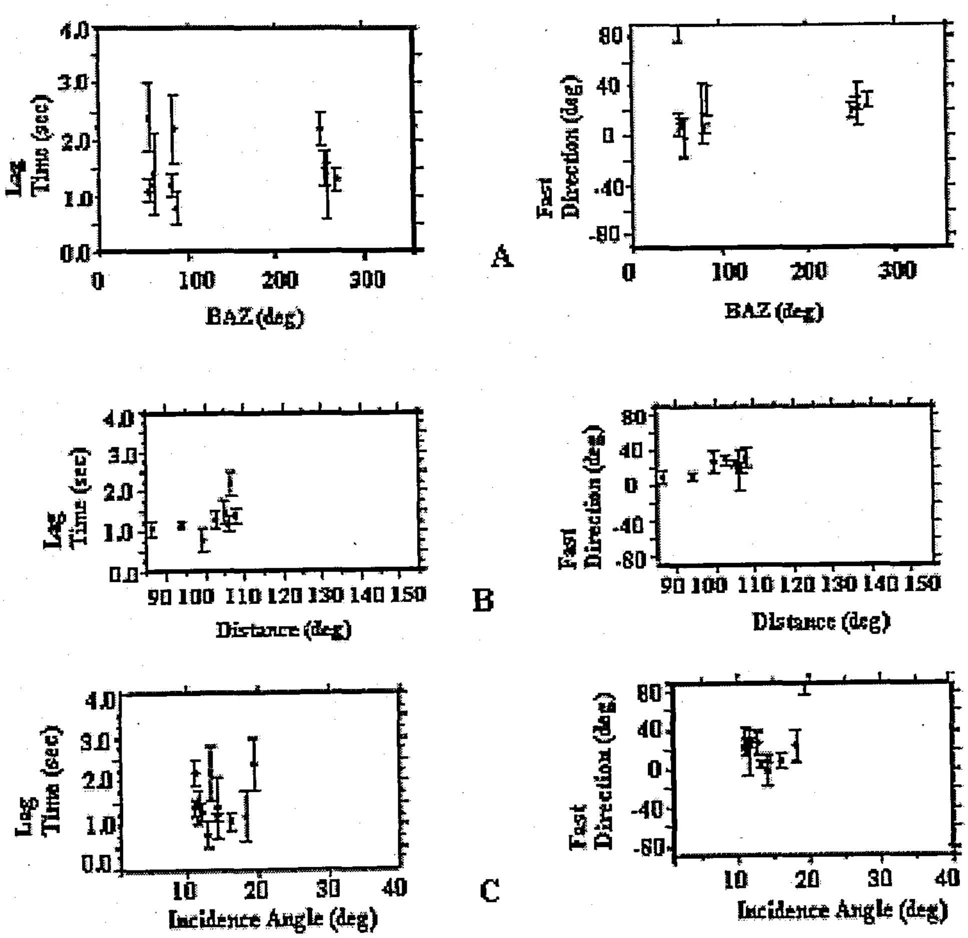

Figure.3.9. Same of the fig.3.8 but for BALB station

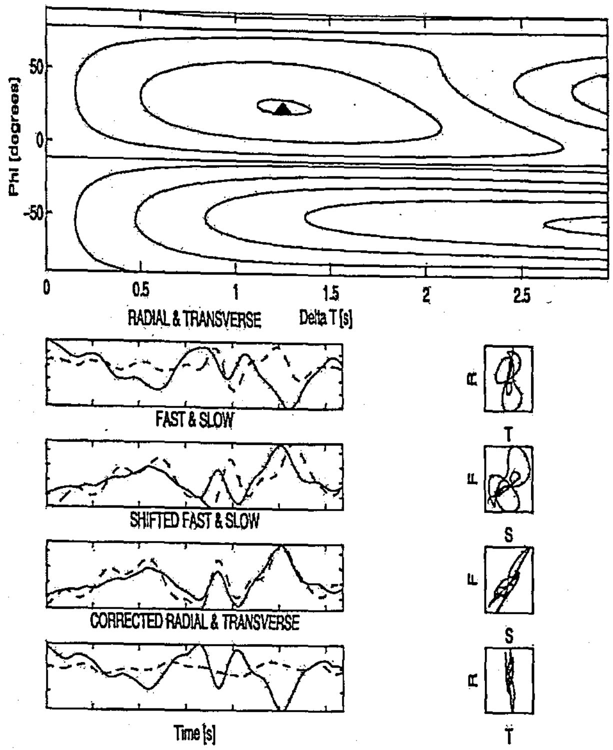

Figure 3.10 This 051642244 event may be shown as a good splitting at BALB station (Φ= 25±17.27°, δt=1.25± 0.59sec).

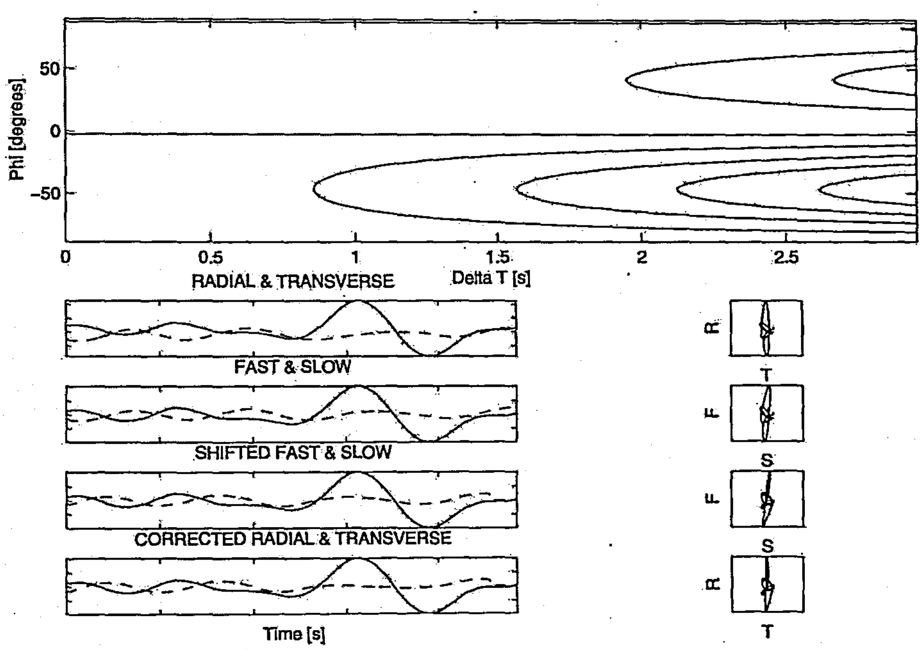

Figure 3.11 This 050611042 event may be shown as a good null at BALB station (Φ= 82° ±27.12, δt=3.0± 3.4sec)

SVSB

Estimated splitting parameters for SVSB station indicate fast polarization directions oriented around purely NE-SW for the events with a back azimuth range between 94°-100° (Table 3.4). The weighted means value of fast polarization directions is 38° ± 3.2°. The mean value of the delay time is 0.8 ± 0.01 seconds. Weighted means of splitting parameters are calculated with all events because they are consistent with each other due to lack of scatter in distribution of parameters. In general, there is very little variation in the fast polarization directions with either ray parameter or BAZ, however, fairly consistent vatiations in lag time with azimuth and incidence angle could be observed. These parameters are plotted as a function of Back azimuth (BAZ), distance and incidence angle at Figure 3.12 in order. Error bars represent 95% confidence intervals for each of the lag time estimates.

Table 3.4. SVSB Splitting Measurements

EVENT ID	Δ (deg)	BAZ (deg)	Φ(deg)	δt (sec)	QUALITY
032400638	93.92	96.20	41.0	0.80	Good
0410815 58	95.71	94.76	36.0	0.90	Good
041140150	92.77	99.80	38.0	0.80	Good
041140150	92.77	99.80	25.0	0.00	Good
052472358	85.08	90.21	42.0	0.80	Good

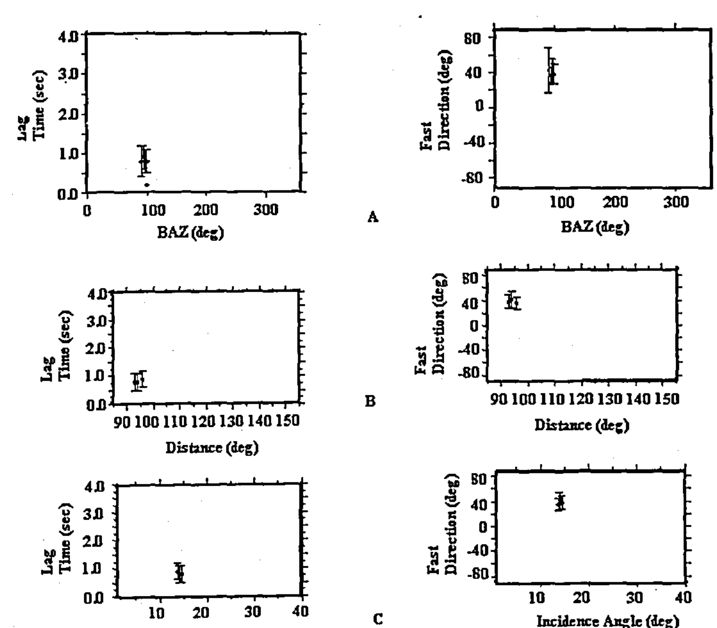

Figure 3.12 A) Splitting versus BAZ (Back azimuth), **B)** Splitting versus distance (deg), **C)** Splitting versus the Moho incidence angle. Error bars represent 95% confidence intervals for each of the lag time estimates.

In summary, taking into account obtained splitting parameters at the used broadband stations, they presents the results of the first detailed measure of seismic polarization anisotropy beneath these stations in Turkey (Figure 3.13). The weighted means of the shear wave splitting parameters for each station are shown in Table 3.5. We have included fast directions with errors less than 20° or delay times less than 0.5 seconds. Our results in the western Anatolia have a N-S fast direction. A part of our results involved BLCB, BODT, DALT, MLSB and FETY stations in which the average value of fast polarization directions is 2.4° ± 13.3° and of the lag time is 1.4 ± 0.25 sec. ISP and ANTB stations have an obvious N-S fast direction that is compatible with the results of mentioned stations above in the Aegean region. This uniformity could be related to present tectonic evolution of these regions. In other words, it is well known that northward subduction of the African plate beneath western Turkey causes extension of the continental crust in the Aegean region.

The stations in the central and eastern part of the Anatolia have a clear NE-SW fast direction and lag time that are similar to the results obtained from temporary broadband stations overall the Anatolian plate (Sandvol, 2003). MALT station suggested that fast direction is more N-S than other stations in the eastern Turkey. On the other hand, the resulting splitting estimates at VANB and CLDR show that fast direction more E-W than NE-SW with respect to another stations in the eastern Turkey.

Seismic anisotropy beneath BR131, and SVSB stations in the central Anatolia has NE-SW fast direction and lag time similar to this observed from ANTO station within the Anatolian plate (Vinnik, 1992). The variations in shear wave splitting lag times with incidence angle could indicate a purely horizontal symmetry axis for stations ANTB, CLDR, DALT, FETY, HDMB, URFA where more steeply incident waves will have smaller lag times rather than rapid lateral variations in the thickness and or strength of the anisotropic fabric. The variations in lag times decrease with increasing incidence angle. This is consistent with an inclined symmetry axis for these stations including BALB, BLCB, BR131, CORM, ISKB, ISP, MALT, and SVSB. These variations could not obviously be observed at EDRB. It has also high value of the delay time with respect to another stations in its vicinity. The results at these stations also show nearly N-S fast direction. The fast polarization directions could not lead to relatively uniformity in the Marmara region because this is located near to the stable Eurasia plate with respect to the active Anatolia plate. Simple average splitting parameters for each station are used to interpret with tectonic structure of Turkey and discuss previous studies in following chapter 4.

Table 3.5 Measurements

Station name	Number of investigated&useful events	Mean ValueΦ±ΔΦ (deg)	Mean Value δt±Δδ (sec)
ANTB	5/1	-7.0°± 13.7	1.4± 0.5
BALB	21/11	19.1°±23.2	1.56 ± 0.26
BLCB	7/2	14.1°±12.7	1.6±0.1
BR131	14/6	-6.5°±7	1.4±0.16
CANB	4/1	30.0°±13.0	1.2±0.2
CORM	9/2	40.2°±0.8	0.7±0.1
EDRB	25	23° ± 18.4	1.75 ± 0.5
DALT	11/4	3° ±5.9	1.8±0.9
FETY	8/5	−32° ± 24	1.1 ± 0.5
HDMB	7/2	65.0°± 19.7	1.3±0.2
ISKB	36/17	37.0± 16.9	1.2±0.3
ISP	117/50	3° ± 9.2	1.8 ± 0.15
KVTB	3/1	25±0.4	3.04±0.4
MALT	26/7	26.8± 12.3	0.9±0.4
MLSB	13/2	22.0°±2.0	1.5± 0.3
PTKB	6/4	26.1°±0.7	3.0±0.2
SVSK	4/4	36.4° ± 8.4	0.8 ± 0.1
URFA	7/4	19.6°± 4.7	1.2±0.2
VANB	15/2	64.9°± 2.6	1.4±0.2

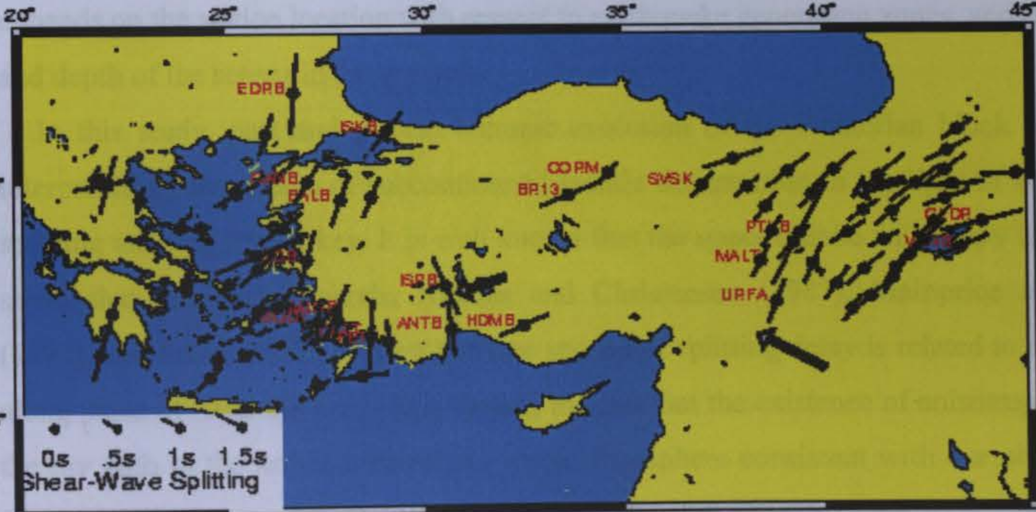

Figure 3.13 Shear Wave Splitting map for Turkey (red points show stations used in this study)

4. DISCUSSION AND CONCLUSION

In this study, we tried to get data from almost all of broadband stations in Turkey. However, we could not observe SKS and SKKS phases at some stations such as CUKT station. There are some causes that are responsible for these kinds of problems. Firstly, CUKT, DATB, MERS, KARA, KOZT, KRTS, SIRT,and SEMD stations etc. were installed approximately 3 or 4 months ago. Especially, it is well known that recording times is very crucial for the analysis of teleseimic shear wave splitting. Indeed, new installed stations could thus not produce sufficient data. Also, signal to noise ratio is too low at some stations such as KVTB station. In other words, it is very difficult to distinguis signal from noise for these stations. Another reason is that signal does not contain an adequate frequency bandwidth to calculate the error bars, perhaps due to large earthquake source dimensions, attenuation along the raypath, and or intracrustal scattering. Almost all of the investigated earthquakes have occured in the south America and the Tonga and Fuji Islands. Recording times to get events (earthquakes) of practical use depend on the environment the seismic station is deployed in. The earthquakes used in the study from Tonga and Fuji Islands have some problems because noise is too high there. For this reason sufficent data could not available for these azimuts. For teleseismic splitting studies, it also depends on the station location with respect to earthquake generation zones, and the quality and depth of the sensor in the ground.

In this study, past and present tectonic evolution of the Anatolian block have been interpreted by the means of subcontinental mantle deformation in the light of shear wave splitting analysis for Turkey. It is well known that the upper mantle anisotropy is based on strain that reorients minerals. Nicolas and Christensen (1987), Mainprice and Silver (1993), and Silver (1996) suggest that one second of splitting delay is related to anisotropy along paths of ~100 km long. This finding implies that the existence of anisotropy through the ray path in the asthenosphere and whole lithosphere consistent with our observations for the Aegean part of Turkey. Fast directions at these stations in the Aegean region are oriented more North-South (N-S) than Northeast-Southwest (NE-SW). For this reason, it can be said that the fast direction in the Aegean region could be also consistent with the extension direction of the lithospheric part of it and its surface deformation seems to be parallel to this. The lateral motion of the lithosphere over a mantle lid could cause upper mantle seismic anisotropy and crustal thinning due to the present-day internal deformation. Moreover, the active thinning of the crust and lateral deformations under lithosphere could cause high heat flow as suggested by Cermák (1978) and İlkışık (1995) in the Aegean extensional region. In other words, this is probably not related to the frozen structure in the upper mantle but related to young internal tectonic activity. In this study, the results are also compatible with the previous studies of Kempler and Ben-Avraham (1987), Le Pichon, et al. (1995), Cianetti, et al. (2001) and Hatzfeld (2001) and beneficial for investigating the deep tectonic structure of the Aegean region. As a summary, this technique gives a crucial opportunity to compare crustal deformation with mantle deformation. In the Aegean region at some areas (eg., BLCB station) variations in spliting paramenters are observed. In this case of this, these variations may depend on the back azimuths that are associated with double anisotropic layers (Silver and Savage, 1994). It is well known that the local thermal activities that are common in the region may cause additional anisotropic layer effect. The double anisotropic layers could also be result from complex lateral deformational interactions between the retreating slab, astenosphere and overriding litosphere. The extensional system in the Aegean region cause supracrustal layer detachment and slide in the extensional direction (Meulenkamp et al., 1988). Most likely, double anisotropic layers implay detached layers in the Aegean region.

Obtained values at ISP station are very satisfying to interpret mantle flow with tectonic activities result in deformation. This internal deformation could be active and intensive based on the subducted slab of oceanic part of the African plate beneath Aegean region. The ISP station is located in so-called Isparta Angle (IA) area where the Hellenic and Cyprian arcs intersect. Extension in the Aegean region is normal to the consumption boundary, whereas there is no extension related to the Cyprian arc (McKenzie, 1978). In case of the southern Aegean region and especially along the subduction boundary, the horizontal anisotropy could have disappeared due to the subduction of the African plate whereas in the northern Aegean, retreat of the subduction zone could continue towards the IA that results in seismic anisotropy. Therefore, fast polarization direction at the ISP station is more N-S oriented than NE-SW at the HDMB station. Also, retreat of the subducted slab could result in complex asthenospheric flow. This situation could create two-layer anisotropy beneath ISP region (Sapaş et al., 2003).

In the western Anatolia, our observations have fundamentally N-S fast direction and lag time that are consistent with results of Hatzfeld (2001). However, the stations in the central and eastern part of the Anatolia have a clear NE-SW fast direction and lag time that are similar to the results obtained from temporary broadband stations of the eastern Turkey Seismic Experiment project within the Anatolian plate (Sandvol, 2003). These observations indicate that the anisotropic fabric may be relatively uniform throughout the upper mantle beneath the Anatolian plate. Previous Pn tomography (Al-Lazki, 2003) and anisotropy (Hatzfeld, 2001), regional wave attenuation of Sn (Gok, 2003) and S wave velocity structure studies (Pearce et al., 1989; Yılmaz, 1993; Al-Lazki et al., 2003) suggest higher average mantle temperatures beneath the eastern part of the Anatolia plate with respect to the rest. This can be interpreted as the presence of asthenospheric material at subcrustal depths resulting from delamination of the mantle lithosphere and/or slab break-off (Sengor, 2003; Keskin, 2003). Assuming 4% upper mantle anisotropy, a 1 sec lag time correspond to a layer of highly oriented pyrolite approximately 120 km thick (Christensen, 1984). This approach is an evidence of the measured anisotropy due to asthenosphere. P-wave tomography of the mantle under the Alpine-Mediterranean area shows that the slab beneath the Bitlis collisional belt is not continuous. Thus, a possible rupture pursues to the west at least up to Cyprus and possibly up to the eastern end of Hellenic arc (Faccenna, 2006). Unless exceptionally high anisotropy exists in the thinned lithosphere, the main contribution to observed delay times (more than 1 sec) must be asthenospheric. In this case, the observed anisotropy have also asthenospheric origin according to the results of this study.

In the southeast Anatolia, our results at URFA station have more N-S fast direction than the NE-SW fast direction. This finding is consistent with the result of MALT station (Sandvol, 2003). This is consistent with the fast directions for events that have a back-azimuth (BAZ) of 270° for stations near the EAF, due to lateral variations in the seismic anisotropy beneath the Anatolian block and the Arabian plate (Sandvol, 2003).

Obtained results for the central Anatolia show that relatively uniform anisotropic fabric could be observed throughout the upper mantle below the Anatolian block because of lattice preferred orientation of olivine minerals (LPO) that develop asthenospheric part of the plate. In the Thrace region, EDRB station has high delay times with respect to other stations in its vicinity. Its results also show nearly N-S fast direction. This station are located in the northern part of the North Anatolian Fault Zone (NAFZ) that follows preexisting suture zones. It is well known that geologic structure of the Anatolian plate is very different from the Eurasian plate. There is a tendency for continental lithosphere to move around the Black Sea. This motion is accommodated by the striking velocity change across the NAFZ and the tendency for motions to turn towards the east around the eastern side of the Black Sea (McClusky et al., 2000). Also, oceanic lithosphere underlying the Black Sea is fundamentally stronger than the continental lithosphere to the south and hence represents a "backstop" resisting deformation and deflecting the impinging continental lithosphere. In summary, the Eurasian plate is not similar to the Anatolian block in terms of internal deformation and inexistence of neotectonic activities. Therefore, the differences in the results of EDRB station could be explained by frozen anisotropy that is related to past deformation .

REFERENCES

Al-Lazki, A., D. Seber,E. Sandvol, N. Turkelli, R. Mohamad, and M. Barazangi Tomographic Pn velocity and anisotropy structure beneath the Anatolian plateau (eastern Turkey) and the surrounding regions. Geophysical Research Letters 30(24), 2003.

Anderson, D. L., Elastic wave propagation in layered anisotropic media, J. geophys. Res., 66, 2953–2963, 1961.

Ando, M., Y. Ishikawa,. and F.Yamazaki, Shear wave polarization anisotropy in the upper mantle beneath Honshu, Japan. Journal of Geophysical Research 88(B7), 1983.

Ansel, V. and H. Nataf,. Anisotropy beneath 9 stations of the geoscope broadband network as deduced from shear-wave splitting. Geophysical Research Letters 16(5), 1989.

Aubouin, J., M. Bonneau, J. Davidson, J. Leboulanger, P., MATESCO, S. zamberakis-A. Lekkas, Escquisse structurale de lÕarc "g"en externe: des Dinarides aux Taurides. Bulletin de la Soci"t" g"ologique de France28, 327-336, 1976.

Babuska, V. & M., Cara, Seismic Anisotropy in th Earth, Kluwer Academic Publishers, Dordrecht, 1991.

Barruol, G. And H. Kern, Seismic anisotropy and shear-wave splitting in lower-crustal and upper-mantle rocks from the Ivrea Zone - experimental and calculated data: Phys. Earth Planet. Inter., 96, 175-194, 1996.

Barruol, G. and D. Mainprice, A quantitative evaluation of the contribution of crustal rocks to the shear-wave splitting of teleseismic SKS waves: Phys. Earth Planet. Inter., 78, 281-300, 1993.

Bates, D. M. and D. G. Watts, Nonlinear regression analysis and its applications, Wiley, NY, 1988.

Ben-Menahem, A., and S. J. Singh, Seismic waves and sources, Springer-Verlag Inc., New York, 1981.

Ben Ismail, W. & D. Mainprice, An olivine fabric database: an overview of upper mantle fabrics and seismic anisotropy. Tectonophysics 296, 145–158, 1998.

Bowman, J. R. and M. Ando, Shear-wave splitting in the upper-mantle wedge above the Tonga subduction zone, Geophys. J. R. Astron. Soc., 88, 25–41, 1987.

Cermák, V. Heat Flow Map of Europe (1:5.0 Mio)., Nath. Comm. Geodesy Geophys. Potsdons, 1978.

Christoffel, E. B., Uber die Fortpflanzung von Stossen durch elastische feste Korper, Ann. Mater.,8, 193-243, 1877.

Cianetti, S., P. Gasperini, C. Giunchi, and E. Boschi, Numerical modeling of the Aegean-Anatolian region: geodynamical constraints from observed rheological heterogeneities, Geophys. J. Int., *146*, 760–780, 2001.

Crampin, S., Seismic-waves propagating through a cracked solid: polarization as a possible dilatancy diagnostic. Geophys J. R. Astr. Soc., 53, 467-496, 1978.

Crampin, S., and R. McGonigle, The variation of delays in stress-induced anisotropic polarization anomalies, Geophys. J. R. Astron. Soc., *64*, 115–131, 1981.

Crampin, S., D. C. Booth, R. Evans, S. Peacock, and J.B. Fletcher, Changes in shear-wave splitting at Anza near the time of the North Palm Springs earthquake: J. Geophys. Res. 95, 11,197-l 1,212., 1990.

Crampin, S., Arguments for EDA. Can. J. Expl. Geophys., 29, 3-17, 1993.

Christensen, N.I., The magnitude, symmetry and origin of upper mantle anisotropy based on fabric analyses of ultramafic tectonites. Geophys. J. R. Astron. Soc. 76, 89–111, 1984.

Efron, B. and R. Tibshirani, `Statistical analsysis in the computer age', Science, 1991.

Eaton, D., A. Frederiksen, and S. Y. Miong, Shear-wave splitting observations in the lower Great Lakes region: Evidence for regional anisotropic domains and keel-modified asthenospheric flow. Submitted to Geophy. Res. Letters, January 7, 2004

Faccenna C., O. Bellier , J. Martinod ,C. Piromallo and V. Regard, Slab detachment beneath eastern Anatolia: A possible cause for the formation of the North Anatolian fault Earth and Planetary Science Letters 242 85– 97 , 2006.

Forsyth, D. W., The early structural evolution and anisotropy of the oceanic upper mantle, Geophys. J. Roy. Astr. Soc. 43:103-62, 1975.

Gamar, F. and P. Bernard, Shear wave anisotropy in the Erzincan basin and its relationship with crustal strain. J. Geophys. Res., 102, 20373-20393, 1997.

Gok, R., E. Sandvol, N. Turkelli, D. Seber, and M. Barazangi, Sn Attenuation in the Anatolian and Iranian Plateaus and Surrounding Regions, Geophysical Research Letters, 30, 8042, 2003.

Hales A. L. and J. L. Roberst, The travel times of S and SKS Bulletin of the Seismological Society of America, 60, 461-489,1970.

Hatzfeld, D. et al., Shear wave anisotropy in the upper mantle beneath the Aegean related internal deformation,. J. Geophys. Res., 106, 30 737-30 754, 2001.

Hess, H. H., Seismic anisotropy of the uppermost mantle under oceans, Nature, 203, 629-631, 1964.

İlkışık, O. M., Ege Bölgesi nde Yerkabuğunun Jeotermik Yapısı., Unpublished Report, 1995.

Jackson, J.A. and D. P. McKenzi, The relation between plate motions and seismic moment tensors, and the rates of active deformation in the Mediterranean and the Middle East, Geophys. J. R. Astr. Soc. 93, 45–73, 1988.

Jacobshagen, V., Geologie von Griechenland: Berlin-Stuttgart, Borntraeger, 279 p, 1986.

Jenkins and Watts, Spectral Analysis and Its Applications, Holden-Day, 1968.

Jung, H. And S Karato, Water-induced fabric transitions in olivine, Science, 293: 1460-1463, 2001.

Jung, H. And S. Karato, Effects of water on the size of dynamically recrystallized grains of olivine, *J. Struct. Geol.* , 23: 1337-1344, 2001.

Kaneshima, S., Origin of crustal anisotropy: Shear wave splitting studies in Japan. J. Geophys. Res., 95, 11121-11133, 1990.

Karato, S., M. Toriumi, T. Fujii, Dynamic recrystallization of olivine single crystals during high-temperature creep, Geophysical Research Letters 7, 649±652, 1980.

Karato, S. I., and P. Wu, Rheology of the upper mantle; a synthesis, Science, 260, 771–778, 1993.

Karato, S. I., The Dynamic Structure of the Deep Earth, An interdisciplinary approach, Princeton University press, 2003.

Kelvin, Lord (W. Thomson), Baltimore Lectures, Cambridge Univ. Press New York, 1904.

Kempler, D., and Z. Ben-Avraham, The tectonic evolution of the Cyprean Arc. Ann. Tecton., 1:58–71, 1987.

Kennett, B. L. N., and E. R. Engdahl, Traveltimes for global earthquake location and phase identification, Geophys. J. Int., 105, 429-465, 1991.

Keskin, M., J. A. Pearce, and J.G. Mitchell, Volcano-stratigraphy and geochemistry of collisionrelated volcanism on the Erzurum-Kars Plateau, North Eastern Turkey, Journal of Volcanology and Geothermal Research, 85/1-4, 355-404, 1998.

Kind, R., G. L. Kosarev, L. I. Makeyeva, and L. P. Vinnik, Observations of laterally inhomogenous anisotropy in the continental lithosphere, Nature, 318, 358-361, 1985.

Kreemer, C., N. Chamot-Rooke, and X. Le Pichon, Constraints on the evolution and vertical coherency of deformation in the Northern Aegean from a comparison of geodetic, geologic, and seismologic data, Earth and Planetary Science Letters, 225, 329-346, 2004.

Kubo,A.,Y. Hiramatsu, M. Kanao, M. Ando, T. Terashima, An Analysis of the SKS Splitting at Syowa Station in Antarctica,Proceedings of the NIPR Symposium on Antarctic Geosciences, ,8,25-34,National Institute of Polar Research Tokyo, 1995.

Le Pichon, X., N. Chamot-Rooke, S. Lallemant, R. Noomen, and G. Veis,Geodetic determination of the kinematics of central Greece with respect to Europe: Implications for eastern Mediterranean tectonics, J. Geophys. Res, 100, 12,675-12,690, 1995.

Love, A. E. H., A treatise on the mathematical Theory of Elasticity 4 th edition, Dover pub. New York, 1944.

Mainprice, D., and P. Silver, Interpretation of SKS-waves using samples from the subcontinental lithosphere: Physics of the Earth and Planetary Interiors, v. 78, p. 257–280, 1993.

Mainprice, D. and M. Humbert, Methods of calculating petrophysical properties from lattice preferred orientation data, Surv. Geophys., **15,** 575–592, 1994.

Meulenkamp, J. E., Wortel, M. J. R., Van Wamel, W. A., Spakman, W. & Hoogerduyn Strating, E., 1988. On the Hellenic Subduction Zone and the Geodynamic Evolution of Crete since the Late Middle Miocene., Tectonophysics, 146, 203-215.

McClusky et al., GPS constraints on plate kinematics and dynamics in the eastern Mediterranean and Caucasus, J. Geophys. Res. 105., 5695-5719, 2000.

McKenzie, D., Active tectonics of the Mediterranean, Geophys. J. R. Astr. Soc., 30 (2), 109-185, 1972.

McKenzie, D.P., Active tectonics of the Alpine-Himalayan belt: The Aegean Sea and surrounding regions, Geophys. J. R. Astron. Soc., *55*, 217-254, 1978.

Menke, W. and V. Levin, A waveform-based method for interpreting SKS splitting observations, with application to one and two layer anisotropic Earth models, GJI, 154,379-392, 2003.

Musgrave, M. J. P.,The Propagation of Elastic Waves in Crystals and Other Anisotropic Media", Reports on Progress in Physics 22, 74-96, 1959.

Nicolas, A., Principles of Rock Deformation, 208 pp., D. Reidel, Norwell, Mass., 1984.

Nicolas, A., and N. I., Christensen, Formation of anisotropy in upper mantle peridotites: A review, *in* Fuchs, K., and Froidevaux, C., eds., Composition, structure and dynamics of the lithosphere/asthenosphere system: Washington, D.C., American Geophysical Union, p. 111–123, 1987.

Nuttli O., The effect of the Earth surface on the S wave particle motion. Bull Seis. Soc. Am. 51, 237-246, 1961.

Ozalaybey, S., and M. K. Savage, Double-layer anisotropy resolved from S phases, Geophys. J. Int., 117, 653-664, 1994.

Papoulis, A., Probability, Random Variables, and Stochastic Processes. McGraw-Hill Book Company, NY, USA, 1991.

Peacock, S., S. Crampin, D.C. Booth, and J.B. Fletche, Shear-wave splitting in the Anza seismic gap, Southern California: temporal variations as possible precursors, *J. geophys. Res.*, 93, 3339–3356, 1988.

Pearce, J. A., J. F. Bender, S. E. De Long , W. S. F. Kidd, P. J. Low , Y. Güner, F Saroglu, Y. Yilmaz, S. Moorbath , and J. G. Mitchell, Genesisof collision volcanism in Eastern Anatolia, Turkey, J. Volcanology and Geothermal Research, 44, 189-229, 1990.

Peng, Z. and Y. Ben-Zion Spatio-temporal variations of crustal anisotropy from similar events in aftershocks of the 1999 M7.4 Izmit and M7.1 Duzce, Turkey, earthquake sequences, Geophys. J. Int. ,160(3), 1027-1043, 2005.

Royden, L., The tectonic expression of slab pull at continental convergent boundaries: Tectonics, v. 12, p. 303–325, 1993.

Ryberg, T., G. Rümpker, C. Haberland, D.Stromeyer, and M. Weber, Simultaneous inversion of shear wave splitting observations from seismic arrays, Journal of Geophysical Research, 110, B3, 2005.

Sandvol, E., and T. Hearn, Bootstrapping Shear-Wave Splitting Errors, Bulletin of the Seismological Soc. of America, 84, 1971– 1977, 1994.

Sandvol, E., N. Turkelli, E. Zor, R. Gok, T. Bekler, C. Gurbuz, D. Seber, and M. Barazangi, Shear wave splitting in a young continent-continent collision: An example from Eastern Turkey: Geophysical Research Letters, v. 30, p. 4-1 - 4-4, 2003.

Sapaş A. S. Yolsal, A. B. Güney, Invetigation of SKS splitting in the upper mantle beneath the Isparta region, International workshop on the North Anatolian, East Anatolian and Dead Fault sytems: recent progressin tectonics and Paleoseismology and field training course in paleoseismology 31 Agust to 12 september, 2003 METU Ankara,Turkey, Abstracts of oral and Posters presentations , p. 144.

Savage, M.K., Peppin, W.A. and Vetter, U.R., Shear wave anisotropy and stress direction in and near Long Valley Caldera, California, 1979--1988. Journal of Geophysical Research 95(B7), 1990.

Savage, M.K., Seismic anisotropy and mantle deformation: What have we learned from shear wave splitting?, Rev. Geophys., 37, 65-106, 1999.

Sengor, A.M.C., S. Ozeren, T. Genc, and E. Zor, East Anatolian high plateau as a mantle-supported, north-south shortened domal structure, Geophys. Res. Lett., 30, 2003.

Shih, X. R., R. P. Meyer, R. P. & J.F. Schneider, J. F., An automated, analytic method to determine shear wave anisotropy, Tectonophysics, 165, 271-278, 1989

Silver, P. G., and W. W. Chan, Implications for continental structure and evolution from seismic anisotropy, Nature, *335*, 34-39, 1988.

Silver, P.G. and W.W. Chan, Shear wave splitting and subcontinental mantle deformation, J. Geophys. Res., 96, 16429-16454, 1991.

Silver, P.G. and M. K. Savage, The interpretation of shear wave splitting parameters in the presence of two anisotropic layers, Geophys .J. Int., 119, 949-963, 1994.

Silver, P. G., Seismic anisotropy beneath the continents: Probing the depths of geology, Ann. Rev. Earth and Planet. Sci., 24, *385-432*, 1996.

Smith, M. L. and F. A. Dahlen, The azimuthal dependence of Love and Rayleigh wave propagation in a slightly anisotropic medium, J. Geophys. Res., 78, 3321-3333, 1973.

Sonder, L., and England, P., Effects of temperature dependent rheology on large scale continental extension: Journal of Geophysical Research, v. 94, p. 7603–7619, 1989.

Tichelaar, B. W., and L. R. Ruff, How good are our best models?, EOS, 70, 593-606, 1989.

Tod, S.R., The effects on seismic waves of interconnected nearly aligned cracks, Geophys. J. Int., 146, 249–263, 2001.

Udias, A.Principles of Seismology ,Cambridge University Press 1999

Vinnik, L. P., G. L. Kosarev, and L. I. Makeyeva, Anisotropy of the lithosphere from the observations of SKS and SKKS, Proc, Acad. Sci., USSR, 278, 1335-1339, 1984.

Vinnik, L. P., V. Farra, and B. Romanowicz, Azimuthal anisotropy in the Earth from observations of SKS at Geoscope and NARS broadband stations, Bull. Seismol. Soc. Am., *79,* 1542-1558, 1989.

Vinnik LP, Makeyeva LI, Milev A, Usenko Y, Global Patterns of azimuthal anisotropy and deformation in the continental mantle, Geophys. J. Int., 111, 433-447, 1992.

Walker, K.T., G.H.R Bokelmann, S. L. Klemperer, Shear-wave splitting to test mantle deformation models around Hawaii, Geophys. Res. Lett., 28, 4319-4322, & 2003, Reply to Comment by L. P. Vinnik et al., Geophys. Res. Lett., 28, 1676, 2001.

Winterstein, D. F. and M.A. Meadows, Shear-wave polarizations and subsurface stress directions at Lost Hills field: Geophysics, 56, 1331-1348, 1991.

Zatsepin, S.V. and Crampin, S., The metastable poro-reactive and interactive rockmass: anisotropic poro-elasticity. 65th Ann. Int. SEG Meeting. Houston, Expanded Abstracts, 918-921, 1995.

Zatsepin, S. V. and Crampin, S., Modelling the compliance of crustal rock: I - response of shear-wave spiitting to differential stress. Geophysical Journal International, submitted, 1995a.

Zatsepin, S. V. and Crampin, S., Modelling the compliance of in situ rock: a new formulation for the equation of state. 57th EAEG Meeting, Glasgow, 1995b.

Zhang, S., and Karato, S., Lattice preferred orientation of olivine aggregates deformed in simple shear: Nature, v. 375, p. 774–777, 1995.

Zhao, L.; Z. Tianyu, Using shear wave splitting measurements to investigate the upper mantle anisotropy beneath the North China Craton: Distinct variation from east to west Geophys. Res. Lett., Vol. 32, 2005.

APPENDIX A

List of Earthquakes used in this study

EVENT ID	Date	Origin time	Lat.	Lon.	Mag.	Depth (km)	Station
96306 0332	96/11/01	03:32	-1.30	149.52	6.10	33	ISPB
96309 1724	96/11/04	17:24	7.31	-77.39	6.30	14	ISPB
96317 1659	96/11/12	16:59	-14.99	-75.68	7.70	33	ISPB
96319 07 58	96/11/14	07:58	-11.38	166.46	6.00	109	ISPB
96326 07 43	96/11/21	07:43	6.66	126.46	5.90	52	ISPB
96365 1941	96/12/30	19:41	-3.99	128.10	6.20	33	ISPB
97 001 2232	97/01/01	22:32	-0.13	123.82	5.90	115	ISPB
97011 20 28	97/01/11	20:28	18.22	-102.76	7.20	33	ISPB
97 01711 20	97/01/17	11:20	-8.90	123.54	6.20	110	ISPB
97 02302 15	97/01/23	02:15	-22.00	-65.72	7.10	276	ISPB
97 40 12 32	97/02/09	12:32	-14.49	-76.28	6.10	33	ISPB
97123 1646	97/05/03	16:46	-31.79	-179.38	6.90	108	ISPB
97128 1329	97/05/08	13:29	51.72	-170.80	6.00	33	ISPB
97129 0906	97/05/09	09:06	13.20	144.70	6.10	29	ISPB
97142 07 50	97/05/22	07:50	18.68	-101.60	6.50	70	ISPB
97153 2124	97/06/02	21:24	-57.78	-25.47	6.10	33	ISPB
9716821 0 3	97/06/17	21:03	51.35	-179.33	6.60	33	ISPB
97175 230 4	97/06/24	23:04	-1.92	127.90	6.40	33	ISPB
97187 09 54	97/07/06	09:54	-30.06	-71.87	6.80	19	ISPB
97189 02 24	97/07/08	02:24	23.80	142.70	5.80	33	ISPB
97190 1924	97/07/09	19:24	10.60	-63.49	7.00	19	ISPB
97200 1422	97/07/19	14:22	16.33	-98.22	6.90	33	ISPB
97201 1014	97/07/20	10:14	-22.98	-66.30	6.10	256	ISPB
97212 2154	97/07/31	21:54	-6.64	130.92	6.00	58	ISPB
9722209 20	97/08/10	09:20	-16.01	124.33	6.60	10	ISPB
97245 1213	97/09/02	12:13	3.85	-75.75	6.80	198	ISPB
97301 06 15	97/10/28	06:15	-4.37	-76.68	7.20	112	ISPB
97329 1214	97/11/25	12:14	1.24	122.54	7.00	24	ISPB
97332 2253	97/11/28	22:53	-13.74	-68.79	6.70	586	ISPB
97345 07 56	97/12/11	07:56	3.93	-75.79	6.40	177	ISPB
97351 04 38	97/12/17	04:38	51.19	178.87	6.60	20	ISPB
98 00106 11	98/01/01	06:11	23.91	141.91	6.60	95	ISPB
9801004 54	98/01/10	04:54	-12.03	-72.07	6.40	33	ISPB
98 01008 20	98/01/10	08:20	14.37	-91.47	6.60	33	ISPB
9801309 50	98/01/13	09:50	-4.10	129.12	5.90	44	ISPB
98091 22 42	98/04/01	22:42	-40.32	-74.87	6.70	9	ISPB
9809322 01	98/04/03	22:01	-8.15	-74.24	6.60	164	ISPB
98110 2259	98/04/20	22:59	18.52	-101.20	6.00	67	ISPB
9813505 58	98/05/15	05:58	14.18	144.88	6.10	154	ISPB
982101800	98/07/29	18:00	-2.69	138.90	6.10	33	ISPB
98216 1859	98/08/04	18:59	-0.59	-80.39	7.20	33	ISPB
98235 1357	98/08/23	13:57	11.66	-88.04	6.70	54	ISPB
98240 1240	98/08/28	12:40	-0.15	125.02	6.20	66	ISPB
9824201 48	98/08/30	01:48	17.09	148.13	6.30	33	ISPB
9824508 37	98/09/02	08:37	5.41	126.76	6.80	50	ISPB
98246 1737	98/09/03	17:37	-29.45	-71.71	6.60	27	ISPB

9825109 10	98/09/08	09:10	13.26	144.01	6.10	141	ISPB
98264 0652	98/09/21	06:52	0.26	122.47	6.10	147	ISPB
9826501 16	98/09/22	01:16	11.82	143.15	6.00	9	ISPB
98271 1923	98/09/28	19:23	3.84	126.41	6.40	30	ISPB
98281 04 51	98/10/08	04:51	-16.12	-71.40	6.40	136	ISPB
98300 2116	98/10/27	21:16	2.92	128.62	5.90	60	ISPB
98301 1625	98/10/28	16:25	0.84	125.97	7.10	33	ISPB
9831207 25	98/11/08	07:25	-9.14	121.42	6.40	33	ISPB
98333 1410	98/11/29	14:10	-2.07	124.89	8.30	33	ISPB
98350 1745	98/12/16	17:45	1.12	126.18	6.20	33	ISPB
9906008 51	99/03/01	08:51	-2.97	126.53	5.70	33	ISPB
990 6117 45	99/03/02	17:45	-22.72	-68.50	5.90	110	ISPB
99 06400 33	99/03/05	00:33	-20.42	-68.90	5.80	110	ISPB
99079 10 47	99/03/20	10:47	51.59	-177.67	7.00	33	ISPB
99 09306 17	99/04/03	06:17	-16.66	-72.66	6.80	87	ISPB
9909511 08	99/04/05	11:08	-5.59	149.57	7.40	150	ISPB
99127 1413	99/05/07	14:13	56.42	-152.94	6.20	20	ISPB
9913600 51	99/05/16	00:51	-4.75	152.49	7.10	73	ISKB
9915300 23	99/06/02	00:23	0.05	123.48	5.80	161	ISPB
99166 2042	99/06/15	20:42	18.39	-97.44	7.00	70	ISPB, ISKB
99169 1055	99/06/18	10:55	5.51	126.64	6.40	33	ISPB
99172 1743	99/06/21	17:43	18.32	-101.54	6.30	68	ISPB, ISKB
99173 0047	99/06/22	00:47	-4.51	133.95	6.00	33	ISPB
992580301	99/09/15	03:01	-20.93	-67.28	6.40	218	ISPB, ISKB
99273 1631	99/09/30	16:31	16.06	-96.93	7.50	60	ISPB, ISKB
9928307 03	99/10/10	07:03	-1.99	134.28	6.20	33	ISPB
9928601 33	99/10/13	01:33	54.66	-161.19	6.40	30	ISPB
9929102 43	99/10/18	02:43	-56.12	-26.58	6.60	33	ISPB
9929308 28	99/10/20	08:28	-6.94	129.34	5.80	189	ISPB
99322 1427	99/11/18	14:27	0.52	126.07	6.00	33	ISPB
9932503 51	99/11/21	03:51	-21.75	-68.78	6.10	101	ISPB
99334 04 01	99/11/30	04:01	-18.90	-69.17	6.60	128	ISPB
99335 1923	99/12/01	19:23	17.65	-82.36	6.30	10	ISPB
99340 2312	99/12/06	23:12	57.41	-154.49	7.00	66	ISPB
9934709 30	99/12/13	09:30	2.08	127.11	5.90	84	ISPB
9935300 48	99/12/19	00:48	12.87	144.57	6.00	50	ISPB
00057 18 24	00/02/26	18:24	9.41	-78.53	6.10	65	ISPB, ISKB
000 6322 09	00/03/03	22:09	-7.32	128.49	6.40	141	ISPB, ISKB
0007222 21	00/03/12	22:21	14.98	-92.44	6.30	62	ISKB
000881100	00/03/28	11:00	22.34	143.73	7.60	126	ISKB
0009415 20	00/04/03	15:20	4.08	125.61	6.20	150	ISPB
0011409 27	00/04/23	09:27	-28.31	-62.99	7.00	608	ISKB
0011417 01	00/04/23	17:01	-28.38	-62.94	6.10	609	ISKB
00133 18 43	00/05/12	18:43	-23.55	-66.45	7.20	225	ISPB, ISKB
0016617 00	00/06/14	17:00	4.54	127.72	6.30	89	ISKB
0016807 55	00/06/16	07:55	-33.88	-70.09	6.40	120	ISKB
00220 14 33	00/08/07	14:33	-7.02	123.36	6.50	648	ISKB
0022804 30	00/08/15	04:30	-31.51	179.73	6.60	357	ISKB
003010421	00/10/27	04:21	26.27	140.46	6.30	388	ISKB
003530 119	00/12/18	01:19	-21.18	-179.12	6.70	628	ISKB
0035807 13	00/12/23	07:13	-7.87	135.82	6.00	61	MALT
01013 17 33	01/01/13	17:33	13.05	-88.66	7.80	60	ISPB, ISKB
01 04705 59	01/02/16	05:59	-7.16	117.49	6.10	521	ISPB, MALT
01059 18 54	01/02/28	18:54	47.15	-122.73	6.80	51	MALT
01073 18 56	01/03/14	18:56	0.45	121.89	6.00	109	ISPB, ISKB
01118 04 49	01/04/28	04:49	-18.06	-176.94	6.90	351	ISPB
0114505 06	01/05/25	05:06	-7.87	110.18	6.30	143	ISPB

0115402 41	01/06/03	02:41	-29.67	-178.63	7.20		178	ISPB
01180 18 35	01/06/29	18:35	-19.52	-66.25	6.10		273	ISPB, ISKB
01184 13 10	01/07/03	13:10	21.64	142.98	6.50		290	ISPB, ISKB
01186 13 53	01/07/05	13:53	-16.09	-73.99	6.60		62	ISPB, ISKB
0126102 19	01/09/18	02:19	-7.51	127.74	6.00		131	BALB
0126503 23	01/09/22	03:23	3.87	-75.97	6.00		178	ISPB, BALB
01332 14 32	01/11/28	14:32	15.57	-93.11	6.40		84	ISPB, ISKB
01343 18 15	01/12/09	18:15	0.00	122.87	6.10		156	ISPB
02001 11 29	02/01/01	11:29	6.30	125.65	6.30		138	ISPB
02016 23 09	02/01/16	23:09	15.50	-93.13	6.40		80	ISPB, MALT
0207822 14	02/03/19	22:14	-6.49	129.90	6.10		148	ISPB, ISKB
0208704 56	02/03/28	04:56	-21.66	-68.33	6.50		125	ISPB, EDRB, ISKB
02091 19 59	02/04/01	19:59	-29.67	-71.38	6.40		71	ISPB, EDRB
0210816 08	02/04/18	16:08	-27.53	-70.59	6.70		62	EDRB
0211616 06	02/04/26	16:06	13.09	144.62	7.10		85	ISPB, EDRB
02214 2311	02/08/02	23:11	29.28	138.97	6.30		426	BALB
0227619 05	02/10/03	19:05	-7.53	115.66	6.00		315	ISPB
0228520 09	02/10/12	20:09	-8.30	-71.74	6.90		534	ISPB, ISKB, MALT
0231601 46	02/11/12	01:46	-56.55	-27.54	6.20		120	ISPB
0306902 09	03/03/10	02:09	1.69	127.30	6.40		93	ISPB
0311722 57	03/04/27	22:57	-8.19	-71.59	6.00		559	BALB, EDRB
0312515 50	03/05/05	15:50	0.22	127.35	6.40		123	ISPB, BALB, EDRB, ISKB
0313407 40	03/05/14	07:40	-8.06	107.32	6.00		79	BALB
03146 23 13	03/05/26	23:13	6.76	123.71	6.90		565	ISPB, BALB, BR131, EDRB
0317106 19	03/06/20	06:19	-7.61	-71.72	7.10		558	ISPB,BR131,
0318205 52	03/07/01	05:52	4.53	122.51	6.00		635	BR131
0320811 41	03/07/27	11:41	-20.13	-65.18	6.00		345	ISPB, BALB, MALT
0324006 38	03/08/28	06:38	-7.32	126.05	6.00		409	BR131, SVSB
03315 18 48	03/11/11	18:48	22.32	143.25	6.00		101	ISPB, BALB, BR131, EDRB, MALT, MLSB
0402822 15	04/01/28	22:15	-3.12	127.40	6.70		17	BALB, EDRB, MLSB
0403621 05	04/02/05	21:05	-3.62	135.54	7.10		16	BALB, EDRB, MLSB, VANB,HDMB
0403802 42	04/02/07	02:42	-4.00	135.02	7.50		10	EDRB, HDMB, MLSB, VANB
0403908 58	04/02/08	08:58	-3.66	135.34	5.70		32	EDRB, VANB
0407703 21	04/03/17	03:21	-21.12	-65.59	6.10		289	EDRB, ISKB
0410815 58	04/04/17	15:58	-7.35	128.37	6.10		128	BALB,BR131, ISKB, MLSB, SVSB
041140150	04/04/23	01:50	-9.36	122.84	6.70		65	BALB, EDRB, ISKB, MLSB, SVSB
0417702 35	04/06/25	02:35	-6.71	130.38	6.10		70	BR131
0418009 49	04/06/28	09:49	54.80	-134.25	6.80		20	VANB
0418107 01	04/06/29	07:01	10.74	-87.04	6.30		9	MALT, VANB
04182 23 37	04/06/30	23:37	0.80	124.73	6.30		90	ISPB, BALB,EDRB
0420108 01	04/07/19	08:01	49.62	-126.97	6.40		23	EDRB, VANB
0421003 56	04/07/28	03:56	-0.44	133.09	6.50		13	KVTB
04241 13 41	04/08/28	13:41	-35.17	-70.53	6.50		5	EDRB
04250 12 42	04/09/06	12:42	-55.37	-28.98	6.90		10	DALT, EDRB, MALT, MLSB
04251 11 53	04/09/07	11:53	-28.57	-65.84	6.40		22	MALT
0425703 00	04/09/13	03:00	44.00	151.41	6.10		8	DALT

04272 15 29	04/09/28	15:29	-52.51	28.02	6.40	10	EDRB, VANB
04278 19 20	04/10/04	19:20	14.55	146.99	6.00	7	DALT, EDRB, MLSB, VANB
0428022 30	04/10/06	22:30	-0.67	134.43	6.20	10	DALT, VANB
04283 21 26	04/10/09	21:26	11.42	-86.67	7.00	35	DALT, MLSB
04300 22 53	04/10/26	22:53	-57.07	-24.68	6.40	10	MALT
04307 10 02	04/11/02	10:02	49.28	-128.77	6.70	10	EDRB
0430808 31	04/11/03	08:31	14.47	146.84	6.00	10	MALT
0431706 36	04/11/12	06:36	-26.70	-63.32	6.10	568	BLCB, BR131
0432009 06	04/11/15	09:06	4.70	-77.51	7.20	15	BLCB, EDRB,HDMB, MALT , PTKB
0432508 07	04/11/20	08:07	9.60	-84.17	6.40	16	MALT, PTKB
0433102 25	04/11/26	02:25	-3.61	135.40	5.90	10	BLCB, HDMB, MALT, VANB
0433307 36	04/11/28	07:36	-3.64	135.45	6.20	23	MALT
0434815 23	04/12/13	15:23	13.39	-89.37	6.00	62	EDRB, PTKB
0434923 20	04/12/14	23:20	18.96	-81.41	6.80	10	BLCB, EDRB, FETY, HDMB, MALT, PTKB, URFA, VANB
0501620 17	05/01/16	20:17	10.93	140.84	6.70	24	MALT
0501710 50	05/01/17	10:50	10.99	140.68	6.10	12	MALT
0503302 30	05/02/02	02:30	14.08	144.71	6.30	158	CLRB, CORM
0503612 23	05/02/05	12:23	5.29	123.34	7.10	525	BR131, URFA, VANB
0505000 04	05/02/19	00:04	-5.56	122.13	6.50	10	FETY, MALT
0506110 42	05/03/02	10:42	-6.53	129.93	7.10	201	BALB, BR131, CORM, DALT, EDRB, FETY, MLSB, URFA, VANB, BODT
0506319 05	05/03/04	19:05	2.67	126.41	6.10	59	BODT
0507613 37	05/03/17	13:37	15.14	-91.38	6.10	197	CORM
0507817 34	05/03/19	17:34	-21.89	-179.55	6.30	598	BALB, BLCB
0508012 43	05/03/21	12:43	-24.73	-63.51	6.40	570	BALB, ISKB, MLSB
0508515 40	05/03/26	15:40	-4.89	129.94	6.10	10	MALT
0509610 46	05/04/06	10:46					BALB kontrol et
0509915 16	05/04/09	15:16	56.17	-154.52	6.00	14	BODT, MALT
0510117 08	05/04/11	17:08	-21.98	170.61	6.70	68	BR131, CLRB, MALT
0512523 41	05/05/05	23:41	5.08	-82.41	5.90	10	ANTB
0513809 10	05/05/18	09:10	-56.41	-26.86	6.00	102	BALB,CORM, FETY, BODT, CANB
0515310 56	05/06/02	10:56	-24.22	-67.00	6.10	196	FETY, URFA
0515514 50	05/06/04	14:50	-6.34	146.81	6.10	43	MALT
0516319 26	05/06/12	19:26	-56.29	-27.08	6.00	94	BALB, ANTB, BODT, BR131, DALT, ISKB, MLSB, FETY
0516422 44	05/06/13	22:44	-19.99	-69.20	7.80	115	BALB, ANTB, BLCB, BODT, BR131, CLRB, DALT,EDRB, ISKB, KVTB, MLSB, URFA
0516517 10	05/06/14	17:10	51.23	179.41	6.80	51	ANTB, CANB

0516610 13	05/06/15	10:13	-4.59	153.19	6.30	74	ANTB, BR131, CANB, CORM, DALT, FETY, URFA, VANB
0516806 21	05/06/17	06:21	40.77	-126.57	6.70	10	CANB, MALT
0517708 23	05/06/26	08:23	1.77	125.82	6.00	91	CORM, DALT, HDMB, URFA
0520714 11	05/07/26	14:11	-15.35	-72.96	6.00	110	CANB, DALT
05246 12 38	05/06/26	12:38	-49.93	-8.95	5.70	10	ANTB
0524723 58	05/09/04	23:58	3.00	123.07	6.00	443	BLCB, CEYT, CORM, HDMB, KARA, KOZT, MERS, PTKB, SVSB
0525104 10	05/09/08	04:10	0.77	126.28	5.70	49	ANTB
0525201 20	05/09/09	01:20	-55.65	-27.10	5.70	10	BLCB
0525207 26	05/09/09	07:26	-4.54	153.47	7.70	90	KOZT
0525900 31	05/09/16	00:31	-5.62	153.59	6.10	10	KARA
0527215 50	05/09/29	15:50	-5.44	151.84	6.70	25	CEYT, KARA
05319 23 01	05/11/15	23:01	22.04	144.80	5.80	20	BODT

APPENDIX B

BLCB

Determined splitting parameters at BLCB station indicate fast polarization directions oriented around nearly N-S for the events with a back azimuth range between 61°-296° (Table B.1). The mean value of fast polarization directions is 14.1° ± 12.7 for only two events because of scatter in fast polarization directions. The mean value of the delay time is 1.6± 0.1seconds. Estimated splitting parameters are plotted as a function of Back azimuth (BAZ), distance and incidence angle at Figure B.1 respectively. Figure B.2 is shown as an example how transverse energy is minimized on the corrected Transverse component. Furthermore, error bars represent 95% confidence intervals for each of the lag time estimates. Inconsistent variations are observed as a function of incidence angle with the lag time increasing at BLCB station (Figure B.1).

TABLE B.1 BLCB Splitting Measurements

EVENT	Δ (deg)	BAZ (deg)	Φ (deg)	δt (sec)	QUALITY
04 31706 36	106.31	248.76	-16.0	0.00	Good
0432009 06	98.42	282.77	-81.0	0.00	Good
04331 02 25	106.60	81.28	4.0	0.00	Good
04349 23 20	92.05	296.06	23.0	0.00	Good
04349 23 20	92.05	296.06	-68.0	0.00	Good
05078 17 34	151.87	61.87	2.0	1.70	Good
05164 22 44	106.72	257.66	18.0	1.60	Good
05247 23 58	92.88	83.92	-47.0	0.00	Good

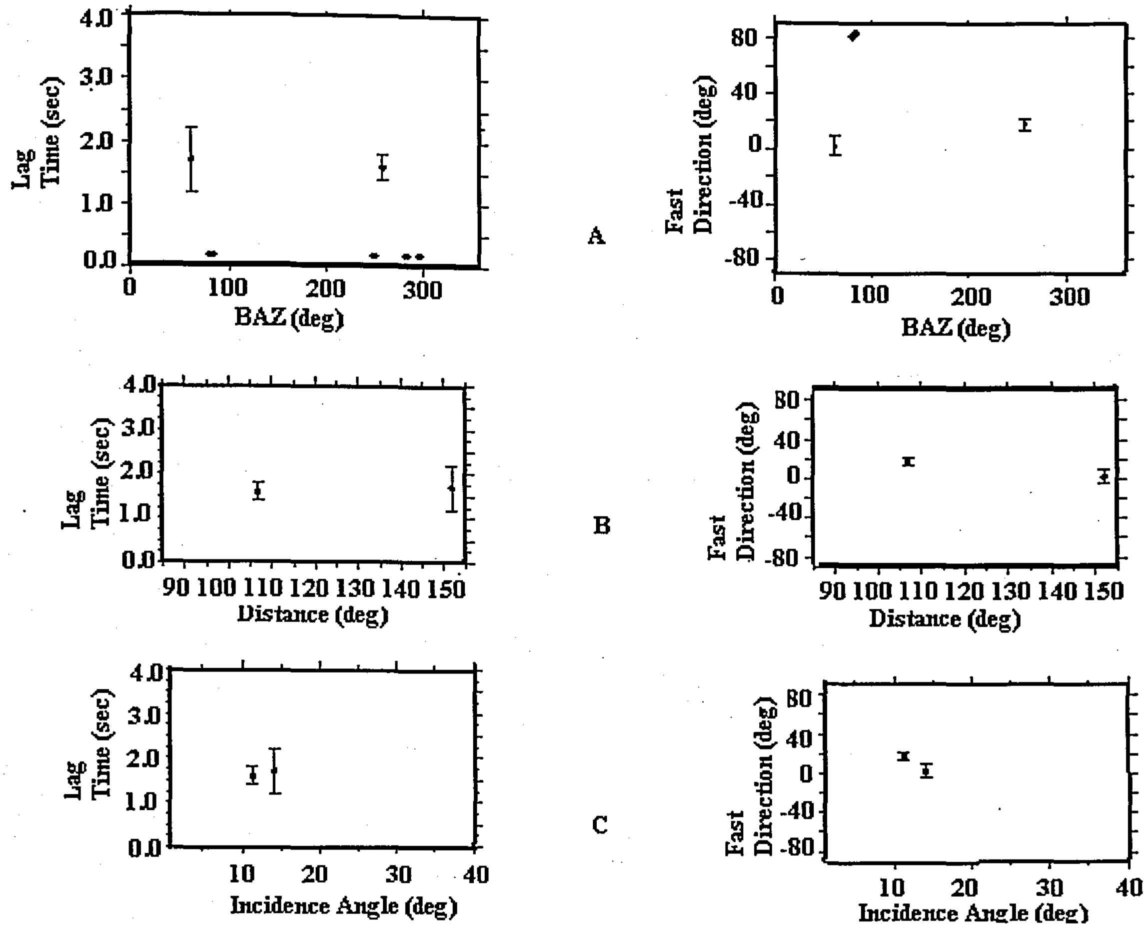

Figure B.1 A) Splitting versus BAZ (Back azimuth), **B)** Splitting versus distance (deg), **C)** Splitting versus the Moho incidence angle. Error bars represent 95% confidence intervals for each of the lag time estimates

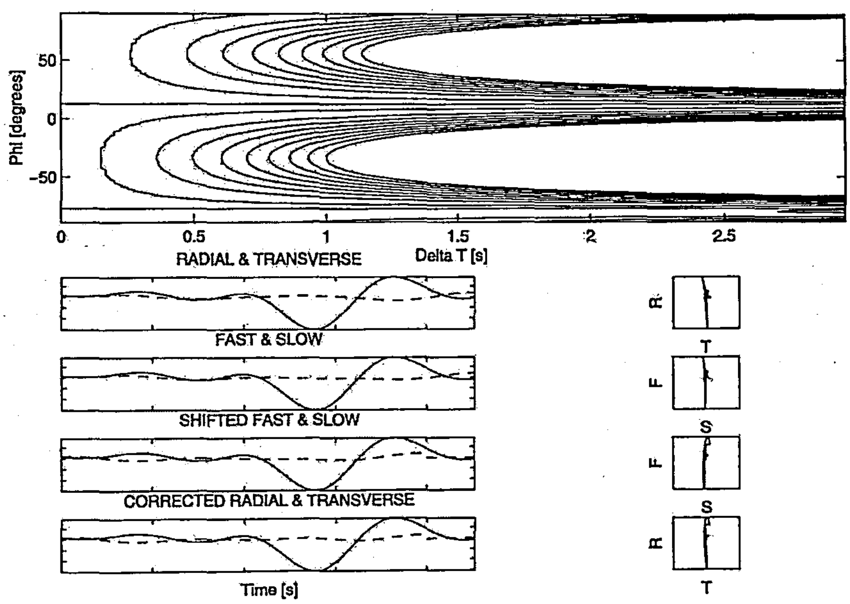

Figure B.2 This 04320 09 06 event may be shown as a good null at BLCB station (Φ= -81° ±2.0, δt=3.0± 1sec).

BODT

The results of BODT station indicate fast polarization directions oriented around N-S for the events with a back azimuth range between 1°- 257° (Table B.2). The mean value of its fast polarization direction is 5.0°±25.1. The mean value of the delay time is 1.1 ± 0.1 seconds. As weighted means of splitting parameters for the station, one event is suitable for our criteria Estimated splitting parameters are plotted as a function of Back azimuth (BAZ), distance and incidence angle at Figure B.3 respectively. In addition, error bars represent 95% confidence intervals for each of the lag time estimates. The azimuthal coverage for BODT station was not good due to lack of appropriate data. As a result of this, it may be not possible to explain clearly relationship between lag time and incidence angle.

TABLE B.2 BODT Splitting Measurements

EVENT	**Δ (deg)**	**BAZ (deg)**	**Φ (deg)**	**δt (sec)**	**QUALITY**
05138 09 10	103.82	207.65	4.0	1.10	Good
05 09915 16	87.12	1.0	-11.0	1.45	Good
0531923 01	96.80	56.0	19.0	0.75	Good
0506319 05	95.66	82.4	-58.0	1.60	Good
05061 10 42	103.97	87.64	84.0	0.00	Good
05163 1926	103.74	207.84	10.0	0.00	Good
0516422 44	106.65	257.42	72.0	0.00	Good

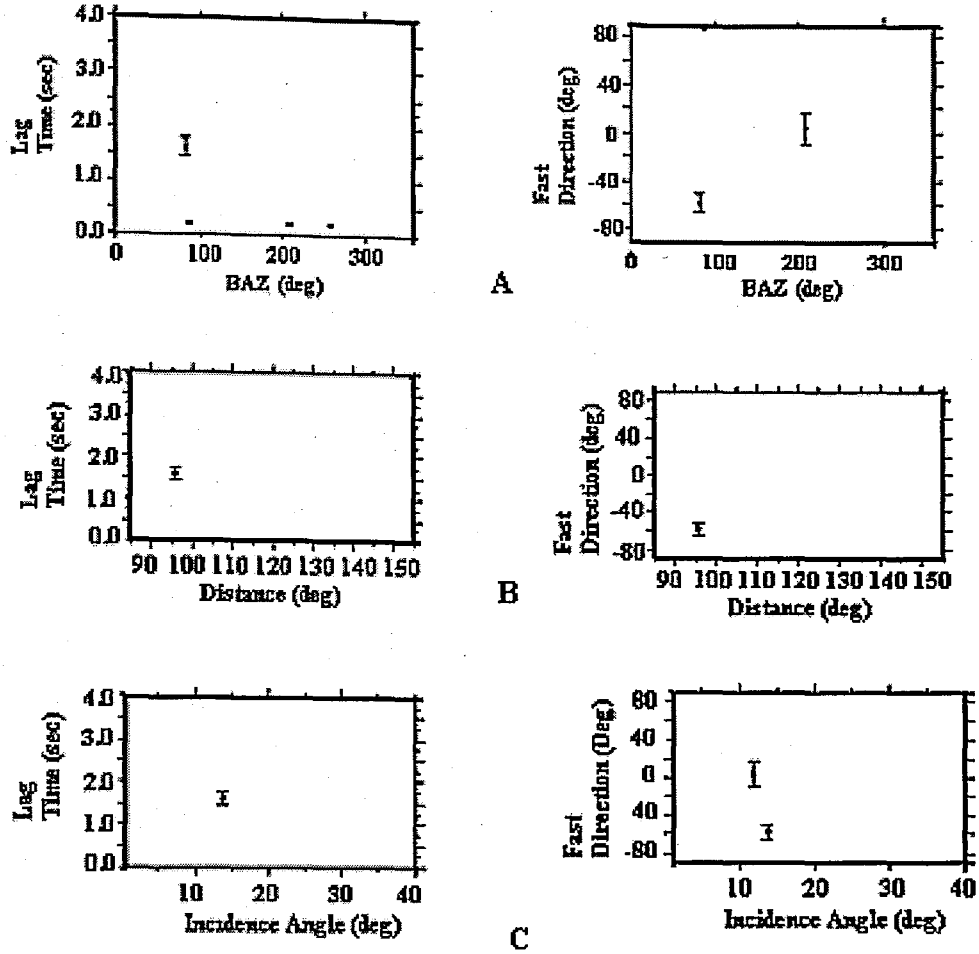

Figure B.3 A) Splitting versus BAZ (Back azimuth), **B)** Splitting versus distance (deg), **C)** Splitting versus the Moho incidence angle. Error bars represent 95% confidence intervals for each of the lag time estimates.

CANB

The estimated splitting parameters for CANB station indicate fast polarization directions oriented around NE-SW for the events with a back azimuth range between 17°-340° (Table B.3). The average value of its fast polarization directions is 30° ± 13°. The mean value of the delay time is 1.2 ± 0.2 seconds for only one event (See Table 3.5) Moreover, obtained estimated splitting parameters are plotted as a function of Back azimuth (BAZ), distance and incidence angle at Figure B.4 respectively. Error bars represent 95% confidence intervals for each of the lag time estimates.

TABLE B.3 CANB Splitting Measurements

EVENT	Δ (deg)	BAZ (deg)	Φ (deg)	δt (sec)	QUALITY
05207 14 11	107.31	264.33	30.0	1.20	Good
05165 17 10	86	17.0	54.0	1.60	Good
05166 02 51	95.43	339.9	2.0	1.60	Good
05168 06 21	96.08	340.2	38.0	1.60	Good

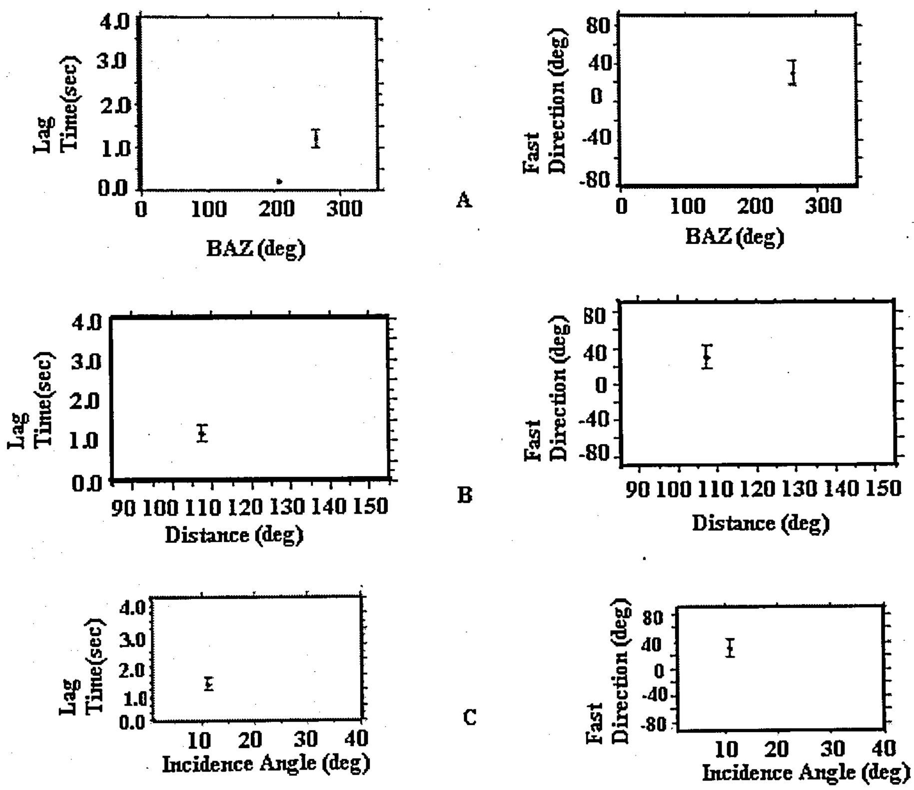

Figure B.4 **A)** Splitting versus BAZ (Back azimuth), **B)** Splitting versus distance (deg), **C)** Splitting versus the Moho incidence angle. Error bars represent 95% confidence intervals for each of the lag time estimates.

CLDR

Estimated splitting parameters at CLDR station indicate fast polarization directions oriented around more E-W than NE-SW for the events with a back azimuth range between 72°- 274° (Table B.4). The average value of fast direction at this station is 75° ± 59° for solely two events The mean value of the delay time is 2.0± 0.4 seconds. Obtained estimated splitting parameters are plotted as a function of Back azimuth (BAZ), distance and incidence angle at Figure B.5 respectively. Also, error bars represent 95% confidence intervals for each of the lag time estimates. Figure B.6 shows that transverse energy is minimized on the corrected Transverse component.

TABLE B.4 CLDR Splitting Measurements

EVENT	Δ (deg)	BAZ (deg)	Φ (deg)	δt (sec)	QUALITY
05 033 0230	89.39	72.41	64.0	0.00	Good
050 33 0230	89.39	72.41	-59.0	0.00	Good
05101 17 08	131.69	85.44	-46.0	1.50	Good
05164 22 44	119.89	267.83	75.0	2.00	Good
05164 22 44	119.89	274.64	-27.0	1.50	Good

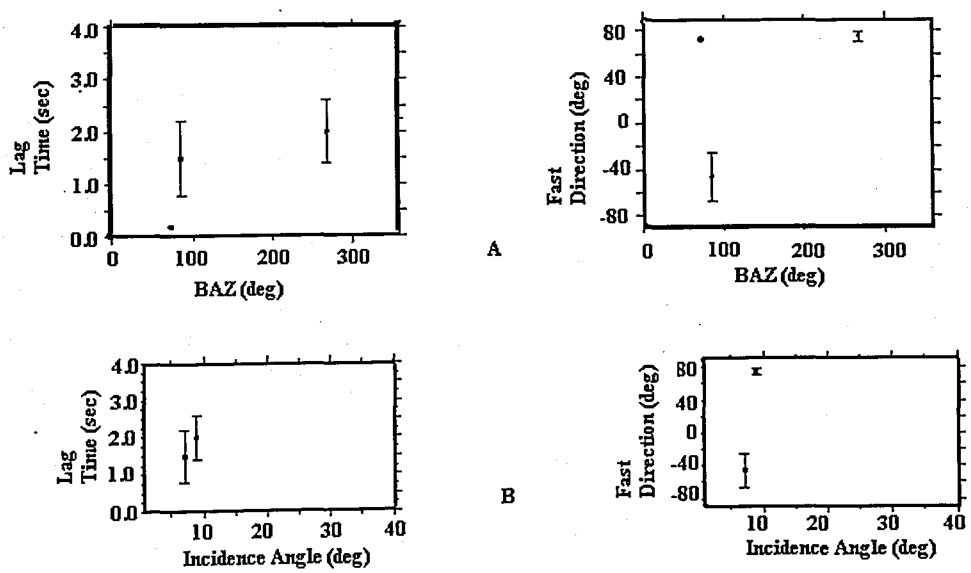

Figure B.5 A) Splitting versus BAZ (Back azimuth), **B)** Splitting versus the Moho incidence angle. Error bars represent 95% confidence intervals for each of the lag time estimates.

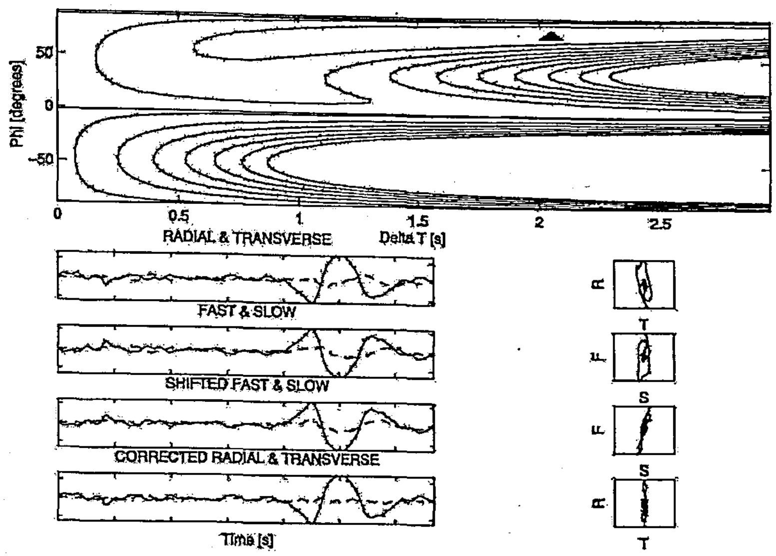

Figure B.6 The event 05164 22 44 is shown as a good example for a null (Φ= 75 ±3.55°, δt=2.05± 0.48 sec).

KVTB

Estimated splitting paremeters at KVTB station demostrate fast polarization directions oriented around N-S for the events with a back azimuth range between 85°-302° (Table B.5). The mean value of fast polarization directions is 25° ± 04°. The mean value of the delay time is 3.04 ± 0.4 seconds (See Table 3.5). Lag time is very high. These high values in splitting parameters are discussed It is clearly seen that these values could incompatible with another stations in Anatolia plate. In following interpretation and discussion this uniformity could be explained with relationship between high delay times and tectonic settings. Determined splitting parameters are plotted as a function of Back azimuth (BAZ), distance and incidence angle at Figure B.7 respectively. Moreover, error bars represent 95% confidence intervals for each of the lag time estimates.

TABLE B.5 KVTB Splitting Measurements

EVENT	Δ (deg)	BAZ (deg)	Φ (deg)	δt (sec)	QUALITY
04210 03 56	95.61	85.7	88.0	3.00	Good
04210 03 56	96.80	302.24	25.0	3.00	Good
05164 22 44	114.00	263.97	28.0	2.80	Good

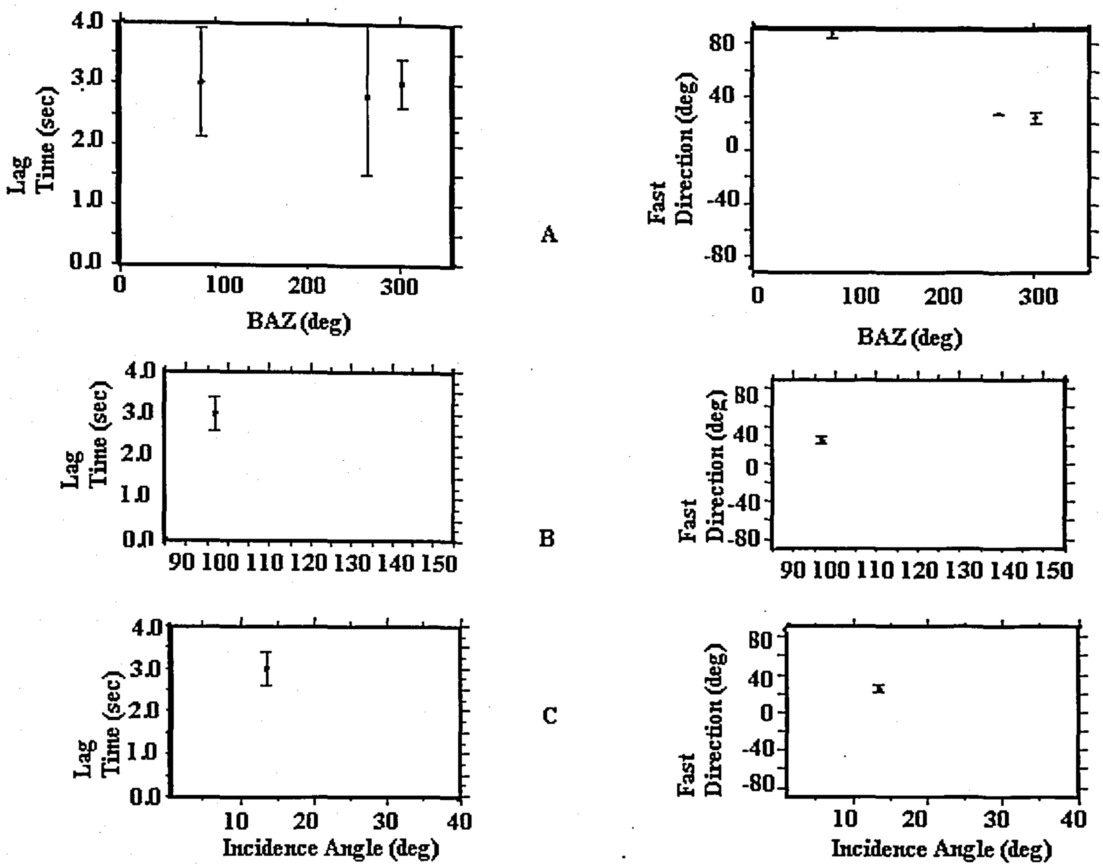

Figure B.7 A) Splitting versus BAZ (Back azimuth), **B)** Splitting versus distance (deg), **C)** Splitting versus the Moho incidence angle. Error bars represent 95% confidence intervals for each of the lag time estimates.

PTKB

The resulting splitting estimates at PTKB station indicate fast polarization directions oriented around NE-SW for the events with a back azimuth range between 99°-306° (Table B.6) The average value of fast polarization directions is 26.1° ± 0.7°. The mean value of the delay time is 3.0 ± 0.2 seconds. The weighted means of splitting parameters are calculated with only four events that are suitable for the criteria. Estimated splitting parameters are plotted as a function of Back azimuth (BAZ), distance and incidence angle at Figure B.8 respectively. Moreover, error bars represent 95% confidence intervals for each of the lag time estimates. The number of analyzed events should be increased in order to get reasonable results from this station

TABLE B.6 PTKB Splitting Measurements

EVENT	**Δ (deg)**	**BAZ (deg)**	**Φ (deg)**	**δt (sec)**	**QUALITY**
04316 21 26	91.56	99.14	69.0	2.40	Good
043200906	107.52	291.24	-80.0	2.70	Good
043250807	108.78	299.78	26.0	0.00	Good
043481523	109.37	306.45	30.0	0.00	Good
043481523	109.37	306.45	20.0	0.00	Good
043492320	100.15	304.32	25.0	0.00	Good

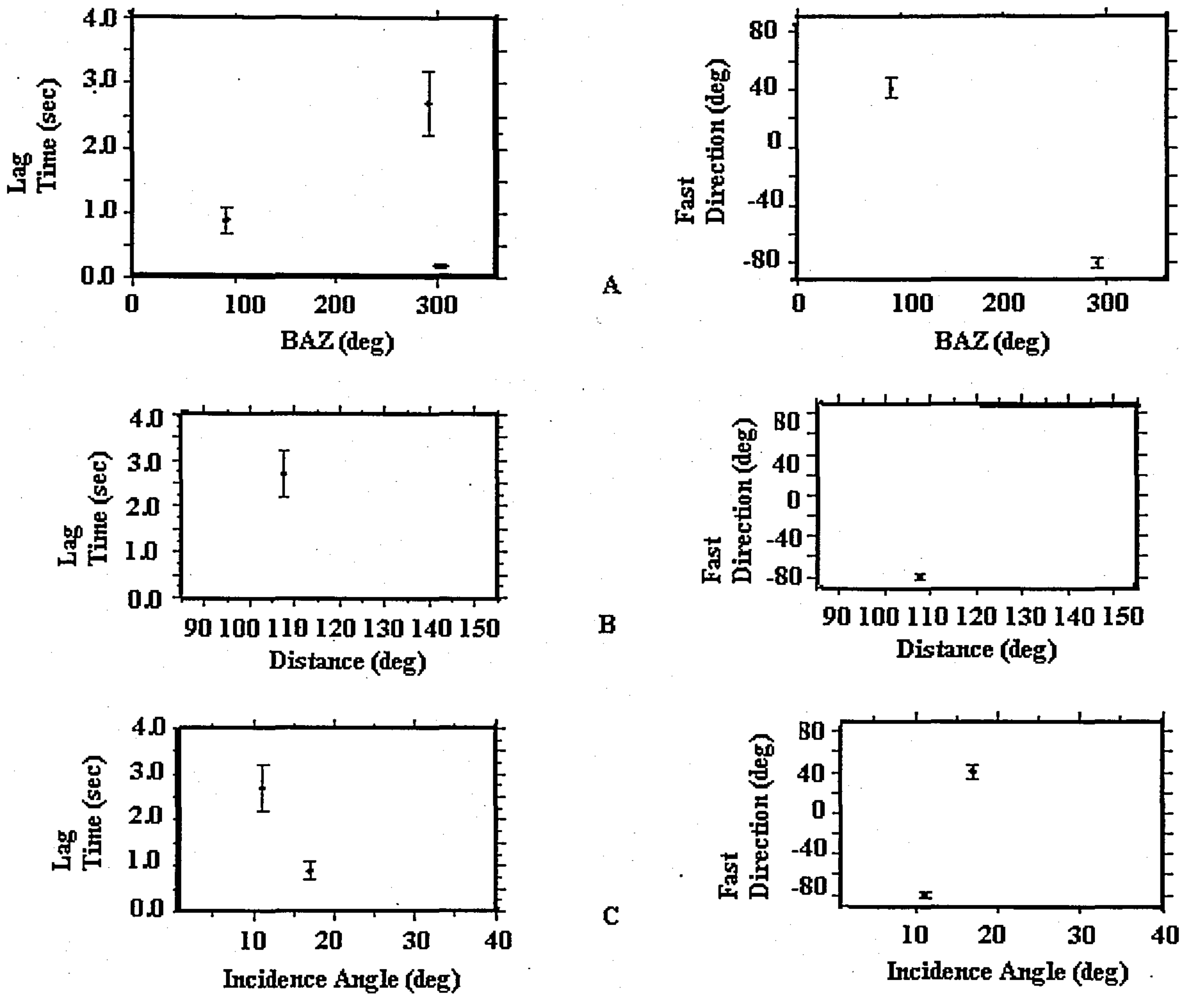

Figure B.8 A) Splitting versus BAZ (Back azimuth), **B)** Splitting versus distance (deg), **C)** Splitting versus the Moho incidence angle. Error bars represent 95% confidence intervals for each of the lag time estimates.

URFA

Obtained splitting parameters at URFA show fast polarization directions oriented around less NE-SW than N-S for the events with a back azimuth range between 67°- 303° (Table B.7). The average value of fast polarization directions is 19° ± 4.7° (four events are useful) The mean value of the delay time is 1.2 ± 0.2 seconds. Moreover, splitting parameters are plotted as a function of Back azimuth (BAZ), distance and incidence angle at Figure B.9 respectively. Error bars represent 95% confidence intervals for each of the lag time estimates.

TABLE B.7 URFA Splitting Measurements

EVENT	Δ (deg)	BAZ (deg)	Φ (deg)	δt (sec)	QUALITY
043492320	100.59	303.71	20.0	1.20	Good
050360334	93.35	67.08	2.0	0.00	Good
050611042	94.80	94.51	24.0	1.10	Good
051531056	116.42	258.79	13.0	1.50	Good
051642244	115.77	263.94	18.0	1.40	Good
051661013	112.05	78.44	-81.0	0.00	Good
051770823	86.55	90.42	29.0	1.00	Good

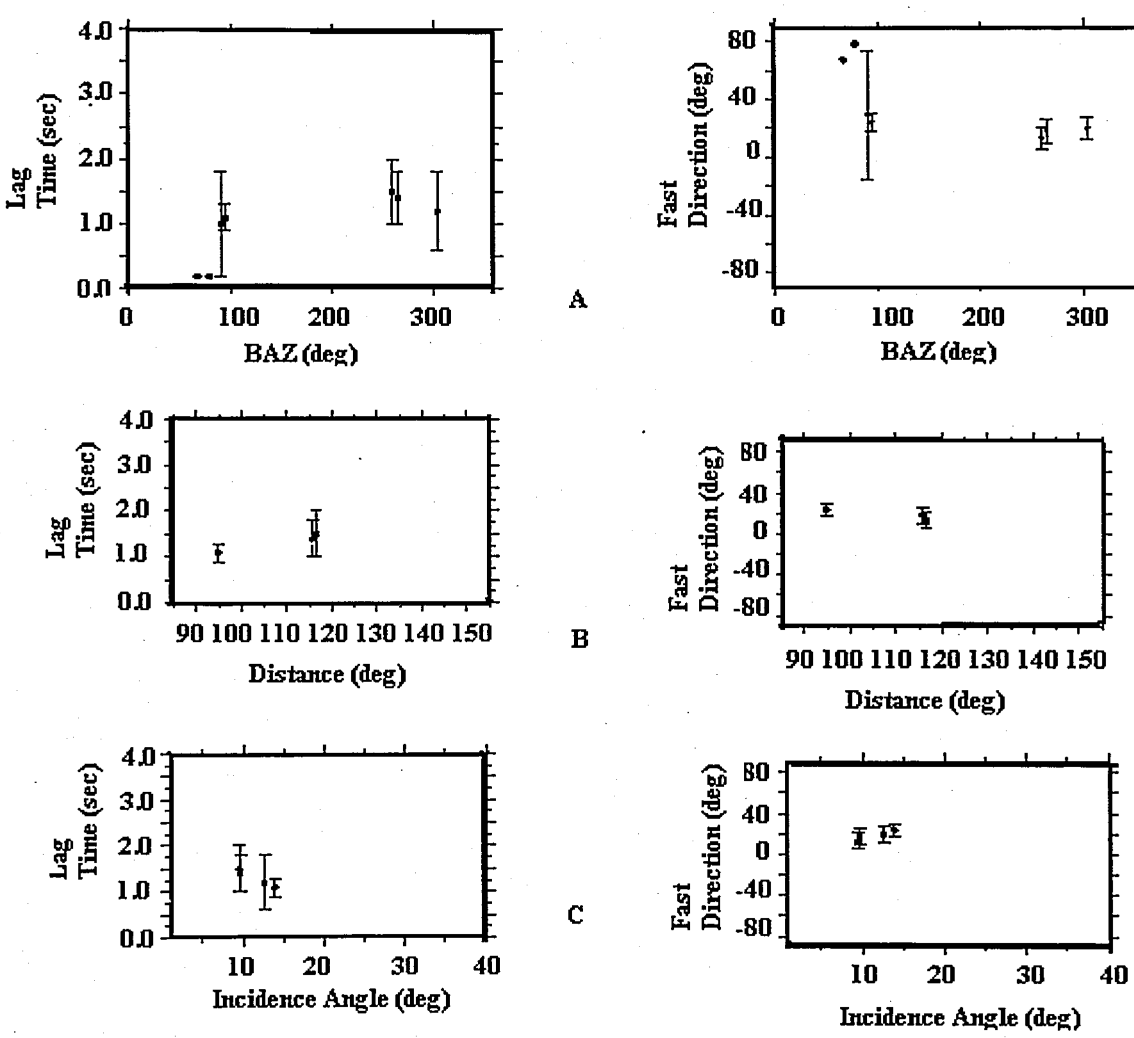

Figure B.9 A) Splitting versus BAZ (Back azimuth), **B)** Splitting versus distance (deg), **C)** Splitting versus the Moho incidence angle. Error bars represent 95% confidence intervals for each of the lag time estimates.

VANB

The resulting splitting estimates at VANB show fast polarization directions oriented around approximately more E-W than NE-SW for the events with a back azimuth range between 70°- 353° (Table B.8). The simple mean value of fast polarization directions is 64.9° ±2.6°. The mean value of the delay time is 1.4 ± 0.2 seconds (See Figure 3.5). Moreover, splitting parameters are plotted as a function of Back azimuth (BAZ), distance and incidence angle (Figure B.10) respectively. Error bars represent 95% confidence intervals for each of the lag time estimates. This event 050611042 recorded by VANB station shows that estimated split parameters (Φ= 70°, δt=0.9 sec) were found with minimizing transverse energy on the Transverse component (Figure B.11).

TABLE B.8 VANB Splitting Measurements

EVENT	**Δ (deg)**	**BAZ (deg)**	**Φ (deg)**	**δt (sec)**	**QUALITY**
04 036210 5	93.91	91.48	77.0	1.10	Good
0403802 42	93.75	92.11	78.0	2.00	Good
0403908 58	93.79	91.65	83.0	0.00	Good
0418009 49	86.95	358.63	-20.0	0.00	Good
0418107 01	112.61	305.88	-59.0	0.00	Good
0420108 01	91.75	353.74	72.0	2.50	Good
0427215 29	91.72	189.33	-2.0	0.00	Good
0427819 20	91.34	70.30	-88.0	0.00	Good
0428022 30	91.23	89.88	4.0	0.00	Good
0433102 25	93.80	91.56	79.0	1.60	Good
0434923 20	102.86	307.14	46.0	0.00	Good
0503603 34	89.58	69.88	-79.0	0.00	Good
0506110 42	91.33	97.23	70.0	0.90	Good
05061 10 42	91.33	97.23	86.0	1.70	Good
05166 10 13	108.30	81.06	75.0	1.90	Good

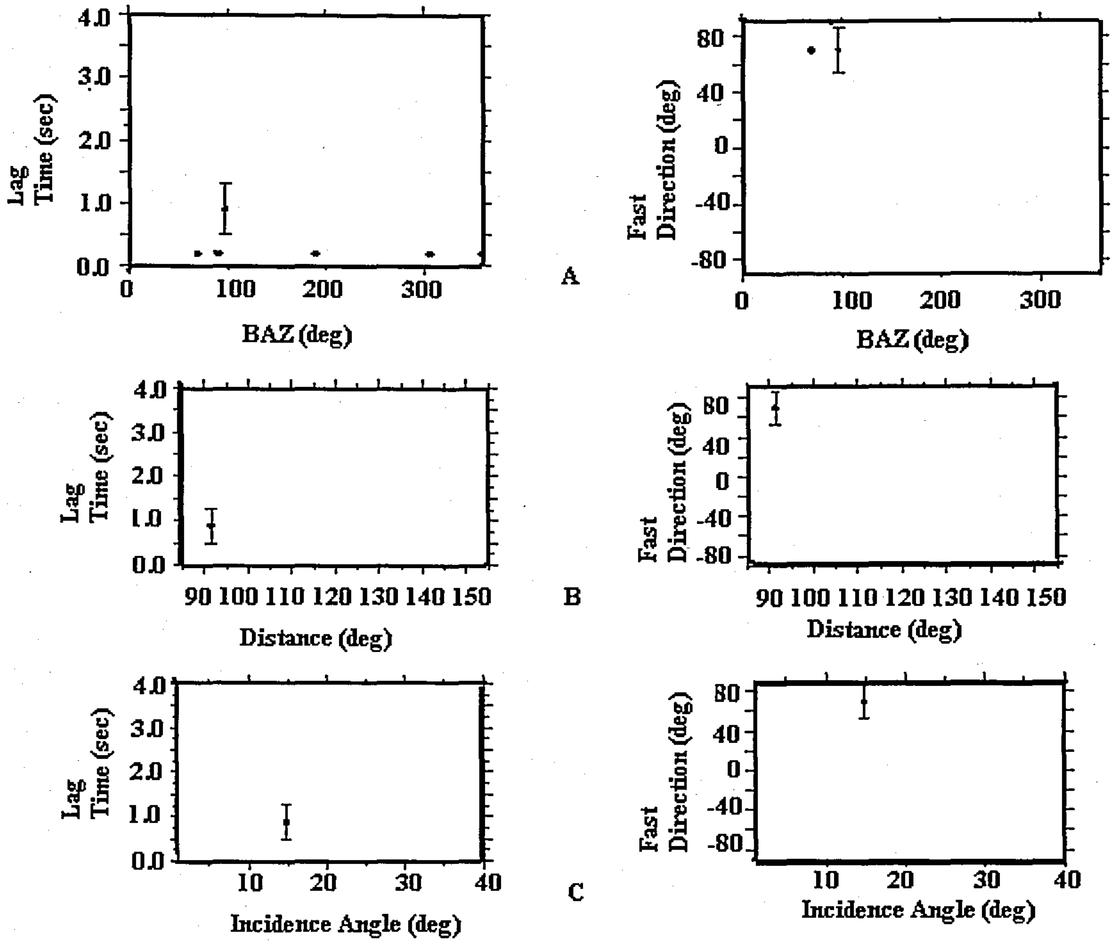

Figure B.10 A) Splitting versus BAZ (Back azimuth), **B)** Splitting versus distance (deg), **C)** Splitting versus the Moho incidence angle. Error bars represent 95% confidence intervals for each of the lag time estimates.

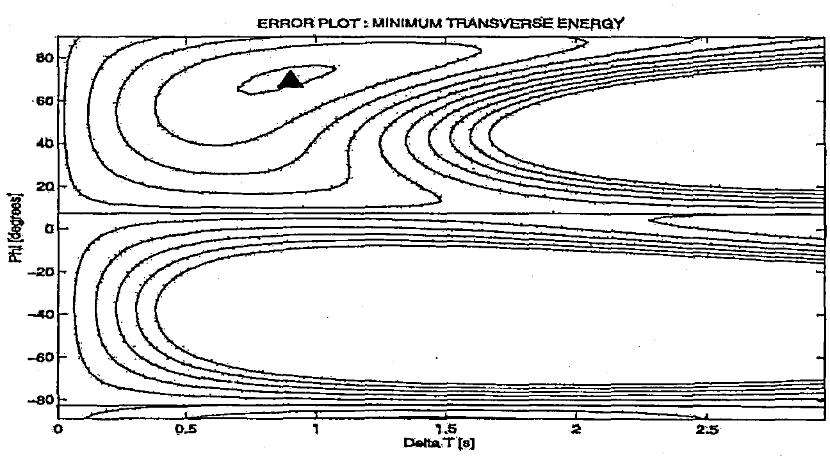

Figure B.11 This event 050611042 recorded by VANB station shows minimum transvers energy (Φ= 70°, δt=0.9 sec).

BR131

The determined splitting parameters at BR131 indicate fast polarization directions oriented around approximately NE-SW for the events with a back azimuth range between 60°-273° (Table B.9). The average value of its fast polarization directions is –6.5° ± 7° The mean value of the delay time is 1.4 ± 0.16 seconds. (See Table 3.5). Estimated splitting parameters are plotted according to back azimuth (BAZ), distance and incidence angle at Figure B.12. Figure 3.13 demostrates that transverse energy is minimized on the corrected Transverse component. Furthermore, error bars represent 95% confidence intervals for each of the lag time estimates. Inconsistent variations are observed as a function of incidence angle with the lag time increament at BR13 station (Figure B.12).

Table B.9 Splitting Measurements at BR13 station.

EVENT ID	Δ (deg)	BAZ (deg	Φ (deg)	δt (sec)	QUALITY
03146 23 13	85.79	84.77	-65.0	0.00	Good
03171 06 19	106.63	273.93	-88.0	1.50	Good
03182 05 52	86.27	87.24	-1.0	1.40	Good
03240 06 38	96.47	94.10	2.0	1.50	Good
03315 18 48	89.96	60.72	-13.0	1.50	Good
04108 15 58	98.28	92.66	72.0	1.50	Good
04177 02 35	99.43	90.89	90.0	0.00	Good
04317 06 36	111.60	252.75	90.0	0.00	Good
05036 12 23	86.43	86.13	61.0	0.80	Good
05061 10 42	98.97	91.03	-89.0	0.00	Good
051011708	139.48	77.11	61.0	1.50	Good
05163 19 26	108.58	210.86	-15.0	1.50	Good
05164 22 44	112.18	261.99	-4.0	1.10	Good
05166 10 13	115.45	73.82	-8.0	1.50	Good

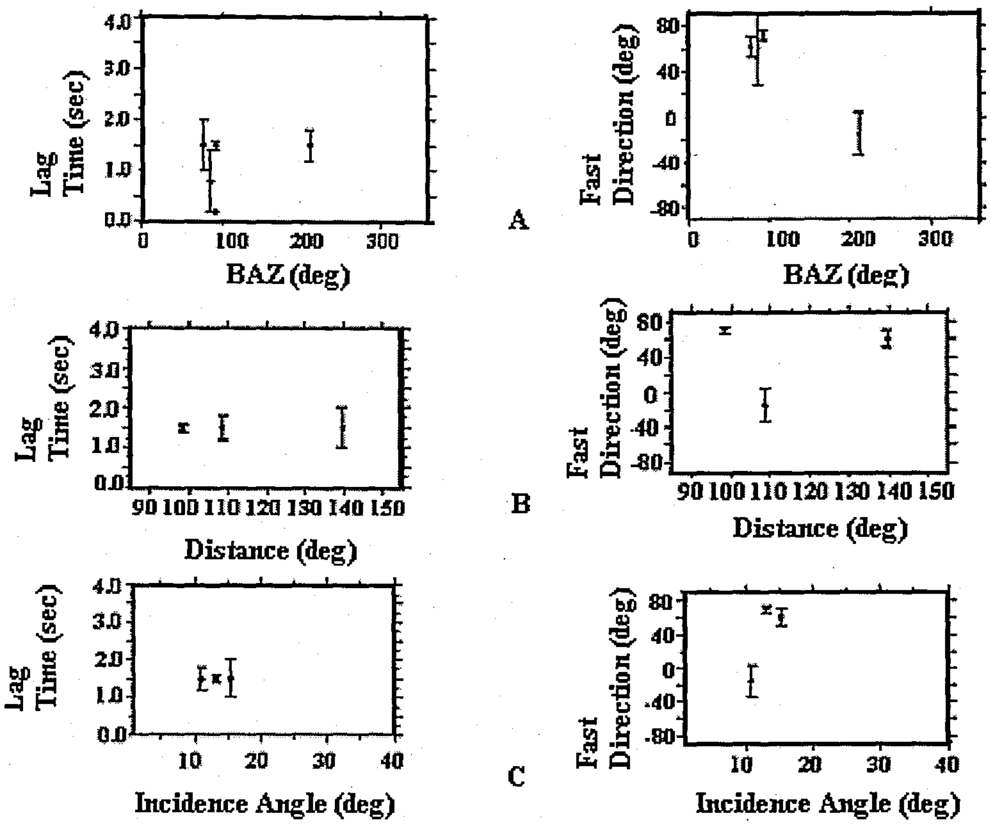

Figure B.12. Same of the fig.B.10 but for station BR13

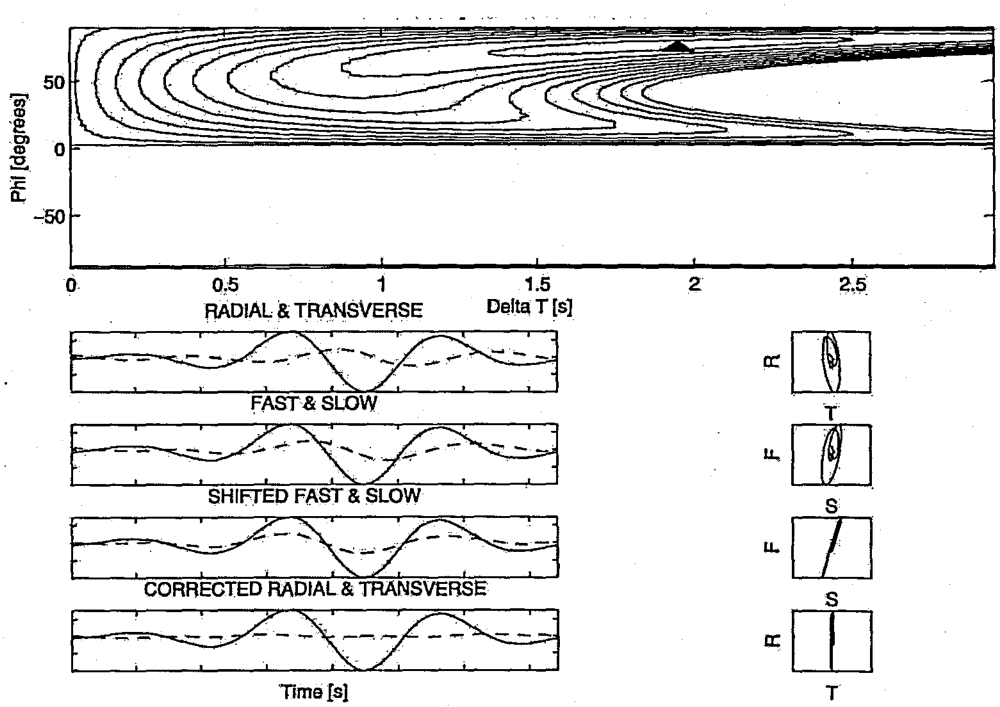

Figure B.13 The event 41081558 may be shown as a good splitting at BR13 station (Φ= 76°, ±4.0°, δt=1.95± 0.35 sec).

CORM

Obtained splitting parameters at CORM station indicate fast polarization directions oriented around nearly NE-SW for the events with a back azimuth range between 66°-305° (Table B.10). The mean value of fast polarization directions at this station is 40.2° ± 0.8°. The mean value of the delay time is 0.7 ± 0.1 seconds (only two events are useful). These estimated splitting parameters are plotted as a function of back azimuth (BAZ), distance and incidence angle at Figure B.14 respectively. Figure B.15 show that transverse energy is minimized on the corrected Transverse component

Table B.10 Splitting Measurements at CORM station

EVENT ID	Δ (deg)	BAZ (deg)	Φ (deg)	δt (sec)	QUALITY
05 033 0230	95.73	66.34	-11.0	0.00	Good
05 06110 42	98.22	91.60	-40.0	2.20	Good
05 07613 37	105.56	305.82	31.0	0.00	Good
05138 09 10	109.34	211.17	-64.0	1.60	Good
05138 09 10	109.34	211.17	-68.0	1.70	Good
05166 10 13	114.60	74.35	78.0	0.00	Good
05177 0823	89.78	87.89	40.0	0.80	Good
05247 23 58	86.89	88.72	41.0	0.70	Good
05247 23 58	86.89	88.72	-51.0	1.80	Good

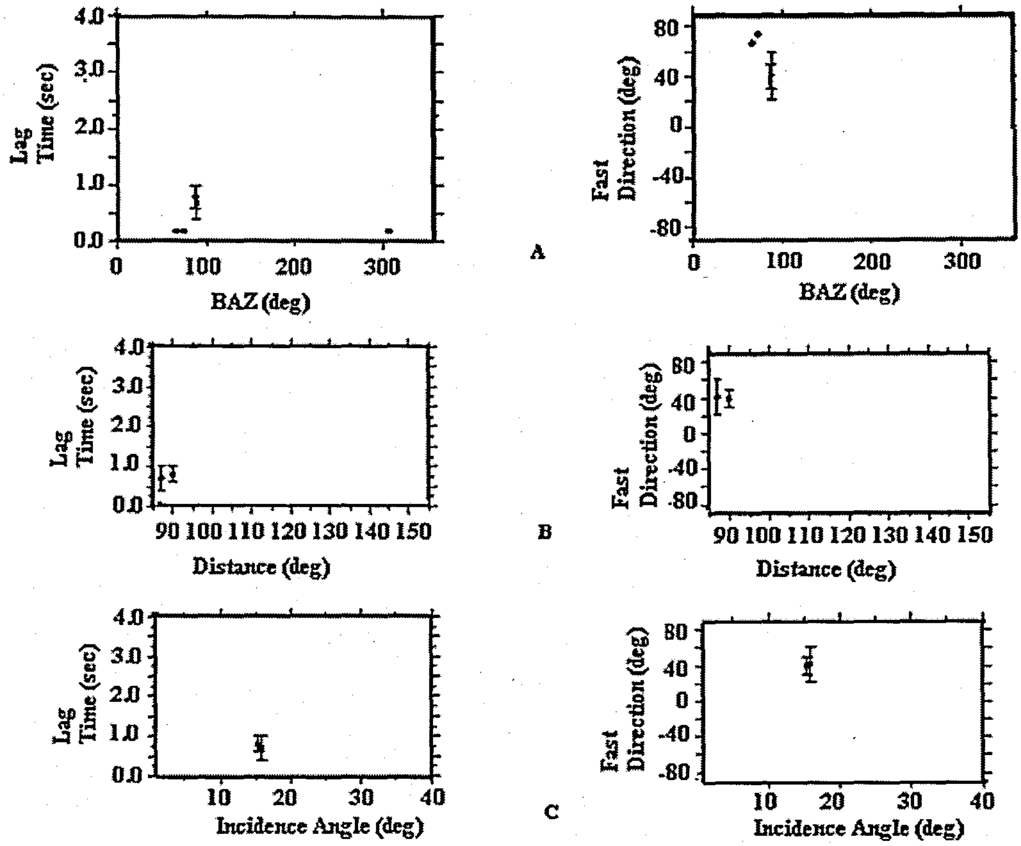

Figure B.14 A) Splitting versus BAZ (Back azimuth), **B)** Splitting versus distance (deg), **C)** Splitting versus the Moho incidence angle. Error bars represent 95% confidence intervals for each of the lag time estimates.

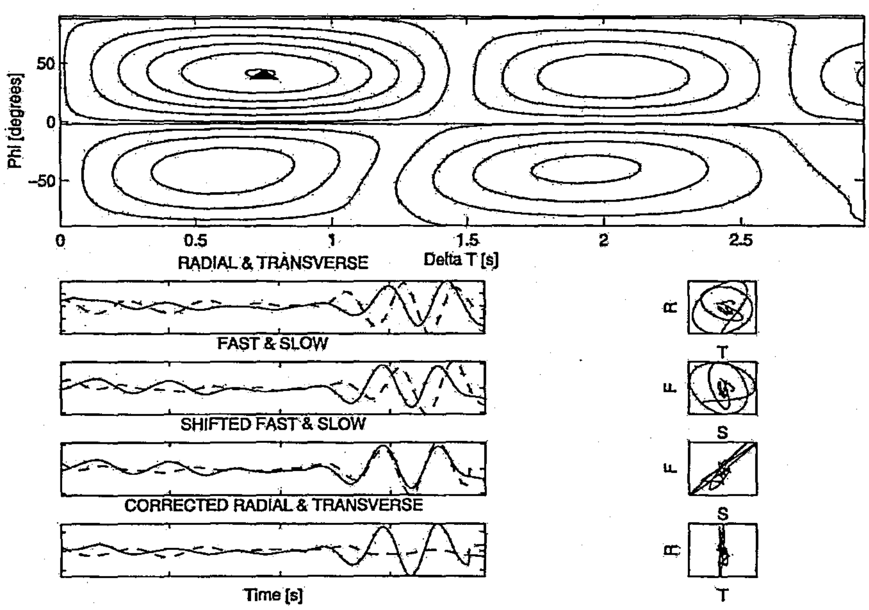

Figure B.15 The event 05177 0823 may be shown as a good splitting at CORUM station (Φ= 40±10°, δt=0.75± 0.2 sec).

DALT

The resulting splitting estimates at DALT indicate fast polarization directions oriented around approximately N-S for the events with a back azimuth range between 37°- 294° (Table B.11). The mean value of fast polarization directions at DALT station is 3° ± 5.9°. The mean value of the delay time is 1.8 ± 0.9 seconds (See Table 3.5). Estimated splitting parameters are plotted as a function of back azimuth (BAZ), distance and incidence angle at Figure B.16 respectively. Error bars represent 95% confidence intervals for each of the lag time estimates. This 042781920 event shows minimizing transverse energy on the corrected Transverse component (Figure B.17). Although the azimuthal coverage for DALT station was not very good, it is obviously seen that consistent variations are observed as a function of incidence angle with the lag time increasing at this station (Figure 3.16.

Table B.11. DALT Splitting Measurements

EVENT ID	Δ (deg)	BAZ (deg)	Φ (deg)	δt (sec)	QUALITY
04250 12 42	104.11	209.80	-7.0	0.90	Good
04257 03 00	84.32	37.58	2.0	2.80	Good
04278 19 20	102.74	60.89	5.0	1.50	Good
04280 22 30	103.03	80.97	3.0	2.50	Good
04283 21 26	102.66	294.70	31.0	0.00	Good
05 0611042	102.92	88.52	-82.0	0.00	Good
05163 1926	103.99	208.37	-75.0	0.00	Good
05164 2244	107.62	258.05	-3.0	0.00	Good
0 5166 1013	120.09	71.60	35.0	0.00	Good
05177 08 23	94.71	84.29	46.0	0.00	Good
05207 14 11	108.21	264.24	-64.0	0.00	Good

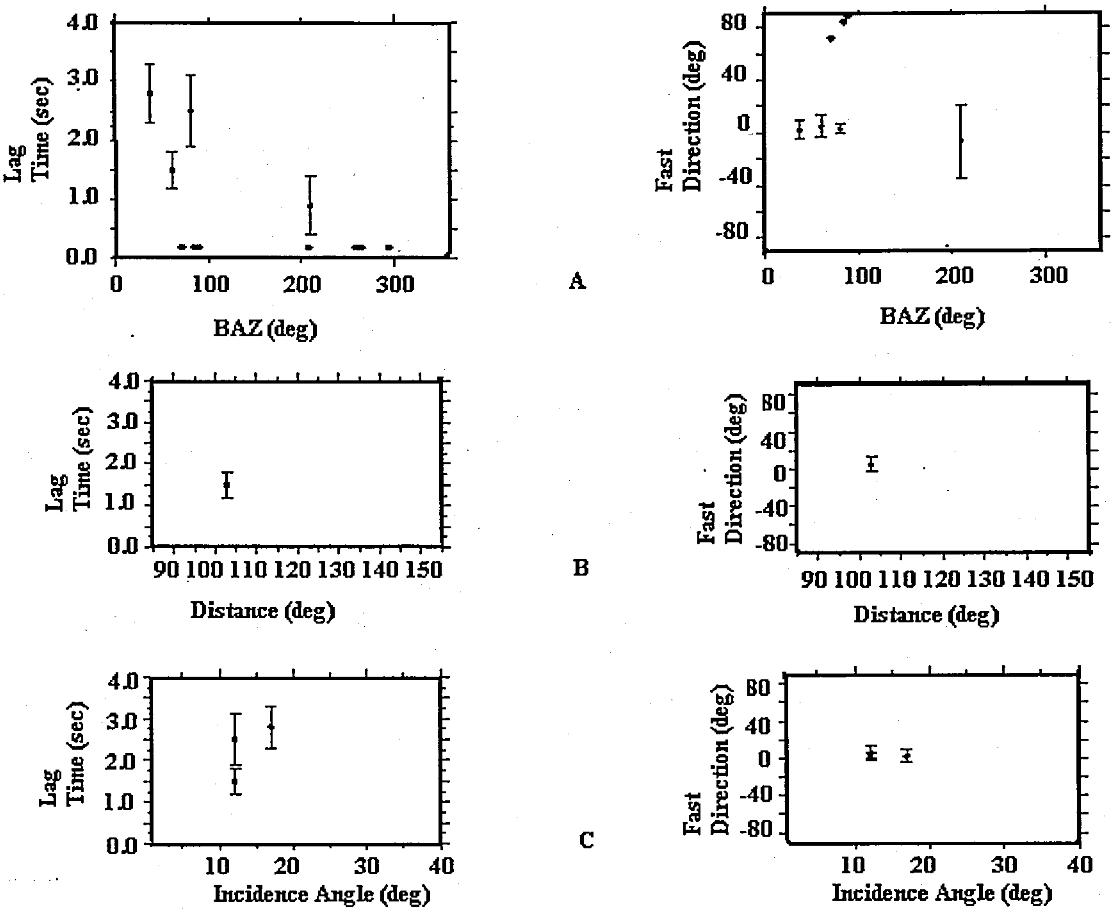

Figure B.16 A) Splitting versus BAZ (Back azimuth), **B)** Splitting versus distance (deg), **C)** Splitting versus the Moho incidence angle. Error bars represent 95% confidence intervals for each of the lag time estimates.

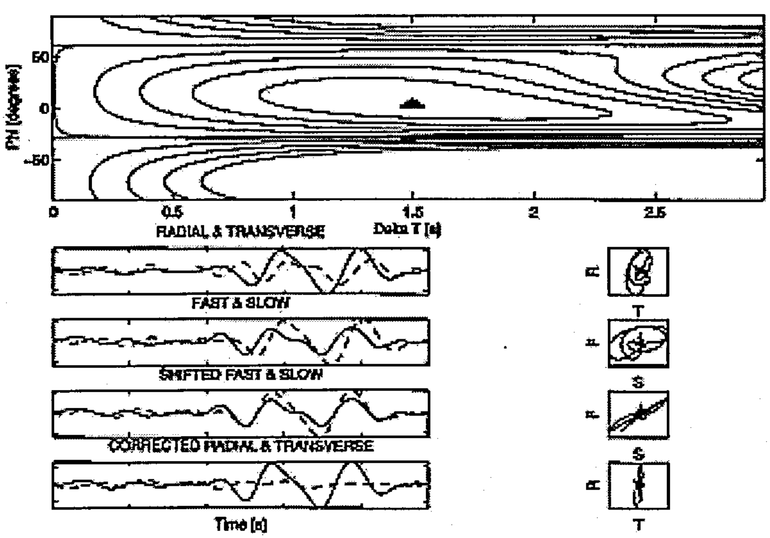

Figure B.17 This 042781920 event may be shown as a good splitting at DALT station (Φ= 5.0 ±8°, δt=1.5± 0.35 sec).

EDRB

The resulting splitting estimates at EDRB show fast polarization directions oriented around approximately N-S for the events with a back azimuth range between 56°-344° (Table B.12). Station EDRB' fast direction is considerably more North-South (23° ± 18.4°) than the other stations in the Marmara region. The mean value of the fast polarization directions is 23° ± 18.4° (95 % confidence level). The mean value of the delay time is 1.75 ± 0.59 seconds (95 % confidence level). Estimated splitting parameters are plotted as a function of back Azimuth (BAZ), distance and incidence angle at Figure B.18 respectively. Moreover, error bars represent 95% confidence intervals for each of the lag time estimates. The azimuthal coverage for EDRB station was very good. Also, consistent variations could not be clearly observed as a function of incidence angle with the lag time increasing at this station (Figure B.18). This 043492320 event shows that transverse energy is minimized on the corrected Transverse component (FigureB.19).

Table B. 12. EDRB Splitting Measurements

EVENT ID	Δ (deg)	BAZ (deg)	Φ (deg)	δt (sec)	QUALITY
02 087 04 56	107.78	256.67	-9.0	0.00	Good
02 087 04 56	107.78	256.67	73.0	0.00	Good
02091 19 59	114.79	251.62	4.0	1.40	Good
02108 16 08	112.97	253.07	73.0	0.00	Good
02108 16 08	112.97	253.07	82.0	0.00	Good
02116 16 06	101.00	61.33	-47.0	0.00	Good
02116 16 06	101.00	61.33	13.0	1.20	Good
03117 22 57	101.61	269.39	66.0	0.90	Good
03125 15 50	97.76	82.74	10.0	0.00	Good
03146 23 13	90.70	80.36	1.0	0.00	Good
03315 18 48	93.31	56.10	24.0	2.40	Good
04 028 22 15	100.01	85.20	82.0	0.00	Good
04 036 21 05	106.37	79.98	75.0	0.00	Good
0403802 42	106.25	80.64	68.0	0.00	Good
04 03908 58	106.26	80.16	3.0	0.00	Good
04 07703 21	105.46	255.44	49.0	0.00	Good
04114 01 50	100.70	92.98	86.0	2.00	Good
04182 23 37	95.43	84.08	80.0	0.00	Good
04201 08 01	86.03	343.22	18.0	0.00	Good
04241 13 41	117.07	246.29	-72.0	0.00	Good
04250 12 42	107.79	209.69	12.0	2.90	Good
04272 15 29	93.99	179.22	13.0	0.00	Good
04278 19 20	101.45	58.60	15.0	2.10	Good

04307 10 02	86.73	344.22	-81.0	0.00	Good
04320 0906	97.43	283.05	-2.0	0.00	Good
0432009 06	97.43	283.05	-2.0	0.00	Good
04348 15 23	99.62	297.59	-54.0	0.00	Good
04349 23 20	90.33	295.93	-39.0	0.00	Good
05 061 10 42	104.15	86.08	74.0	1.10	Good
05164 22 44	107.21	258.51	75.0	0.00	Good

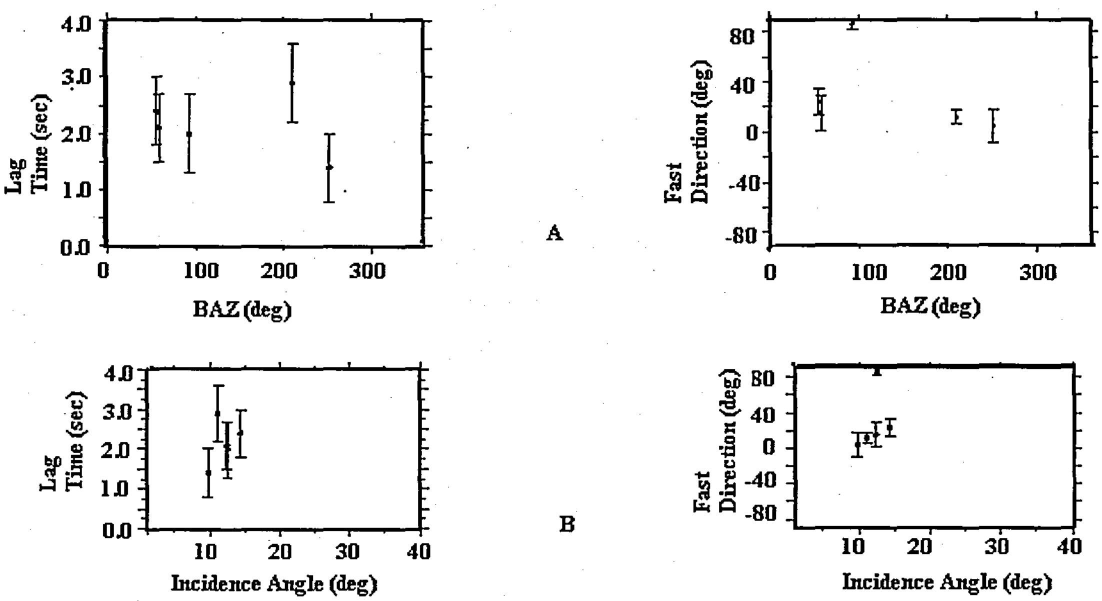

Figure B.18 Same of the fig.B.10 but for station EDRB.

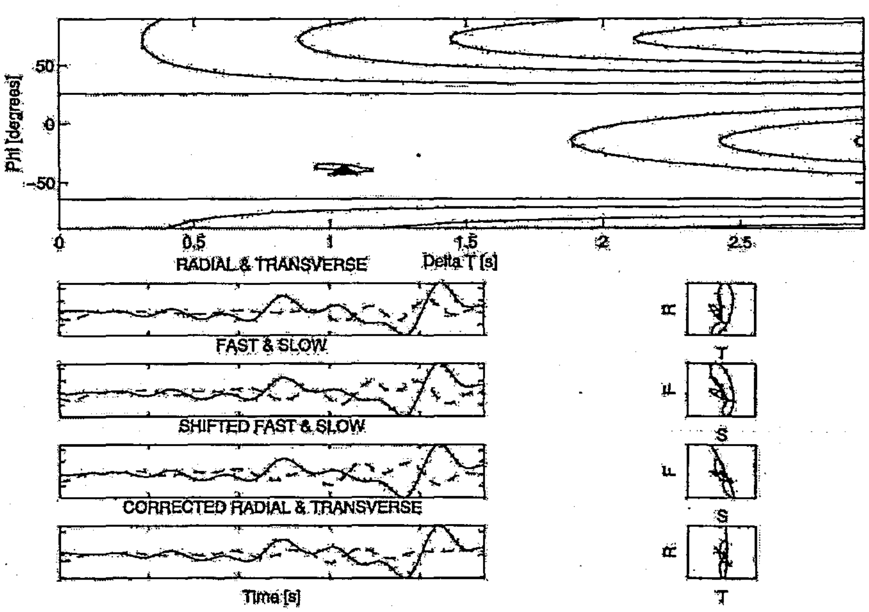

Figure B.19 This 043492320 event is an example at EDRB station for a good splitting estimate (Φ= -39° ± 42, δt=1.05± 1.25 sec).

FETY

The measuring splitting results at FETY indicate fast polarization directions oriented around dominately N-S for the events with a back azimuth range between 72°-297° (Table B.13). The mean value of fast polarization directions is –32° ± 24°. The mean value of the delay time is 1.1 ± 0.5 seconds. Estimated splitting parameters are plotted as a function of Back azimuth (BAZ), distance and incidence angle at Figure B.20 respectively. Moreover, error bars represent 95% confidence intervals for each of the lag time estimates. It is clearly seen that consistent variations are not clearly observed as a function of incidence angle with the lag time increasing at this station (Figure B.20). Transverse energy is minimized on the corrected Transverse component of the event 051380910 (Figure B.21).

Table B.13 FETY Splitting Measurements

EVENT ID	Δ (deg)	BAZ (deg)	Φ (deg)	δt (sec)	QUALITY
04349 2320	94.28	297.25	-63.0	0.00	Good
050611042	102.56	88.81	-60.0	0.60	Good
051380910	104.11	208.35	-19.0	0.80	Good
051531056	108.67	253.39	-15.0	0.00	Good
051531056	108.67	253.39	77.0	0.00	Good
051631926	104.04	208.54	-22.0	1.10	Good
051661013	119.79	72.0	0.0	1.70	Good
05050 00 04	95.72	92.6	-13.0	1.30	Good

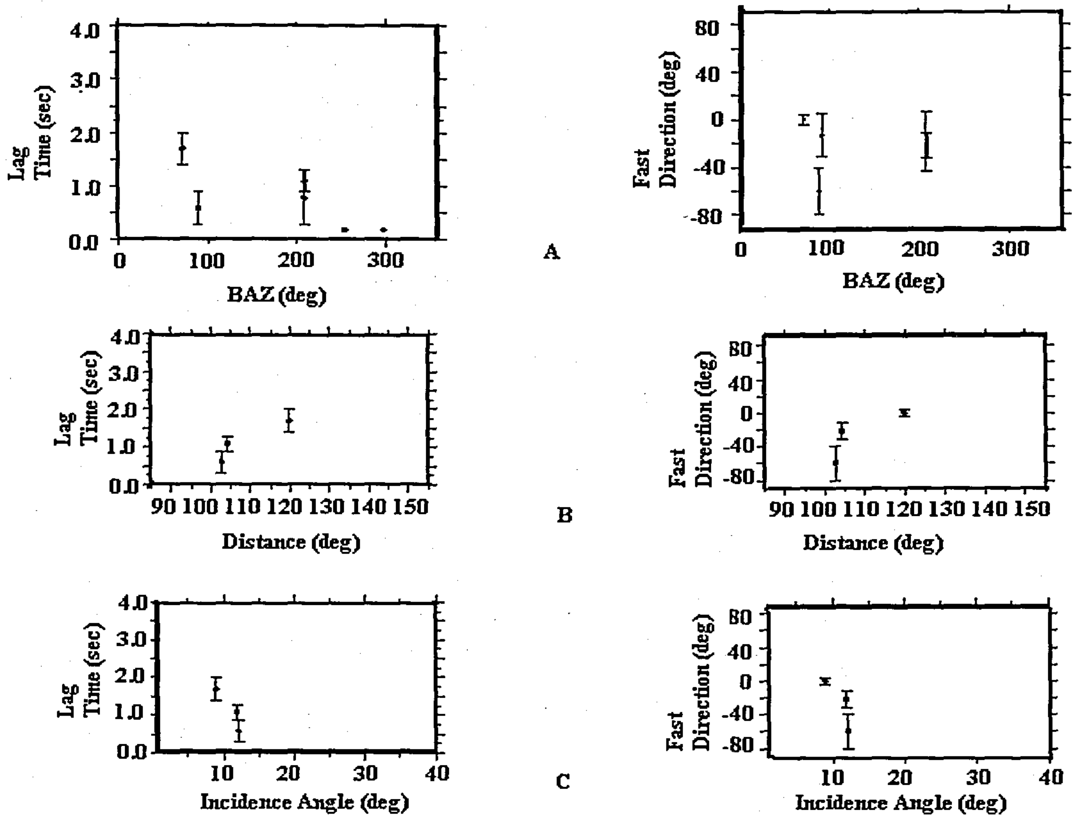

Figure B.20 A) Splitting versus BAZ (Back azimuth), **B)** Splitting versus distance (deg), **C)** Splitting versus the Moho incidence angle. Error bars represent 95% confidence intervals for each of the lag time estimates.

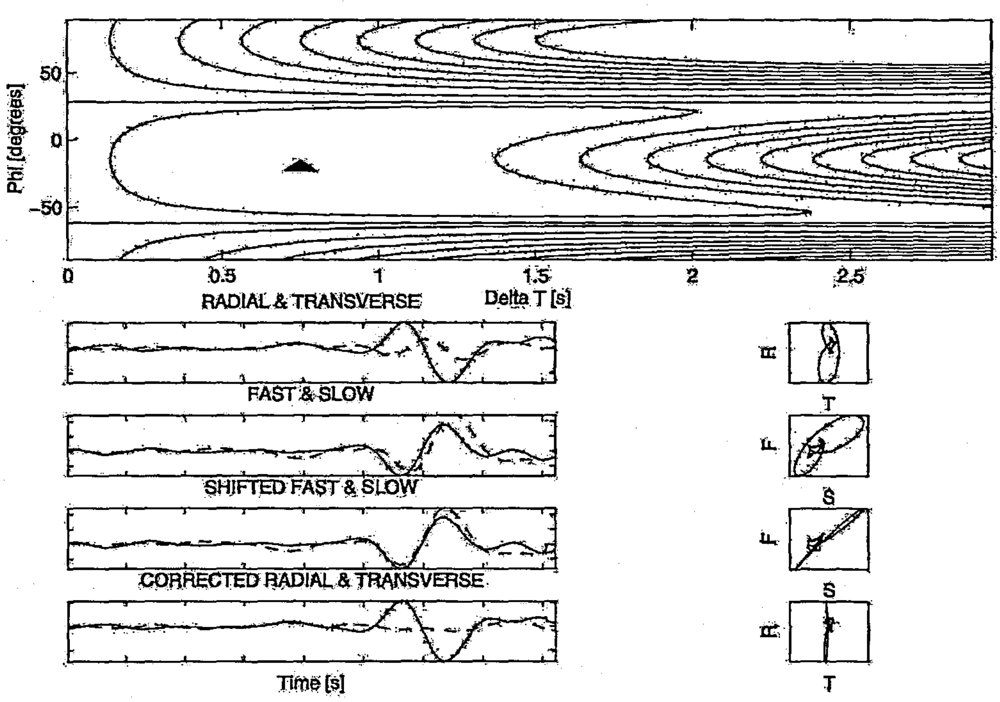

Figure B. 21 This event 051380910 recorded by FETY station (Φ= -19° ± 25, δt=0.7± 0.45sec).

HDMB

The estimated splitting parameters at HDMB show fast polarization directions oriented around approximately NE-SW for the events with a back azimuth range between 85°-299° (Table 3.9). The mean value of fast polarization directions is 65.5° ± 19.7°. The mean value of the delay time is 1.3 ± 0.2 seconds. Obtained splitting parameters are plotted as a function of Back Azimuth (BAZ), distance and incidence angle at Figure B.22 in order. In addition, error bars represent 95% confidence intervals for each of the lag time estimates.

Table B.14 HDMB Splitting Measurements

EVENT	Δ (deg)	BAZ (deg)	Φ (deg)	δt (sec)	QUALITY
0403621 05	102.59	85.02	29.0	0.00	Good
0403802 42	102.41	85.65	87.0	0.00	Good
043200906	102.96	286.03	-82.0	0.00	Good
04331 02 25	102.48	85.09	78.0	0.00	Good
04349 23 20	96.53	299.43	48.0	1.10	Good
05177 08 23	91.62	86.59	76.0	0.00	Good
05247 23 58	88.68	87.26	75.0	1.50	Good

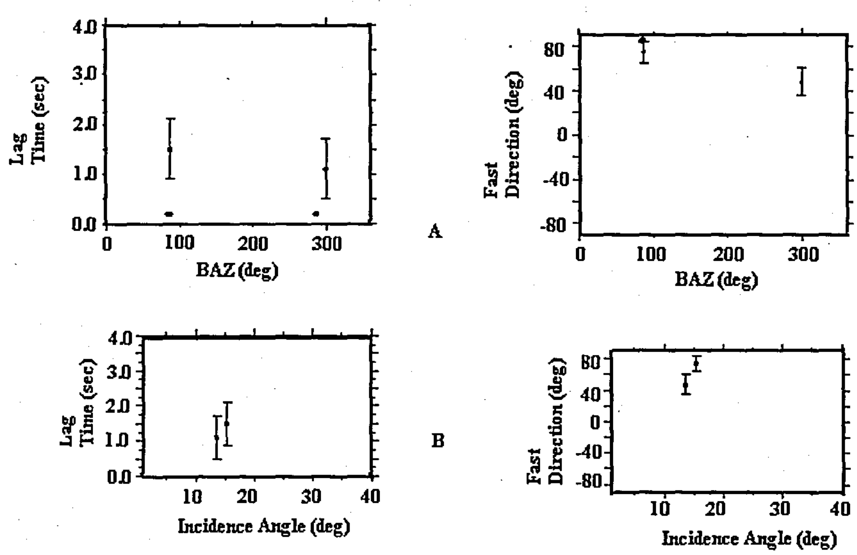

Figure B.22 A) Splitting versus BAZ (Back azimuth), **B)** Splitting versus the Moho incidence angle.

ISKB

Estimated splitting parameters at ISKB station show fast polarization directions oriented around nearly NE-SW for the events with a back azimuth range between 56°-311° (Table B.15). The mean value of fast polarization directions is 37.0 °± 16.9. The mean value of the delay time is 1.2 ± 0.3 seconds (See Table 3.5). Estimated splitting parameters are very satisfied to interpret mantle flow with tectonic activities resulting in development of deformation in region. In addition, azimuthal coverage for ISKB station is very good. Acquired splitting parameters are plotted as a function of back azimuth (BAZ), distance and incidence angle at Figure B.23 respectively. Error bars represent 95% confidence intervals for each of the lag time estimates. Consistent variations are observed as a function of incidence angle with the lag time increasing at this station (Figure B.23). This event 001661700 indicates that transverse energy is minimized on the corrected Transverse component (Figure B.24).

Table B.15. ISKB Splitting Measurements

EVENT	Δ (deg)	BAZ (deg)	Φ (deg)	δt (sec)	QUALITY
99136 00 51	117.9	70.34	37.0	1.60	Good
99166 20 42	102.82	308.48	31.0	2.60	Good
99166 20 42	102.82	308.48	32.0	0.00	Good
99172 17 43	105.25	311.62	33.0	2.70	Good
99172 17 43	105.25	311.62	34.0	1.60	Good
99258 0301	108.09	257.79	34.0	1.10	Good
99273 16 31	104.32	306.59	32.0	0.00	Good
00 05708 11	99.42	62.53	38.0	1.50	Good
00 063220 9	101.87	89.38	53.0	1.40	Good
00072 22 21	102.34	302.49	-67.0	2.20	Good
00 08811 00	92.57	57.37	42.0	0.00	Good
00114 09 27	109.43	249.12	39.0	1.60	Good
00114 170 1	109.43	249.03	41.0	1.60	Good
00133 18 43	109.06	255.12	50.0	1.20	Good
0016617 00	93.56	80.91	37.0	1.40	Good
00168 07 55	117.59	247.93	50.0	2.00	Good
00220 14 33	97.80	92.49	71.0	1.20	Good
00228 04 30	154.61	77.33	54.0	1.50	Good
00301 04 21	87.69	56.79	35.0	0.00	Good
00353 01 19	148.99	58.81	11.0	0.00	Good
01013 17 33	101.30	298.39	-61.0	0.00	Good
01 07318 56	91.85	87.81	-24.0	1.90	Good
01180 18 35	106.46	258.33	39.0	1.10	Good
01184 13 10	92.60	58.36	39.0	0.00	Good

01186 13 53	110.14	265.96	42.0	1.10	Good
01332 14 32	102.32	303.38	-83.0	1.10	Good
02 07822 14	102.40	87.81	44.0	1.10	Good
0208704 56	109.31	257.82	36.0	0.80	Good
0228520 09	103.54	270.76	45.0	0.90	Good
03125 15 50	96.12	84.39	49.0	1.40	Good
04 07703 21	106.96	256.62	39.0	1.20	Good
04108 15 58	101.80	89.48	49.0	1.40	Good
04114 01 50	98.91	94.62	43.0	1.10	Good
05080 12 43	107.64	252.42	31.0	1.00	Good
05163 19 26	107.91	209.14	-74.0	0.00	Good
0516422 44	108.78	259.68	0.0	2.80	Good

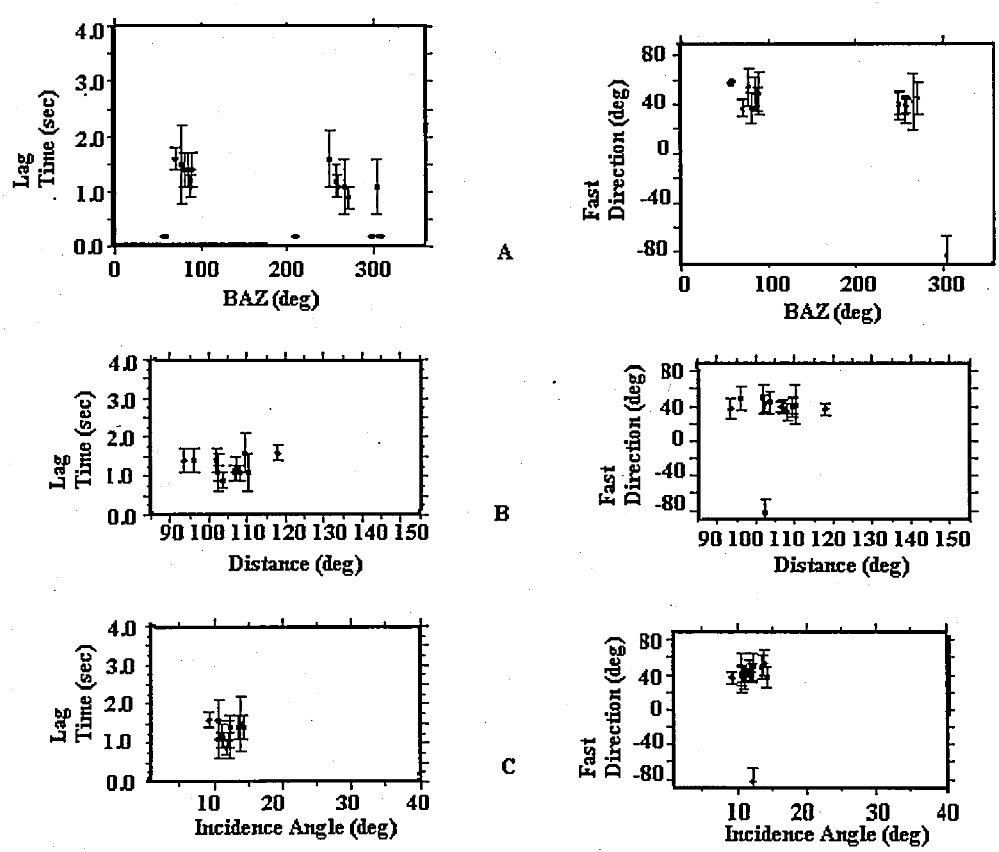

Figure B.23 A) Splitting versus BAZ (Back azimuth), **B)** Splitting versus distance (deg), **C)** Splitting versus the Moho incidence angle. Error bars represent 95% confidence intervals for each of the lag time estimates.

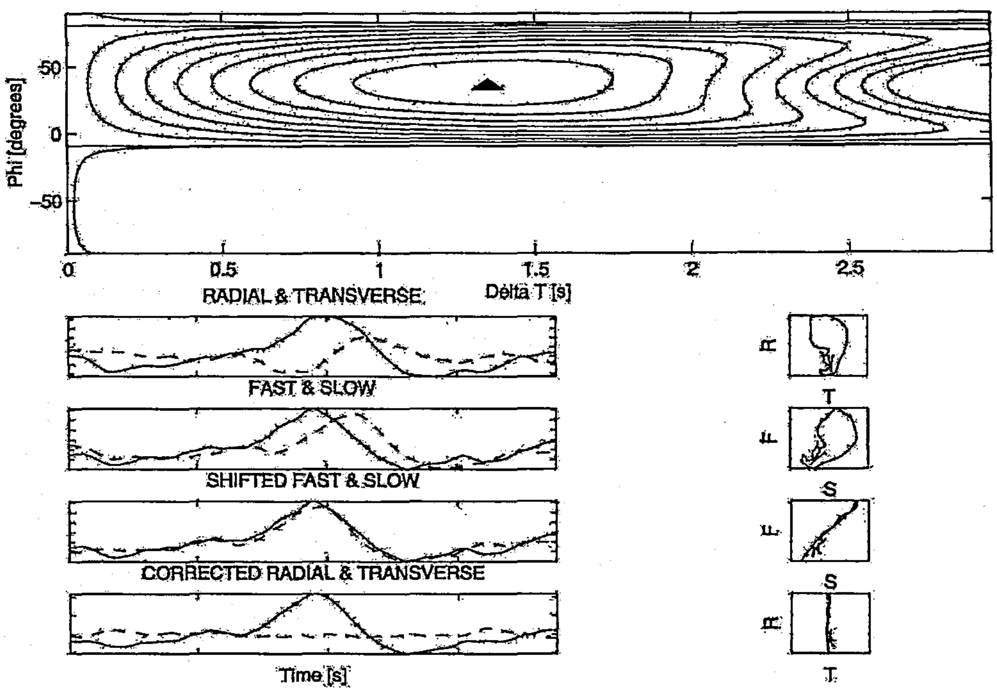

Figure B.24 This 001661700 event may be shown as a good example for estimated splitting parameters at ISKB station (Φ= 37° ± 12, δt=1.35± 0.3 sec).

ISP

Determined splitting parameters at ISP indicate fast polarization directions oriented around approximately N-S for the events with a back azimuth range between 1°-312° (Table B.16). The mean value of fast polarization directions is 3° ± 9.2°. The mean value of the delay time is 1.8 ± 0.15 seconds (See Table 3.5). We acquired very efficient results from ISP station. In addition, azimuthal coverage for the ISP station is better than other stations except for ISKB station that are mentioned above. Almost events may get a cluster between 10° and 15° of incidence angle and come from between 100-120 degrees of distance. Obtained splitting parameters are plotted as a function of Back azimuth (BAZ), distance and incidence angle at Figure B.25 respectively. Error bars represent 95% confidence intervals for each of the lag time estimates.

Table B.16. ISP Splitting Measurements

EVENT ID	Δ (deg)	BAZ (deg)	Φ (deg)	δt (sec)	QUALITY
96306 0332	113.43	72.35	-27.0	0.00	Good
96309 1724	99.47	286.88	26.0	0.00	Good
96317 1659	111.74	267.60	77.0	0.00	Good
96319 0758	132.67	68.04	41.0	0.00	Good

96326 0743	90.63	81.14	16.0	0.00	Good
96365 1941	98.42	88.52	70.0	0.00	Good
9700122 32	92.69	88.08	48.0	2.70	Good
97001 2232	92.69	88.08	-66.0	0.00	Good
97 0112028	109.04	312.94	-12.0	1.90	Good
97 0171120	97.76	95.21	-6.0	1.90	Good
97023 0215	107.90	255.81	-6.0	2.60	Good
97 40 12 32	111.93	268.40	-86.0	0.00	Good
97123 1646	154.78	85.21	79.0	0.00	Good
97128 1329	88.90	13.08	7.0	1.60	Good
971290906	100.22	64.53	-8.0	2.20	Good
9714207 50	108.00	312.33	0.0	1.60	Good
97153 2124	106.16	207.54	-46.0	1.80	Good
97168210 3	87.43	18.21	-64.0	0.00	Good
97175 2304	97.01	87.00	1.0	0.00	Good
9718709 54	116.85	251.64	-8.0	0.00	Good
9718902 24	91.65	58.06	45.0	0.00	Good
97190 1924	86.72	280.78	-68.0	0.00	Good
97200 1422	107.77	308.15	-33.0	1.90	Good
97201 1014	108.89	255.27	80.0	0.00	Good
97212 2154	102.24	88.91	85.0	2.40	Good
9722209 20	102.59	100.52	7.0	0.00	Good
97245 1213	100.41	283.14	-8.0	1.10	Good
9730106 15	106.24	277.19	-69.0	2.20	Good
97329 1214	90.84	87.79	7.0	0.00	Good
97332 2253	105.58	264.58	-81.0	0.00	Good
9734507 56	100.39	283.22	-3.0	1.10	Good
9735104 38	87.12	19.31	12.0	0.00	Good
9800106 11	91.04	58.46	2.0	1.50	Good
98 0100454	107.18	267.98	-83.0	2.50	Good
98 0100820	104.83	301.77	2.0	1.80	Good
98 0130950	99.29	87.98	15.0	1.10	Good
9809122 42	123.66	242.34	-16.0	0.00	Good
98 0932201	106.60	272.54	-63.0	0.90	Good
98110 2259	107.89	311.91	-4.0	1.60	Good
9813505 58	99.68	63.68	11.0	1.50	Good
982101800	106.14	80.69	-2.0	0.00	Good
98216 1859	106.80	282.66	-67.0	0.00	Good
98235 1357	104.37	297.35	2.0	1.60	Good
98240 1240	93.65	87.37	71.0	1.20	Good
9824201 48	99.94	59.36	-12.0	2.00	Good
9824508 37	91.63	81.93	16.0	1.00	Good
98246 1737	116.43	252.15	67.0	0.00	Good
9825109 10	99.68	64.95	-9.0	0.00	Good
98264 0652	91.38	88.61	70.0	1.60	Good
9826501 16	100.02	66.59	-3.0	1.60	Good
982711923	92.31	83.38	-88.0	0.00	Good

9828104 51	109.01	264.10	-90.0	0.00	Good
983002116	94.62	82.74	22.0	0.00	Good
983011625	93.80	86.01	4.0	0.00	Good
983011625	93.80	86.01	20.0	2.20	Good
983120725	96.23	96.67	-88.0	0.00	Good
98333 1410	94.72	88.96	65.0	2.20	Good
98350 1745	93.79	85.66	6.0	0.00	Good
990600851	96.56	88.67	8.0	2.00	Good
99 0611745	110.44	256.70	84.0	0.00	Good
99064 0033	109.48	258.94	85.0	2.50	Good
9907910 47	87.61	17.16	-53.0	0.00	Good
99 0930617	110.31	264.36	-89.0	0.00	Good
990951108	116.22	75.91	-85.0	0.00	Good
991271413	86.08	1.93	-52.0	0.00	Good
991530023	92.31	88.15	87.0	0.00	Good
99166 2042	105.73	308.94	2.0	1.50	Good
99169 1055	91.47	81.93	1.0	1.30	Good
99169 1055	91.47	81.93	2.0	2.70	Good
99172 1743	108.25	312.05	25.0	0.00	Good
99173 0047	103.35	85.31	80.0	0.00	Good
99258 0301	108.50	257.59	83.0	0.00	Good
99273 1631	107.17	306.98	20.0	0.00	Good
99283 0703	102.08	83.08	0.0	2.50	Good
99286 0133	87.34	6.78	-62.0	0.00	Good
99291 0243	105.37	209.19	-40.0	2.90	Good
9929308 28	101.17	90.13	-88.0	0.00	Good
99322 1427	94.07	86.20	2.0	2.40	Good
9932503 51	110.12	257.70	-5.0	0.00	Good
993340401	108.84	260.41	87.0	0.00	Good
99335 1923	96.29	297.89	18.0	0.00	Good
99340 2312	85.03	2.72	-43.0	0.00	Good
99347 0930	93.95	84.33	-4.0	0.00	Good
99353 0048	100.34	64.86	-16.0	0.00	Good
00 0571824	98.97	289.23	9.0	2.10	Good
00063220 9	100.73	90.95	85.0	1.40	Good
00 0941520	91.54	83.68	76.0	0.00	Good
00133 1843	109.32	254.85	-8.0	0.00	Good
01 0131733	103.84	298.80	15.0	0.00	Good
0104705 59	91.95	97.48	-8.0	1.50	Good
010731856	90.81	88.81	83.0	0.00	Good
011180449	148.95	58.25	-20.0	0.00	Good
011450506	86.69	102.51	-7.0	1.50	Good
011540241	154.50	80.08	-5.0	0.00	Good
011801835	106.92	258.23	-3.0	2.50	Good
011841310	93.30	59.45	-12.0	1.60	Good
011861353	111.03	265.64	90.0	0.00	Good
012650323	100.56	283.30	8.0	2.50	Good

013321432	105.06	303.80	12.0	2.00	Good
013431815	91.86	88.57	2.0	0.00	Good
020011129	90.22	81.92	85.0	0.00	Good
020162309	105.12	303.77	12.0	2.00	Good
020782214	101.35	89.41	84.0	0.00	Good
020870456	109.72	257.53	-7.0	0.00	Good
020911959	116.29	251.78	-7.0	2.50	Good
021161606	100.23	64.66	-13.0	2.30	Good
022761905	90.74	98.88	-75.0	0.00	Good
022761905	90.74	98.88	68.0	0.00	Good
02285 2009	104.71	270.88	-69.0	1.10	Good
0231601 46	106.05	209.27	-32.0	1.20	Good
03 0690209	94.33	84.52	67.0	0.00	Good
0312515 50	95.27	85.65	68.0	0.00	Good
0314623 13	88.41	82.74	-64.0	0.00	Good
0317106 19	104.29	271.43	-61.0	0.70	Good
0320811 41	106.44	257.11	3.0	2.50	Good
0331518 48	93.02	58.79	11.0	1.30	Good
0418223 37	92.84	86.80	64.0	1.10	Good

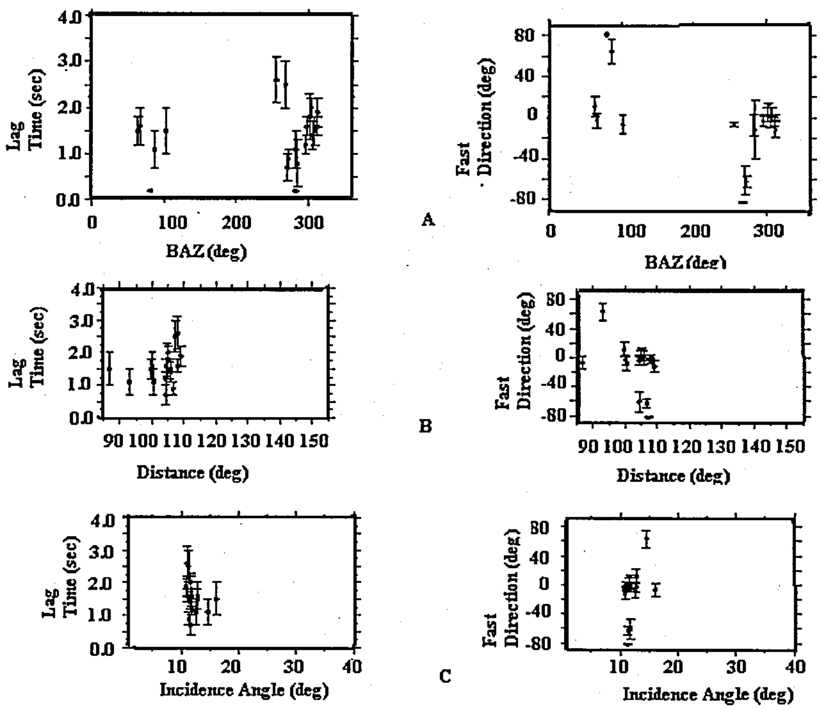

Figure B.25 A) Splitting versus BAZ (Back azimuth), **B)** Splitting versus distance (deg), **C)** Splitting versus the Moho incidence angle. Error bars represent 95% confidence intervals

MALT

The results of estimated splitting parameters at MALT indicate almost fast polarization directions oriented around more N-S than NE-SW for the events with a back azimuth range between 7°-349° (Table B.17). The mean value of fast polarization direction is 26.8± 12.3°. The mean value of the delay time is 0.9±0.4 seconds. It is clearly seen that azimuthal coverage for MALT station is very good. Determined splitting parameters are plotted as a function of back azimuth (BAZ), distance and incidence angle at Figure B.26. Error bars represent 95% confidence intervals for each of the lag time estimates.

Table B.17. MALT Splitting Measurements

EVENT ID	Δ (deg)	BAZ (deg)	Φ (deg)	δt (sec)	QUALITY
0035807 13	100.62	91.65	76.0	1.90	Good
010470559	85.89	102.37	27.0	1.60	Good
010591854	93.26	347.24	82.0	0.00	Good
020162309	109.82	309.93	19.0	1.10	Good
022852009	110.91	276.01	56.0	0.00	Good
0320811 41	112.66	261.74	12.0	1.30	Good
033151848	87.32	63.66	33.0	0.70	Good
033151848	87.32	63.66	33.0	0.80	Good
041810701	109.53	301.88	5.0	0.80	Good
042501242	109.53	214.00	29.0	0.00	Good
042511153	117.66	254.25	36.0	0.00	Good
043002253	108.83	210.97	29.0	0.00	Good
043080831	95.01	67.31	-18.0	0.00	Good
043200906	107.02	290.39	22.0	0.00	Good
043250807	108.40	298.89	-54.0	1.60	Good
043310225	97.70	88.52	90.0	0.00	Good
043330736	97.75	88.51	15.0	1.10	Good
043492320	99.85	303.57	-49.0	0.00	Good
050162017	92.85	73.80	-8.0	1.80	Good
050171050	92.70	73.86	35.0	0.70	Good
050500004	88.48	98.23	57.0	0.00	Good
050851540	94.19	92.90	-83.0	0.00	Good
050991516	85.24	7.23	-74.0	0.00	Good
051011220	105.85	81.77	79.0	0.00	Good
051551450	108.32	83.51	3.0	0.00	Good
051680621	100.11	348.48	89.0	0.00	Good

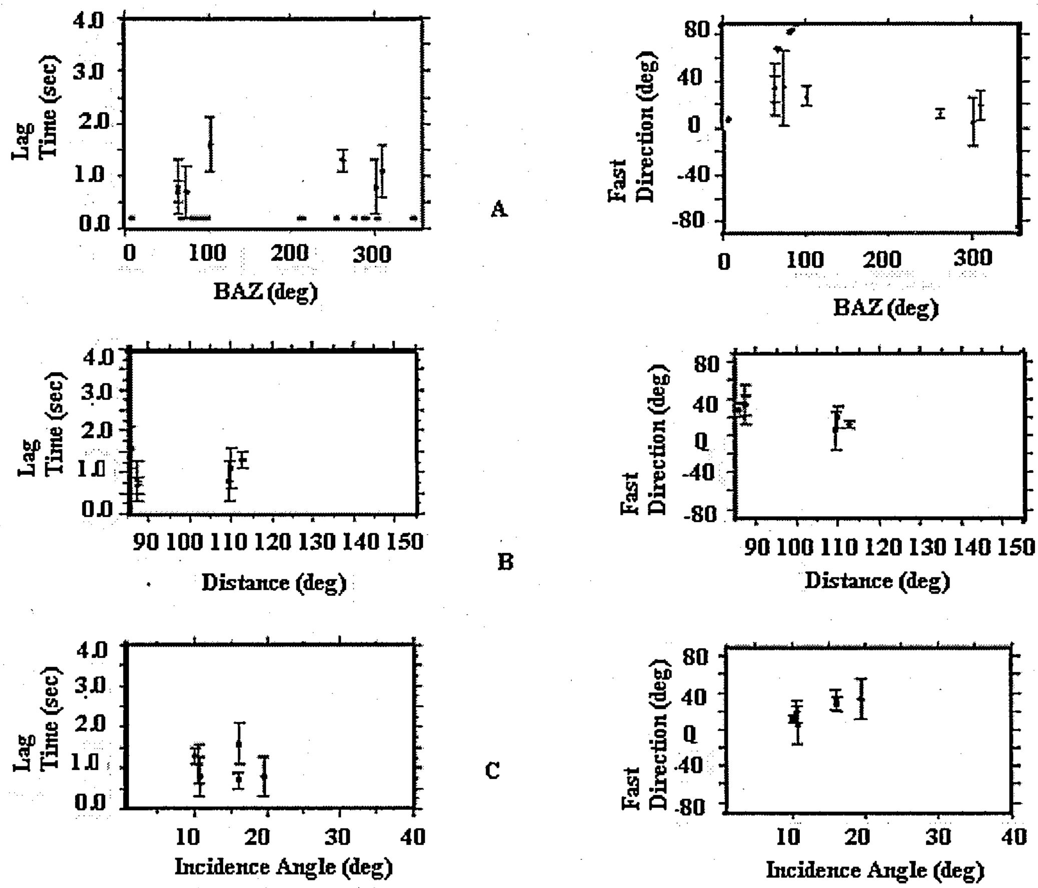

Figure B.26 A) Splitting versus BAZ (Back azimuth), **B)** Splitting versus distance (deg), **C)** Splitting versus the Moho incidence angle. Error bars represent 95% confidence intervals for each of the lag time estimates.

MLSB

Determined splitting parameters for MLBS station indicate fast polarization directions oriented around N-S for the events with a back azimuth range between 57°-295° (Table B.18). The average mean value of fast polarization directions is 22.0°±2°. The mean value of the delay time is 1.5± 0.3 seconds. Estimated splitting parameters are plotted as a function of back azimuth (BAZ), distance and incidence angle at Figure B.27 respectively. Error bars represent 95% confidence intervals for each of the lag time estimates.

Table B.18. MLSB Splitting Measurements

EVENT	Δ (deg)	BAZ (deg)	Φ(deg)	δt (sec	QUALITY
033151848	95.15	57.07	74.0	1.20	Good
040282215	99.54	86.65	87.0	0.00	Good
040362105	106.30	81.99	-20.0	0.00	Good
040380242	106.12	82.63	79.0	0.00	Good
041081558	102.83	89.49	0.0	0.00	Good
041140150	99.61	94.44	2.0	1.10	Good
042501242	104.23	209.50	12.0	1.70	Good
042781920	103.08	60.19	54.0	0.00	Good
042832126	101.82	294.23	17.0	0.00	Good
050611042	103.59	87.87	17.0	1.20	Good
050801243	105.50	250.64	74.0	0.00	Good
051631926	104.12	208.07	-20.0	0.80	Good
051642244	107.06	257.74	-20.0	0.80	Good

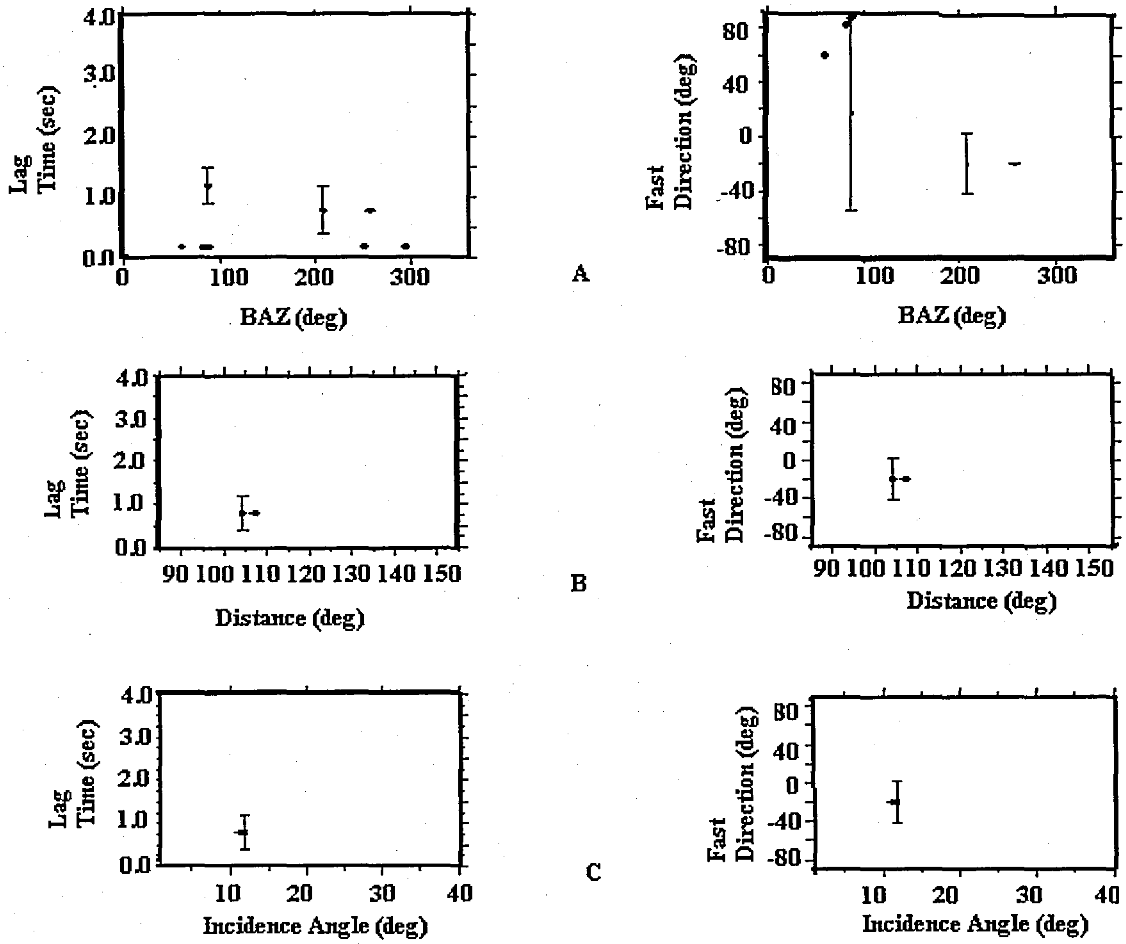

Figure B.27 A) Splitting versus BAZ (Back azimuth), B) Splitting versus distance (deg), C) Splitting versus the Moho incidence angle. Error bars represent 95% confidence intervals for each of the lag time estimates.